RECEIVER IMPLEMENTATIONS FOR A CDMA CELLULAR SYSTEM

by

George Aliftiras

Thesis submitted to the Faculty of the
Virginia Polytechnic Institute and State University
in partial fulfillment of the requirements for the degree of

MASTER OF SCIENCE
in
Electrical Engineering

Approved:

Dr. Brian D. Woerner
(Chairman)

Dr. Theodore S. Rappaport

Dr. Charles W. Bostian

July 1996
Blacksburg, Virginia

Keywords: CDMA, multiuser receiver, interference cancellation, quantization

Receiver Implementations for a CDMA Cellular System

by

George Aliftiras

Committee Chairman: Dr. Brian D. Woerner

Electrical Engineering

Abstract

The communications industry is experiencing an explosion in the demand for personal communications services (PCS). Several digital technologies have been proposed to replace overburdened analog systems. One system that has gained increasing popularity in North America is a 1.25 MHz Code Division Multiple Access (CDMA) system (IS-95). In CDMA systems, multiple access interference limits the capacity of any system using conventional single user correlation or matched filter receivers. Previous research has shown that multiuser detection receivers that employ interference cancellation techniques can significantly improve the capacity of a CDMA system. This thesis studies two such structures: the successive interference cancellation scheme and the parallel interference cancellation scheme. These multiuser receivers are integrated into an IS-95 compatible receiver model which is simulated in software.

This thesis develops simulation software that simulates IS-95 with conventional and multiuser receivers in multipath channels and when near-far conditions exist. Simulation results present the robustness of multiuser receivers to near-far in a practical system. In addition to multiuser implemenations, quantization effects from finite bit analog to digital converters (ADC) in CDMA systems will also be simulated.

Acknowledgements

I am sincerely grateful to Dr. Brian Woerner for being my advisor and providing guidance for this thesis work. His insight and motivation were invaluable. I would also like to express my appreciation to my committee members, Dr. Theodore Rappaport and Dr. Charles Bostian for their corrections and comments on this work.

I would like to thank Bradley Department of Electrical Engineering and Texas Instruments for providing me the financial assistance and sponsoring projects I have been doing during my study at Virginia Tech.

I am grateful to all the members of the Mobile and Portable Radio Research Group (MPRG) who assisted me through my thesis. I would especially like to thank Mike Buehrer, Brian Fox, Jason Hale, George Mizusawa, and Ning Yang for their help with my research. I would also like to thank Steve Swanchara for his unfailing assistance in my dealing with C. I greatly appreciate the help provided by all the MPRG staff members during my time here.

Finally, I dedicate this work to my family and friends who have provided support and encouragement during my academic studies.

Contents

List of Tables

List of Figures

Chapter 1

Introduction

Universal communications continues to be the goal of telecommunications companies worldwide. In order to provide ubiquitous coverage, service providers must eliminate the wirelines that keep users tethered to a stationary network. Wireless communications is the solution to eliminating fixed physical media for communications. Advances in semiconductor devices which began following World War II have motivated the development of wireless communications equipment. Of the varied forms of wireless communications, cellular radio and personal comunications services (PCS) have been growing at high rates over the past few years. There were approximately 30 million cellular radio users at the of 1994 and growth continues at 45% levels annually [Fla95]. This rapid growth has increased demand for wireless services that will integrate seamlessly with existing backbone networks and allow future service expansion.

1.1 CDMA in Wireless Communications

A problem facing the wireless communications industry is the limited available frequency spectrum. A conventional system might assign a channel or set of channels to service a geographical region. This region is typically chosen so that the coverage area is maximized. The capacity of the region is then limited to the number of channels allocated. This pattern of assigned channels is then repeated over an entire geographic region. While resolving the problem of spectral congestion, the reuse of channels results in co-channel interference. Care must be taken to limit the interference that will occur between these clusters of cells as this interference dominates the capacity of the system [Lee89]. The current analog cellular standard, Advanced Mobile Phone System (AMPS), is based upon frequency modulation (FM). While analog FM works well for voice, it lacks the flexibility in configuration for handling digital video and data sources. The integration of voice, video, and data services has pushed the demand for digital systems significantly. Digital modulation techniques are indifferent to the source of the transmission and can be designed to sufficiently handle the requirements for all types of service. Powerful forward error correcting (FEC) codes and advances in speech coding further enhance the capabilities of digital systems. While the transit to digital technology is undeniable, questions still remain about the choice of modulation and access technique.

The AMPS system uses frequency division multiple access (FDMA) to separate the duplex channels on which each user communicates. Each user is assigned a duplex channel in FDMA. Typically, a seven cell cluster is used to implement an AMPS system. FDMA performs poorly in a cellular environment and leads to low capacity limits [Lee91], [Jun93]. In an effort to increase capacity, a digital standard for the United States was proposed. The United States Digital Cellular (USDC) or Electronic Industry Association Interim Standard-54 (IS-54) uses time division multiple access (TDMA) to share each frequency channel between three users, but maintains the same 30 kHz channel bandwidth as the AMPS system [EIA90]. Service providers may allocate some of their current AMPS channels to an IS-54 system while still supporting existing AMPS users. In TDMA, multiple users share a forward and reverse frequency assignment and are reserved a time slot during which only they are allowed to transmit. The user is inactive during other time slots. IS-54, may support 3 full-rate or 6 half-rate users in each channel, when the data rates are compressed by speech coding techniques. IS-54 has been revised to include all digital control channels and standardized as IS-136.

While IS-54 (IS-136) may triple the capacity of current AMPS service, there is still a need for a solution that will increase capacity by a greater factor, in expectation of a coming boom in personal communications. A CDMA system (IS-95) has been recently standardized for this reason [EIA92]. For cellular, IS-95 would replace 40 analog channels (1.25 MHz of spectrum) but in a PCS application the entire band might be dedicated to a CDMA layout. It is important to note that in the cellular case, IS-95 *does not overlay* existing narrowband channels within the same cell. Very broadband signals that might overlay a cellular band have been suggested but not yet implemented. Resistance to narrowband jamming is of less concern in a cellular arena since the FCC strictly regulates transmissions in the cellular band. CDMA appears capable of greatly increasing the capacity of a cellular system; some claim by a factor of 10-14 [Gil91]. These claims are contigent upon the performance of the power control algorithm and the duty cycle of the voice activity detection.

Another TDMA technology has recently been adopted for use in the PCS band. The Globale System for Mobile (GSM) was developed in Europe as a second generation cellular system and has now become the world's most popular standard for new personal communications equipment. The GSM system will be frequency upshifted to 1.9 GHz and renamed DCS 1900 for PCS use. The primary competetion for any CDMA system for PCS will most likely come from GSM systems that will be setup in the United States.

1.1.1 Advantages of CDMA in Cellular

A CDMA system has several advantages over narrowband TDMA or FDMA systems. One important feature of spread spectrum is the inherent resistance to multipath fading. Any two multipath components of a signal separated by a time greater than a pulse duration are highly uncorrelated and resolvable. Multipath combining receivers may take advantage of this and actually improve the signal to noise ratio. Even without multipath combining, these interfering components will be rejected by the receiver because of the cross-correlation properties of CDMA. CDMA systems also undergo a "gradual" degradation in signal to noise ratio as the number of users is increased. This soft capacity limit allows operators to push the number of active users beyond the design value, unlike other multiple access techniques. In designing a CDMA layout, it is possible to assume an average load and still handle peak traffic times because of this soft capacity. FDMA and TDMA do not allow more users beyond a fixed limit but they can guarantee a minimum quality of service for the active users, whereas an overloaded CDMA system will see gradually increasing bit error rates before it begins dropping calls.

In CDMA, the frequency reuse factor is one. The same duplex channel is allocated to all users in every cell in the system. Switching channels is not necessary for the roaming user and algorithms for supporting handoffs at the base station are simplified. Users at the boundary of two cells will have the probability of being dropped significantly reduced because the system can afford to maintain a user's radio link with in two different cells temporarily through a procedure called "soft handoff". CDMA is an interference limited system so through the use of multisectored antennas and voice activity detection it is possible to increase the capacity. Multisectored antennas focus the antenna energy, spatially reducing the interference for users in other sectors. Adaptive antenna patterns where individual spot beams are given for each user have also been studied [Lib94]. Further capacity gains are possible by suppressing the transmitter during quiet periods of speech. Voice inactivity is exploited greatly in IS-95 by permitting a transmitter to turn off during inactivity or reduce the transmission power level.

1.1.2 Disadvantages of CDMA in Cellular

While CDMA promises great capacity gains, there are still many technical issues that need resolving. Synchronization to PN sequences is still a difficult task for a receiver with Doppler and multipath effects further complicating the issue. IS-95's solution to the problem is to provide short and long PN sequences. The short PN sequence has a significantly shorter repeat period, speeding up acquisition. A serious disadvantage in CDMA, is the near-far effect. Ideal performance of a CDMA system depends on the received powers having equal strengths at the receiver. This has not been a problem in satellite based CDMA systems where the powers are fairly constant. Wireless system will undergo power fades as the user moves about the cell and as multipath components induce deep fades. A weak user might be drowned out by users who are near the base station tower. To maintain uniform power levels, a power control loop is used by either the mobile, base station, or both. A power variation of as little as 1-2 dB may still reduce capacity by 15-20% [Cam92]. Similar capacity reductions were also demonstrated in the presence of multicellular interference and imperfect power control [Mil92]. Another potential disadvantage of CDMA is a quality that was mentioned previously, voice activity detection. This greatly improves capacity because of the pauses naturally occurring in speech. There are few such pauses in most data transfer and video applications. In a CDMA system designed to take advantage of voice activity detection, data and video users will force the system to a lower capacity.

1.2 Simulation of Communications Systems

It is often difficult to use analytic techniques to evaluate the performance for complex communications systems. Performance evaluation is central to the design and selection of communications systems. The extreme difficulty in obtaining closed form expressions for the performance of a system through analytical techniques has boosted the interest in simulation of systems. Simulation allows the designer to implement variations in a system and observe the effects in a timely manner while minimizing the gross assumptions needed for analytic techniques.

The field of simulation may be divided into two areas that often overlap: the simulation of hardware level designs and the simulation of systems. Hardware level designs are often simulated using tools for the appropriate medium, analog or digital. Circuit level simulations using products such as SPICE often evaluate the transient behavior of a device, for example, the acquisition time of a phase-locked loop. Many packages have already been developed that perform the system function [Sha88]. These typically consist of block oriented subsytem models that allow integration for the simulation. The engineer may iterate this process with modifications. These areas of simulation overlap when the performance of a particular piece of hardware may adversely effect the system. Due to the rigorous computations needed for most system simulations, the hardware evaluation is often lumped into a single parameter such as timing or phase tracking errors. The majority of these simulations evaluate either the bit error rate (BER) or some measure of change in the signal to noise ratio (SNR). It is necessary to make the distinction as to when analytic techniques are sufficient and when simulation is the only solution.

The usefulness of analytic techniques is often limited by the linearity of the system. Analysis of systems often uses a channel consisting of additive white Gaussian noise (AWGN) since the error function may be used to develop a closed form expression. The stochastic properties of the noise are maintained so long as the filter at the receiver is linear [Sta94]. The performance of convolutional codes combined with interleaving in a bursty environment is often desired. Analytic work on coding operations has only yielded upper and lower bounds with white noise. In the case of a wireless environment, analytic methods may poorly describe the channel environment. Often, the Rayleigh fading model is used so that an analytic expression may be derived. With the advent of wideband channel sounding methods, real-world channel profiles may be measured at different locations and imported into the simulation. The software developed in this work allows for channel profiles to be imported given the length of the profiles and the data is in baseband quadrature form at the system sampling rate. The software allows several profiles to be imported so that each simulated user may experience time-varying channels.

1.3 Purpose of Research

The objective of this research is to simulate and evaluate the performance of different receiver implementations with respect to the IS-95 CDMA standard proposed for second generation cellular and PCS. It is well known that multiuser receivers improve the capacity of CDMA systems and provide some resistance to the near-far problem. The simulation software developed for this research implements parallel and successive interference cancellation methods in combination with the IS-95 standard. Quantization effects in the receiver are also simulated for both the IS-95 standard and a simpler spread spectrum model. This thesis bridges the work and results provided by [LiY93] and [Kau95]. It also develops further areas that were not covered in the previous work and are pertinent to the simulation of IS-95 such as noncoherent demodulation. This work will provide crucial information leading to the implementation of interference cancellation in a real-world system. The quantization results are also useful in the handling of multimode receivers where there is a potential tradeoff between narrowband and wideband CDMA quantization requirements.

Li developed software based on the IS-95 standard that used the same foundation as the BERSIM 2.0 software developed by the Mobile and Portable Radio Research Group (MPRG)at Virginia Tech. The BERSIM tool was originally coded by Fung [Fun91] in the programming language PASCAL and was later rewritten by Thoma [Tho92] into ANSI C. The results given by Li showed the performance of IS-95, both forward and reverse channels, in several real-world channel models. That simulation tool, however, did not look at the performance of the reverse channel with noncoherent reception as it is practically implemented in hardware. The simulator in this work uses noncoherent demodulation. Striglis [Str94] and Kaul investigated the use of a multistage RAKE receiver. Kaul then applied the same methods of a multistage RAKE to multiple stages of interference cancellation. Parallel interference cancellation was used in that work along with adaptive receivers that used the information in the channel. In practical systems, instantaneous phase and amplitude measurements from the channel are not readily available.

For both successive and parallel interference cancellation, we compare them in a near-far and multipath environment. Only one stage of parallel interference cancellation is used to minimize the complexity in the receiver. It will be shown that the use of noncoherent demodulation can reduce the expected advantages of interference cancellation and RAKE receivers. Quantization effects for a range of one to eight bits are shown for both a simple spread spectrum receiver and an IS-95 receiver. By comparing to the results of infinite quantization levels, we can see how many bits are necessary to maintain near optimal conditions.

1.3.1 Outline of Thesis

The remainder of the thesis is organized as follows. Chapter 2 discusses direct sequence spread spectrum (DS/SS) and the IS-95 standard. The transmitter for the IS-95 reverse channel is presented along with detailed descriptions of the function of each system component. The basic operation of the DS/SS system is given for comparison to the IS-95 system and as a reference for the simulation on quantization effects.

Chapter 3 is a review of some of the receiver structures that have appeared in the literature over the years. The superheterodyne receiver structure is repeated here only for the purposes of reviewing the concept of analog to digital conversion methods. The nature of quantization is also reviewed. The differences between conventional single user receivers and the RAKE receiver are described. Several methods for implementing RAKE receivers is also given. The major forms of multiuser receivers are listed with a brief description of each receiver's advantages and disadvantages.

Chapter 4 presents the simulation method used in this thesis. The mathematical model for baseband simulation is described. The implementation of the transmitter, channel, and receiver in software is explained. The critical issue of scaling of AWGN power is covered along with a discussion of the modeling of the multiple access interference present in a CDMA system. The models for the successive and parallel interference cancellation are shown as well.

Chapter 5 covers the results of the simulations. All the results are measures of the bit error rate (BER). We present the results for the performance of the IS-95 reverse channel with hard and soft Viterbi decoding and with a variable number of bits in the quantizer. This is contrasted with the simple DS/SS system with quantization. Performance of IS-95 under in the near-far conditions and in a multipath environment is also presented. We also demonstrate performance improvements with the implementation of parallel and successive interference cancellation designed for IS-95. The interference cancellation cases are examined in near-far and multipath conditions.

Chapter 6 concludes the thesis and summarizes the results of the work. Areas for future work are also detailed.

Chapter 2

Spread Spectrum System Model

The common goal of communications systems is to maximize information transfer while minimizing the bandwidth occupied. Almost all conventional communications systems used in practice followed this guideline. The most notable exception is wideband FM used for broadcast radio. In that case, bandwidth expansion is used to improve signal fidelity. For modern digital modulation schemes, the bandwidth occupied is directly proportional to the information rate of the source. Spread spectrum systems are distinct from other digital modulation schemes in that they purposefully increase the bandwidth occupied by the modulated signal. The factor by which the bandwidth is expanded is often described as the processing gain (G_p) of the system. In a spread spectrum system, another signal is used to "spread" the bandwidth of the information signal. This spreading is fundamentally different from the bandwidth expansion of wideband FM. Wideband FM is generated from the information source solely and is therefore not considered a spread spectrum system. Although many methods exist for generating spread spectrum signals, almost all fall into three distinct categories:

1) Direct Sequence Spread Spectrum (DS/SS): DS/SS signals are generated by spreading the information signal with a pseudo-random or pseudo-noise (PN) code sequence. Typically, modulo-two addition of the information signal and the PN sequence is used to create the DS/SS signal. The PN code rate is much higher than the information rate so the spectral characteristics of an RF modulated carrier are dominated by

the PN code rate rather than the information sequence. DS/SS was originally developed for military applications because of its inherent resistance to jamming and the low probability of intercept (LPI) due to the pseudo-randomness of the signal. The resistance to jamming and interference is a function of the processing gain used in the system. At the receiver, the interfering signal is spread by the correlating structure that is used to receive the spread signal. This antijamming capability has made DS/SS popular in the crowded unlicensed band where DS/SS may be used in the presence of narrowband users already present.

2) Frequency Hopped Spread Spectrum (FH/SS): PN sequences are also used in this type of spreading, but instead of operating directly on the information signal the PN sequence controls the RF carrier frequency. In essence, the signal is moved in the frequency domain according to the PN sequence. The PN sequence determines the sequence (or "hopping pattern") of carrier frequencies. Two classes of FH/SS exist: fast and slow frequency hopping. In fast FH/SS, the hopping rate is greater than the data rate. Slow FH/SS uses a hopping rate lower than the data rate. FH/SS has several advantages over DS/SS including resistance to the near-far problem and improved antijamming capabilities. For commercial cellular applications, however, FH/SS has several disadvantages. Fast FH/SS is impractical due to the need for local oscillators that will shift frequencies at very high rates. Acquisition and generation of the signal becomes extremely difficult without expensive hardware when compared to fixed frequency or slow hopping signals. FH/SS signals are also narrowband at any given instant in time and are consequently susceptible to fading. Fading results in burst errors which require powerful coding techniques and interleaving to overcome. In a multiple access situation, there is a probability that two or more transmitters will hop to the same frequency resulting in a collision in which the data will not be resolveable. As the system load increases, the collisions will become more frequent which can only be reduced by increasing the occupied bandwidth.

3) Time Hopped Spread Spectrum (TH/SS): Time hopping is the time domain dual of FH/SS. In TH/SS, a time interval is divided into a large number of time slots and the PN sequence determines the time slot used for transmission. TH/SS often uses extremely short pulses for high spreading gains. The receiver also requires rapid timing acquisition and buffering to store the received data over the time interval.

Time-hopping modulation is extremely vulnerable to interference, narrowband or otherwise. This system finds most applications in ranging or systems where simplicity in the modulation is desired and the data may be pulse modulated [Dix84].

Numerous hybrids that combine two or more of the aforementioned methods have been suggested as suitable applications for spread spectrum. For cellular, PCS, and other commercial communications systems, DS/SS has gained the most poularity. Much of this is due to DS/SS's robustness in multipath and some complexity issues concerning FH/SS. The multiple access technique conventionally used with spread spectrum is CDMA. Since this thesis focuses on the IS-95 standard we will limit the discussion to DS/SS.

2.1 DS/SS Systems

2.1.1 DS/SS Transmitter

For simplicity, we intially describe DS/SS with BPSK modulation. The ith bit of the information signal is assumed to be discrete and takes on values of $b_i \in \{+1, -1\}$. Figure 2.1 shows the block diagram of a DS/SS transmitter.

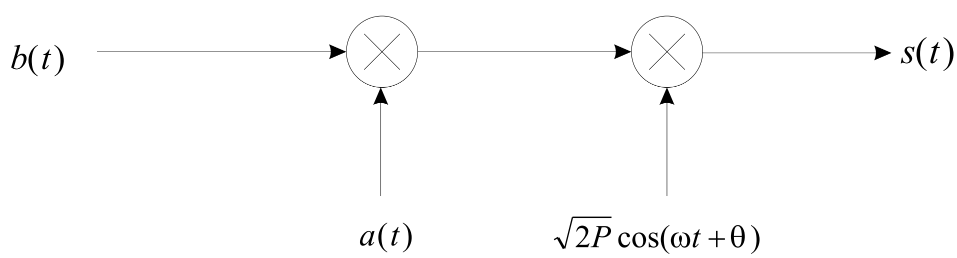

Figure 2.1: DS/SS Transmitter

The data signal $b(t)$ is described as

$$b(t) = \sum_{i=\infty}^{\infty} b_i p_T(t - iT) \tag{2.1}$$

where b_i is an independent identically distributed random variable, $p_T(t)$ is the pulse shape of the bit, and T is the duration of a bit. In this case, we shall assume a rectangular pulse shape. That is

$$p_T(t) = \begin{cases} 1, & 0 \leq t \leq T \\ 0, & t > T \end{cases} \tag{2.2}$$

The data is then spread by the PN sequence $a(t)$ given by

$$a(t) = \sum_{j=-\infty}^{\infty} a_j p_{T_c}(t - jT_c), \tag{2.3}$$

where a_j is the jth chip of a discrete periodic PN sequence assigned to the user and takes on values of $a_j \in \{\pm 1\}$ with a duration of T_c. The chip has pulse shape $p_{T_c}(t)$ which is limited in time to $[0, T_c]$. The processing gain, G_p, by convention is defined as the ratio T/T_c. The transmitted signal $s(t)$ is then

$$s(t) = \sqrt{2P}a(t)b(t)cos(\omega t + \theta). \tag{2.4}$$

2.1.2 DS/SS Receiver

For the above DS/SS example, we must develop a receiver model. In the simplest form, our model might consist of additive white Gaussian noise (AWGN) and a finite propogation delay τ. The received signal would then be

$$r(t) = s(t - \tau) + n(t). \tag{2.5}$$

One possibility for an optimal receiver, a correlation structure, for an AWGN channel is presented in Figure 2.2. This receiver performs the complementary operations of the DS/SS transmitter in Figure 2.1. The received signal is downcoverted to baseband where it is multiplied by the PN sequence. This despread signal is then passed through a correlator that gives a decision statistic Z_i. A threshold comparison is done on Z_i to produce an estimate of b_i. If $Z_i \geq 0$, then $\hat{b}_i = 1$, $Z_i < 0$ then $\hat{b}_i =$ -1. The decision statistic Z_i is given by

$$Z_i = \int_{iT}^{(i+1)T} r(t)a(t)cos(\omega t + \theta)dt. \tag{2.6}$$

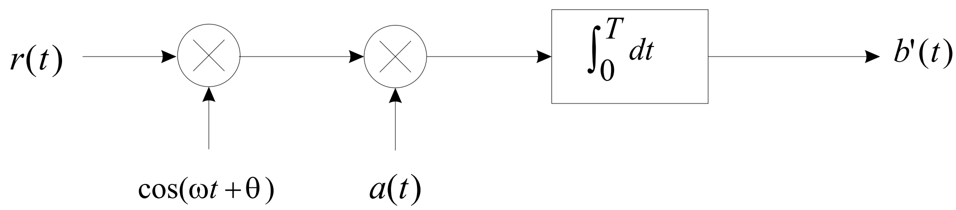

Figure 2.2: DS/SS Receiver

Note that Figure 2.2 is only one of many possible receiver implementations [Pro89]. It is possible to first despread the signal at an intermediate frequency (IF) and then downconvert to decide on the transmitted bit. Other structures are optimal for Gaussian environment including matched filters. The receiver shown here is only optimal for the AWGN channel. In many wireless environments, conditions such as multipath exist which preclude the sole use of an AWGN model. The interference generated from multiple access users may also not be Gaussian. Therefore, the receiver in Figure 2.2 is not necessarily optimal or even guaranteed to give good performance for these cases.

2.2 Model for CDMA System

The system used in the simulation is based on the IS-95 CDMA standard proposed by QUALCOMM. This standard describes both forward and reverse channels which are composed of traffic, paging, pilot, access, and synchronization channels. The forward channel is defined as the link from the base station to the handset and the reverse channel is the link from the handset to the mobile. The forward channel is composed of one pilot channel, up to seven paging channels, up to one synchronization channel, and up to 63 traffic channels. The pilot channel transmits a zero information signal and is used for coherent demodulation at the handset. The synchronization channel is optional and provides relative offset information for the pilot channel. Paging channels are used for call setup and other networking features. The traffic channels represent the physical layer of the system where voice (and possibly data) information is exchanged. One possible configuration is to operate the system with the pilot channel and 63 traffic channels. The reverse channel is composed of access channels and traffic channels. Access channels are used to respond to pages and to initiate contact with the base station. There must be at least one access channel for every paging channel supported. All the channels use DS-CDMA, but only the traffic channels are of critical concern. The simulation models only reverse traffic channels since the receiver structures presented are only practical at the base station. The following descriptions of the reverse traffic channel are taken from the IS-95 standard [EIA92]. Other works have covered the IS-95 standard such as [LiY93] which describes the forward and reverse traffic channels in greater detail.

2.2.1 Reverse Traffic Channel

The IS-95 standard allows for multiple speech data rates in the reverse traffic channel. These include 9600, 4800, 2400, and 1200 bps (subsequent versions of the standard now also allow for a 13.6 kbps voice coder). These varying data rates take into account the voice activity of a particular user. For this simulation, we will limit the data rate to 9600 bps for all users. This generates a worst-case scenario for a CDMA system as the transmitted power will be constant in a full-rate transmission as opposed to a reduced-rate. The interference, consequently, will never be reduced by voice activity detection.

Data on the reverse traffic channel is grouped into 20 ms frames. At 9600 bps, the number of data bits output from the vocoder is 172 which corresponds to a 8.6 kpbs vocoder rate. A 12 bit CRC check is appended to this in order to provide a frame quality indicator. Another 8 bits of padded zeroes are also added. These zeroes flush out and reset the convolutional encoder shift register. This 192 bit frame is then encoded by a 1/3 rate convolutional encoder and interleaved. The interleaved bits are then grouped into code symbols which are orthogonally modulated. These modulation symbols are then spread at a rate of 1.2288 million chips per second (Mcps). Table 2.1 from [EIA92] demonstrates the resulting transmission rates. Figure 2.3 depicts the critical elements of the reverse channel transmitter.

Table 2.1: Reverse Traffic Channel Modulation Parameters

Data Rate = 9600 bps		
Parameter		**Units**
PN Chip Rate	1.2288	Mcps
Code Rate	1/3	bits/code sym
TX Duty Cycle	100	%
Code Symbol Rate	28,800	sps
Modulation	6	code sym/Walsh sym
Walsh Symbol Rate	4800	sps
Walsh Chip Rate	307.20	kcps
Walsh Symbol	208.33	μs
PN Chips/Code Symbol	42.67	PN chips/Code sym
PN Chips/Walsh Symbol	256	PN chip/Walsh sym
PN Chips/Walsh Chip	4	PN chips/Walsh chip

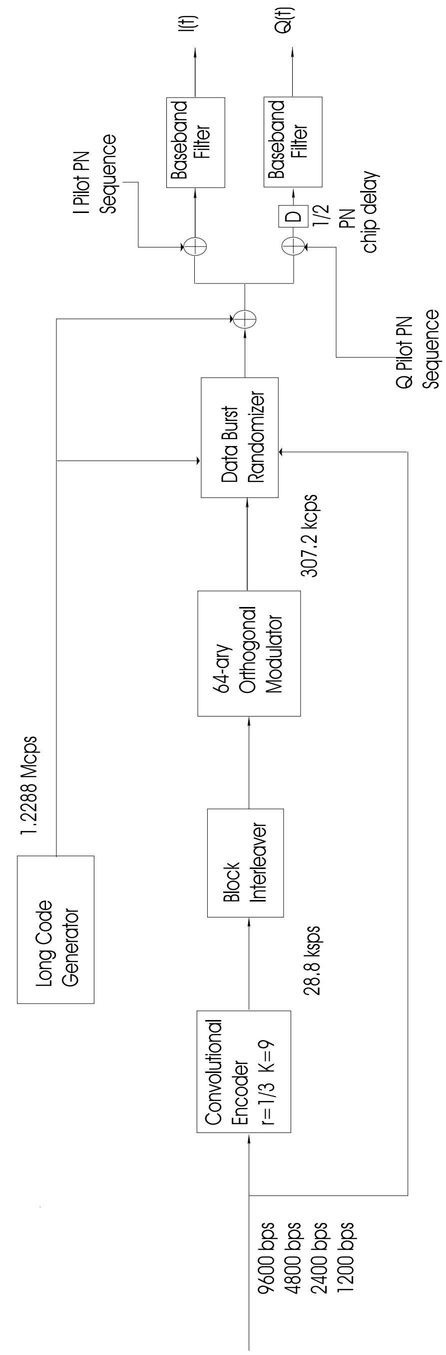

Figure 2.3: Reverse Channel Transmitter for IS-95

Some parameters were not included in this simulation of IS-95 in order to reduce complexity. One of these parameters is the power control mechanism. IS-95 uses both open-loop and closed-loop power control. Open-loop power control is used by the handset. The received power at the handset is used as a reference point so that when the received signal power is low, the handset assumes it is farther away from the base station and boosts its transmit power. The sum of the received and transmitted power in dB must yield a constant. The base station uses closed-loop power control to force the handset to deviate from its current transmitting power level. Every 1.25 ms a power control bit is sent, by puncturing the transmitted bits, that adjusts the handset's power by 1 dB [Whi94]. The power control function was not directly implemented in this simulation. Instead, either ideal power control was assumed or a fixed power differential was assigned to groups of users.

The data burst randomizer used immediately after orthogonal modulation was also not included as this component is a function of the data rate and serves no purpose at 9600 bps.

2.2.2 Convolutional Encoder

Convolutional encoders play an important role in the development of modulation schemes for wireless systems. Convolutional codes add a structured redundancy to the information source that mitigates the effect of random noise corrupting the data stream. Convolutional codes perform better in the marginal regions of bit error rates ($10^{-2} - 10^{-4}$) than block codes such as Reed-Solomon [Ber87]. Since voice communications systems perform satisfactorily in this range and are often designed for those bit error rates convolutional codes are a common element in wireless systems. Convolutional codes gain their name from the fact that the information source is mathematically convolved with the impulse response of the code [Wic95]. This impulse response is defined by generator functions for a particular code. There is a generator function for every output of a convolutional encoder. These convolutional encoders are physically constructed by using shift registers with taps determined by the generator functions. The rate of the encoder is defined as the ratio of inputs to outputs. The number of taps on the shift register determines how many of the ouput bits are influenced by the input bits. The number of influenced output bits is called the constraint length. To avoid confusion, in practice the constraint length of an encoder is usually taken to be the number of memory elements in the shift register plus one. Note that shift registers are readily implemented in any programming language making them easy to simulate. IS-95 defines a rate 1/3 encoder with constraint length K = 9, thus there are eight memory elements in the shift register. The generator functions in octal are $g_0 = 557$, $g_1 = 663$, and $g_2 = 711$. Figure 2.4 shows the necessary taps for the IS-95 reverse channel convolutional encoder.

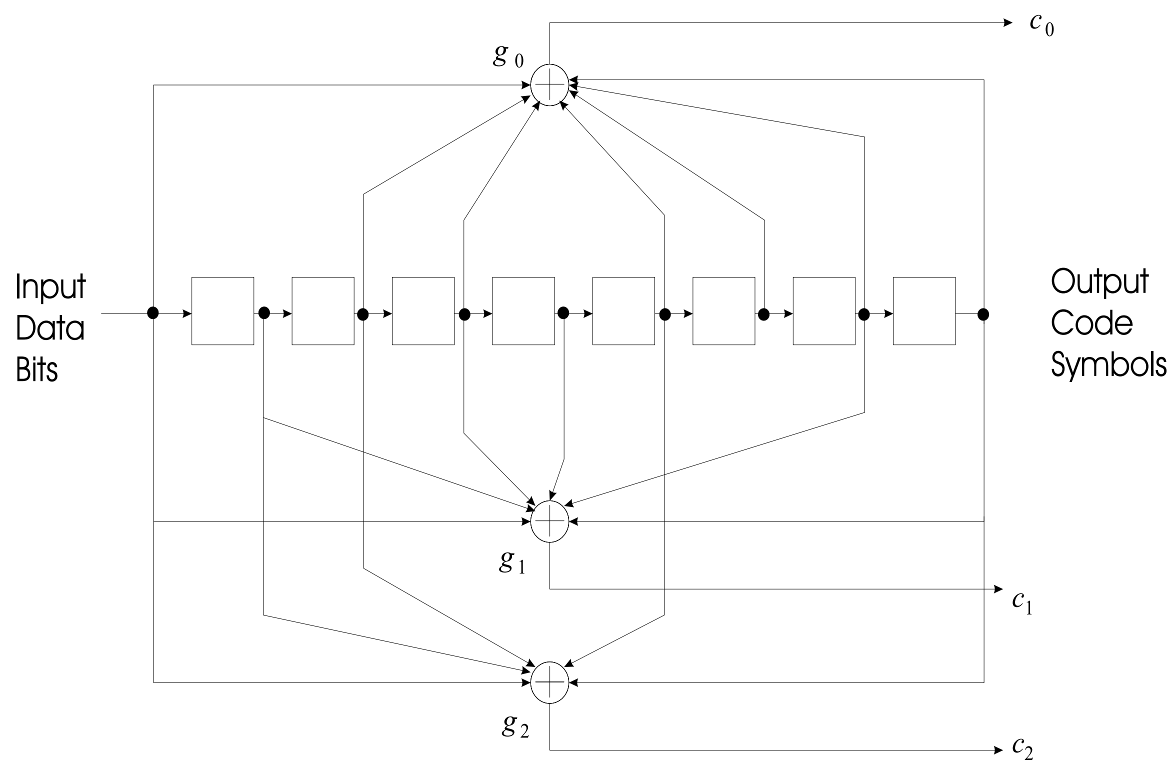

Figure 2.4: Convolutional encoder for IS-95 reverse channel

2.2.3 Interleaving

While convolutional codes perform well in correcting random errors typical in a Gaussian noise environment, they are very susceptible to deep fades. The burst of errors that may occur in a fade common to a multipath environment can be prevented by randomizing the placement of the errors. One possible implementation of interleaving is the block interleaver. Bits are input to an $m \times n$ matrix by columns and read out by rows. The number of rows in the interleaver must be at least as large as the average fading duration expected in the channel to effectively randomize the code symbols. For finite block lengths the maximum separation between symbols cannot be larger than the block size of the interleaver. For a slowly changing channel, such as low-speed vehicles, it may not be possible to completely decorrelate any two symbols. For this reason many interleavers are chosen so that symbols related to an input bit are evenly spaced throughout the interleaver block [Lin92]. In order to achieve such a spread, the number of columns in the interleaver must be greater than the constraint length of the convolutional encoder. IS-95 uses an 32 x 18 matrix which spans the 20 ms frame. For reduced data rates, the interleaver introduces redundancy into the information by repeating symbols.

2.2.4 64-ary Orthogonal Modulator

The modulation type for the reverse channel is 64-ary orthogonal modulation. Every six code symbols select one of 64 possible orthogonal modulation symbols. The modulation symbols are generated using Walsh functions. The 64 modulation symbols are numbered 0 through 63 and are selected according to the following formula [EIA92]

$$\text{Modulation symbol number} = c_0 + 2c_1 + 4c_2 + 8c_3 + 16c_4 + 32c_5,$$

where the c_n represents the nth code symbol. The 64 by 64 matrix of modulation symbols is readily generated by recursion with

$$W_{2n} = \begin{matrix} W_n & W_n \\ W_n & \overline{W}_n \end{matrix}$$

where the seeding function is $W_1 = 0$, and continues with

$$W_2 = \begin{matrix} 0 & 0 \\ 0 & 1 \end{matrix}$$

The value n is a power of 2. The Walsh chip rate is 307.2 kilochips per second (kcps).

2.2.5 Long Code Spreading

After modulation the Walsh chips are spread by direct sequence using the long PN sequence. Each user is uniquely assigned a long PN sequence of period $2^{42} - 1$ chips. Since the sequence is clocked at 1.2288 Mcps, this period corresponds to about 41 days. The long code is defined by the polynomial

$$p(x) = x^{42} + x^{35} + x^{33} + x^{31} + x^{27} + x^{26} + x^{25} + x^{22} + x^{21} + x^{19} +$$

$$x^{18} + x^{17} + x^{16} + x^{10} + x^{7} + x^{6} + x^{5} + x^{3} + x^{2} + x^{1} + 1.$$

Every PN chip is generated by the modulo-2 product of the long code shift register and the long code mask. Figure 2.5 is a diagram of the long PN sequence generator. The initial state of the generator is such that the output is a '1' followed by 41 zeroes. The long code mask has three states: an initialization state, a public mask used for setup that is unique to the handset's electronic serial number (ESN), and a private mask unique to the mobile station identification number (MIN). The initialization state of the mask has the most significant bit (MSB) set to '1' and the remaining 41 bits set to zeroes. The public mask has the ten most significant bits set to '1100011000' with the remaining 32 bits composed of a permutation of the ESN. This permutation has this format:

$$\text{ESN} = (E_{31}, E_{30}, E_{29}, E_{28}, \ldots E_{2}, E_{1}, E_{0})$$

$$\text{Permuted ESN} = (E_{0}, E_{31}, E_{22}, E_{13}, E_{4}, E_{26}, E_{17}, E_{8}, E_{30}$$

$$E_{21}, E_{12}, E_{3}, E_{25}, E_{16}, E_{7}, E_{29}, E_{20}, E_{11}, E_{2}, E_{24}, E_{15}$$

$$E_{6}, E_{28}, E_{19}, E_{10}, E_{1}, E_{23}, E_{14}, E_{5}, E_{27}, E_{18}, E_{9})$$

The private mask is generated through a confidential process and was not used in the simulation. After the initial state is generated, the public mask is used for all frame transmissions. The ESN used was a random bit sequence.

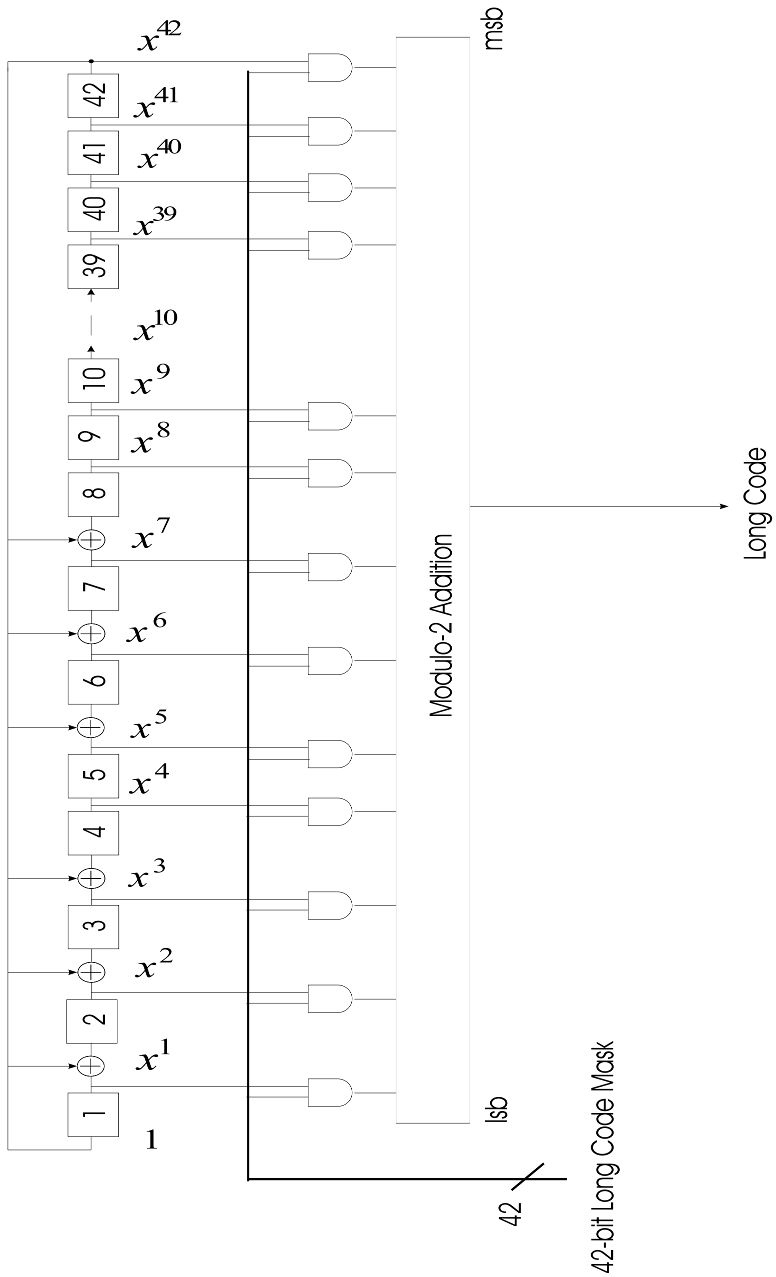

Figure 2.5: Long PN code generator for IS-95

2.2.6 Quadrature Modulation

After the long code spreading, the chips are sent to both in-phase (I) and quadrature (Q) arms where they are further spread by separate I and Q PN sequences. The resulting Q symbol stream is delayed by one half a PN chip (406.901 ns). This is offset quadrature phase shift keying (OQPSK) PN spreading combined with binary phase shift keying data modulation. Figure 2.6 shows the signal constellation for OQPSK. OQPSK is used in the reverse channel to control the spectral characteristics of the RF signal. The lack of 180 degree phase transitions in the signal constellation means that the envelope of a bandlimited (or pulse shaped) signal will not go to zero. Power efficient nonlinear amplification will not cause large sidelobe regeneration improving spectral efficiency [Rap96]. QPSK type modulation may also be detected noncoherently eliminating the need for a pilot tone, consequently improving the power efficiency.

The clock rate of these I and Q chips is matched to the data rate so no bandwidth spreading occurs. The purpose of these sequences is to allow for rapid acquisition of the signal at the receiver and to prevent any I and Q mixing products. Both sequences have a 15 element shift register with a period of $2^{15} - 1$. This is increased to 2^{15} by shifting in a zero after 14 zeroes have occurred to give the "all zeroes" state. The initial state of both these sequences has the MSB set to the value 1 and all remaining registers set to 0. The I PN sequence polynomial is [EIA92]

$$p_I(x) = x^{15} + x^{10} + x^8 + x^7 + x^6 + x^2 + 1.$$

The Q PN sequence polynomial is

$$p_Q(x) = x^{15} + x^{13} + x^{11} + x^{10} + x^{10} + x^9 + x^5 + x^4 + x^3 + 1.$$

These I and Q PN sequences are not guaranteed to be orthogonal over the entire transmission; although, it is hoped that the crosscorrelation is very low. This has consequences when dealing with a noncoherent link such as the reverse channel in IS-95. It will be shown later that mixing of the I and Q channels may degrade the system performance.

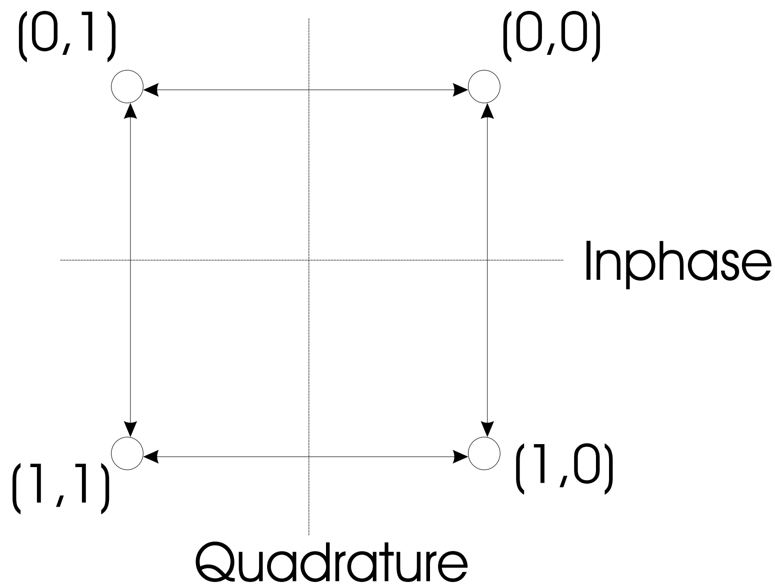

Figure 2.6: IS-95 Reverse Channel Signal Constellation

2.2.7 Baseband Filtering

Pulse-shaping is required for both the I and Q channels. The purpose of this pulse-shaping is to bandlimit the signal to meet FCC regulations. A digital filter is specified with coefficients given in Table 2.2. This pulse-shaping filter is identical for both I and Q channels. These coefficients are separated in time by one fourth a PN chip (203.5 ns).

Most filtering used in mobile communications obeys Nyquist's pulse-shaping criterion for zero intersymbol interference (ISI). His theorem states that the received pulse shape, $p_r(t)$, must have the property

$$p_r(nT) = \begin{cases} 1, & n = 0 \\ 0, & n \neq 0 \end{cases}, \tag{2.7}$$

where T is the symbol period, and n is any integer. For matched filtering, one would convolve the transmitted pulse-shape with a time-reversed version in order to minimize the noise [Zie92]. All sampling instants after convolution must occur at $t = nT$ for there to be zero ISI. For IS-95, the receiver filter is identical to the pulseshaping filter due to symmetry. The convolution of the two filters is shown

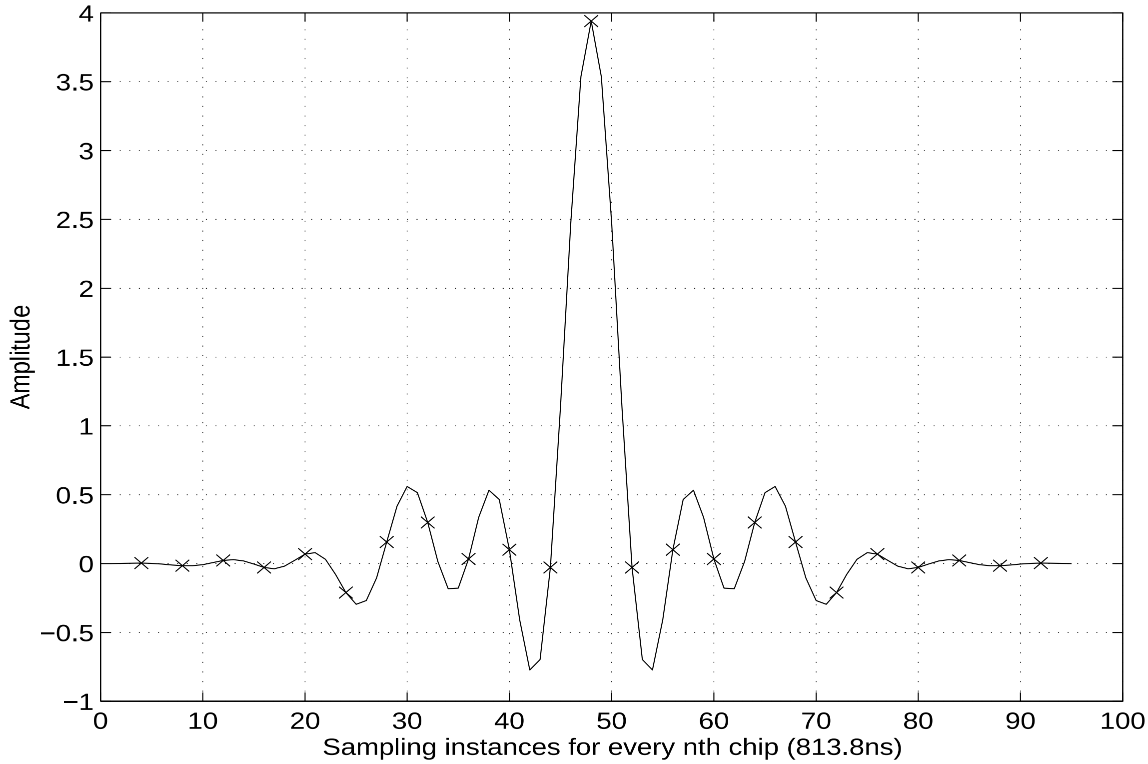

Figure 2.7: Convolution of pulse-shaping filter with matched filter; appropriate sampling instances for each chip are marked with '×'.

in Figure 2.7 with the sampling instances marked by the symbol '×'. It is notable that where the sampling instances occur, the waveform is not equal to zero. The modified pulse-shape has better spectral characteristics than convential raised cosine filter. The resulting ISI is acceptable when attempting to meet stringent bandwdith constraints.

Table 2.2: Filter Coefficients for Baseband Filtering

k	h(k)
0, 47	-2.5288315e-02
1, 46	-3.4167931e-02
2, 45	-3.5752330e-02
3, 44	-1.6733702e-02
4, 43	2.1602514e-02
5, 42	6.4938478e-02
6, 41	9.1002137e-02
7, 40	8.1894974e-02
8, 39	3.7071157e-02
9, 38	-2.1998074e-02
10, 37	-6.0716277e-02
11, 36	-5.1178658e-02
12, 35	7.8745260e-03
13, 34	8.4368728e-02
14, 33	1.2686931e-01
15, 32	9.4528345e-02
16, 31	-1.2839661e-02
17, 30	-1.4347703e-01
18, 29	-2.1182909e-01
19, 27	-1.4051313e-01
20, 27	9.4601918e-02
21, 26	4.4138714e-01
22, 25	7.8587564e-01
23, 24	1.0000000e+00

2.3 Modifications to IS-95

In an attempt to improve the speech quality of IS-95, the physical layer has been modified to accommodate a higher data rate [ANS95]. On the forward link, the convolutional encoder has been modified from a rate 1/2 to a rate 3/4 by puncturing the code stream, i.e. removing symbols that would only increase redundancy. The reverse channel has been modified by reducing the 1/3 rate code to a 1/2 rate code. Consequently, the data rates possible are now increased by 50%. The new speech codec developed by QUALCOMM has been modified to take advantage of the increased data rates by increasing the quantization of the speech and improving voice activity detection. The increased data rate makes the CDMA standard more attractive to data users. In this thesis, however, we focus primarily on the 9600 bps data rate.

2.4 Chapter Summary

The forward and reverse traffic channels for IS-95 use two distinct forms of modulation and coding. The reverse channel is the limiting factor in this CDMA system. To minimize power consumption at the mobile, no pilot channel is used to maintain a coherent reference. This requires the base station receiver to use a noncoherent detection method for demodulation. Orthogonal modulation is an extremely powerful technique that has extremely good energy efficiency in exchange for poor bandwidth efficiency. Kim in [Kim92] has developed results for the performance of 64-ary orthogonal modulation in conjunction with noncoherent reception and direct sequence spreading in a multiple access interference only scenario. Jalloul and Holtzman in [Jal94] continued the same analysis for multipath fading channels. The combination of convolutional coding and orthogonal modulation forms a concatenated code that further improves performance. Analysis of 64-ary orthogonal modulation combined with convolutional coding can be found in [Lin92].

Noncoherent detection is a large liability in a cellular system. This noncoherence results in a mixing product of the I and Q channels at the receiver. The I and Q PN sequences help somewhat in this regard because the cross-correlation between the two signature sequences should be low.

Chapter 3

Receiver Structures

Receivers can be broken down into several components, each representing a portion of the path the signal must traverse. For the purposes of this work, the receiver may be broken down into two critical areas: the analog front end and the digital demodulation structure. The analog front end includes the amplifiers, analog filters, and local oscillators (LOs), automatic gain control (AGC), and the analog to digital converter (ADC). The digital demodulation structure would contain the correlators, digital filters, and decoders that would attempt to estimate the data transmitted across the channel. Some idealizations will be assumed for the analog receiver front end, since simulation of the front end would be impractical. One of the critical issues that will be included is the quantization that occurs in the ADC. Quantization effects in CDMA are a critical issue in the design of hardware because of the despreading operation that correlates the received signal increasing its SNR by the processing gain. If the ADC is placed prior to despreading, the processing gain may overcome some of the quantization error introduced. Several assumptions are made for the digital portion of the receiver, such as acquisition and perfect synchronization with the PN sequences.

3.1 Analog to Digital Conversion

There are several receiver structures that may be used to receive a radio frequency (RF) signal. The superheterodyne receiver (Figure 3.8) has been used conventionally to first downconvert the signal to an intermediate frequency (IF) (or multiple IFs) and then produce a baseband signal. Once at baseband, an ADC is used to generate digital samples and then the demodulation begins. As digital processing has become less costly, newer variations of this architecture have been suggested in order to reduce complexity and cost of designs which rely on analog components. One possibility, the direct downconversion receiver, would take the RF signal and mix it immediately to baseband. Difficulties with this type of implementation are the design of high gain RF amplifiers and preventing LO radiation. A technique that is becoming more preva-

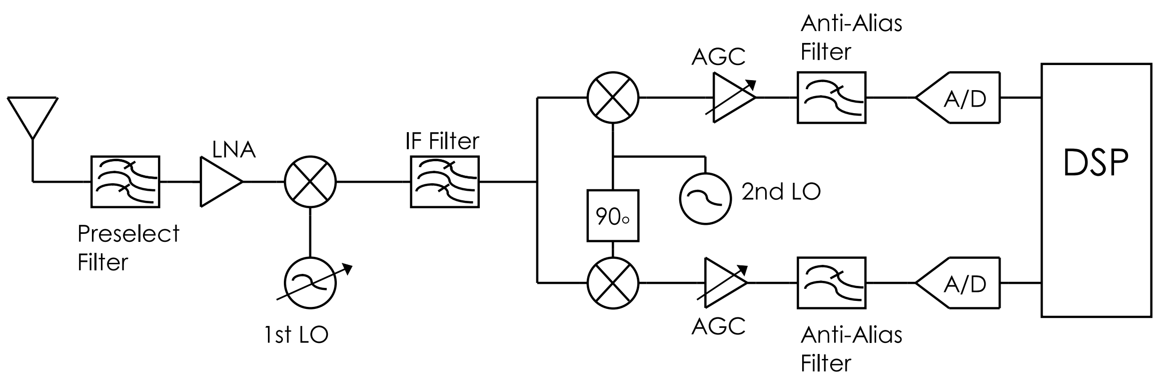

Figure 3.8: Superheterodyne Receiver

lent in base station hardware is IF sampling. Instead of downcoverting to baseband and then sampling the signal at the Nyquist rate of the IF or greater, the signal is subsampled at the IF frequency. The Nyquist sampling criterion is still met so long as the subsampling is performed at twice the information bandwidth of the signal. This technique is popular with FDMA cellular base stations, since there is no need to have a variable LO (we have a fixed IF) or even to have multiple front ends; the entire cellular band is IF subsampled [Hal96]. Digital filtering techniques are then used to select the desired channels. Problems do exist with this type of wideband receiver. Since all the users are being passed by a wideband analog IF filter, the stronger users will occupy more of the dynamic range of the ADC which will reduce the signal to noise ratio (SNR) of a weaker desired user. A CDMA system, however, does not require multiple frequency bands to be digitally converted. Since all users occupy the same frequency band it may be more practical to simply downconvert the signal to baseband and then use an ADC. Received power fluctuations are expected so power control is implemented in most CDMA systems to account for unusually strong or weak users. IS-95 requires dual-mode compatibility with the analog AMPS standard, so the system engineer must make a selection between a wideband receiver to accomodate AMPS users and CDMA users, or two separate receivers for the two classes of users.

The only modelling used for the front end of the receiver in this work is the ADC. It is assumed that the signal has already been decomposed into quadrature signals and is now at baseband. Several types of ADC and AGC are used in practice; many of the design choices are based on available sampling rate, resolution, power consumption, and cost. All these factors are difficult to account for in any analytic techniques or simulation methods involved in a large-scale architecture. Instead, we will only survey the methods found in practice and present some factors that will be useful in choosing a front end architecture.

The AGC is an analog device that scales or limits the received signal to a value that will not overload the ADC. In the case of pulse-shaped signals, such as IS-95 and IS-54, the AGC must track the signal and scale the voltage level of the signal continuously. Dynamic AGC's require feedback from either the digital portion of the circuit to properly scale the received signal or an analog power measurement circuit. Certain modulation schemes, such as Gaussian minimum shift keying (GMSK) used in Digital European Cordless Telephone (DECT), are constant envelope so the received signal can be passed through a limiting strip with little damage to the signal fidelity. Limiter circuits are relatively simple circuits when compared to dynamic AGC's, making receiver design a much easier task.

In its simplest form, an ADC takes an analog signal and converts it to a digital representation. The conventional model for an ADC consists of a sampler and a quantizer as shown in Figure 3.9. The sampling operation must meet or exceed Nyquist's criterion of sampling the signal at twice the information bandwidth of the received signal. There are two elements of sampling that may affect the SNR: finite

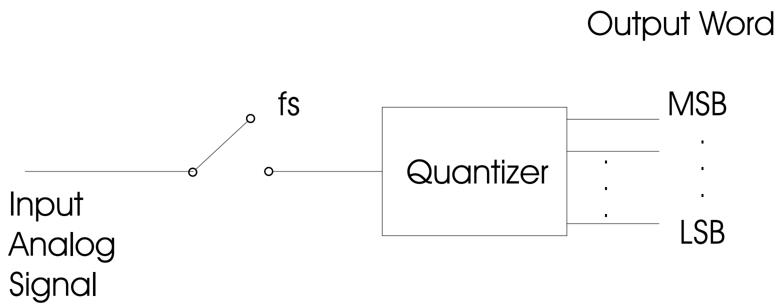

Figure 3.9: Analog to Digital Converter

sampling aperture and aperture jitter. Finite sampling aperture is the inability of the sampler to generate the ideal impulse for sampling. The sampling pulses take on a rectangular shape which results in a sinc(x) waveform in the frequency domain. The lower sidelobes of the sinc(x) waveform will reduce the power of the sampling images causing a drop in the expected SNR. Aperture jitter reflects small timing errors in the sampling instants. This error is a function of the sampling frequency and is small for most applications. The quantizer maps the input voltage to one of multiple output levels. The transfer function of the quantizer is shown in Figure 3.10. The full scale dynamic range of the quantizer is the value of $\pm$ V. The AGC is assumed to have limited the signal voltage to the full scale range to prevent clipping. Most quantizers in a wireless environment are designed to have uniform quantization levels in the full scale range of the device because of the difficulty in generalizing the received signal probability density function (pdf) and applying the Lloyd-Max algorithm to determine optimum nonuniform quantization levels [Max60] [Llo82]. In a CDMA signal environment, it may be possible to apply the central limit theorem and consider the received signal Gaussian. The difficulty then becomes estimating the mean and variance of the signal and optimally adjusting the quantization levels while receiving the signal.

Typically, an ADC's performance is quantified by the following factors: SNR, spurious free dynamic range (SFDR), intermodulation products, and power consumption. For uniform quantizers, the SNR for a general input signal is given by [Azi96]

$$SNR = 10log_{10}\left(\frac{\sigma_x^2}{V^2}\right) + 4.77 + 6.02N(dB) \tag{3.8}$$

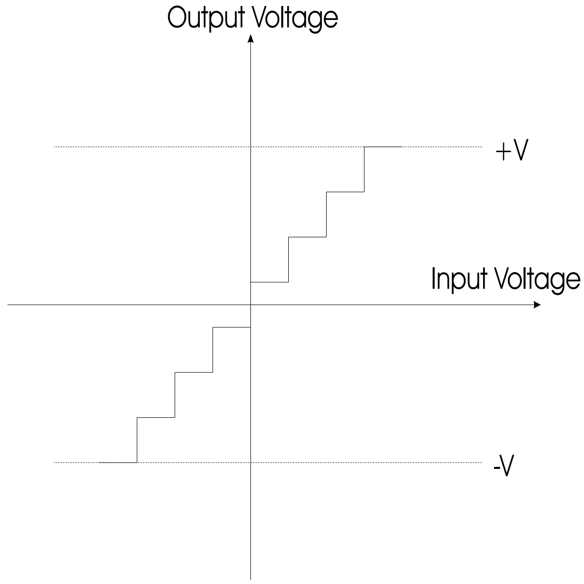

Figure 3.10: Transfer function of a uniform quantizer

where σ_x^2 is the variance of the signal and N is the number of bits. To improve the SNR, it is necessary to increase the number of bits (apparent from Equation (3.8). However, by oversampling the signal we may spread out the noise in the signal so that post-filtering will reduce the integrated noise power in the signal bandwidth. This oversampling technique yields an SNR increase of 3 dB for every octave of over-sampling above the Nyquist rate. The other factors important in ADC performance are not readily derived from even a basic model. These are more often simulated or measured for a particular structure. Clipping can occur when the signal exceeds the full scale range of the ADC which introduces spurious components. This effect is controlled by the choice of AGC. Nonlinearities in the quantizer transfer function also introduce harmonics. In this simulation, we will only deal with the number of bits of resolution in a uniform quantizer with the AGC scaling the signal to the maximum input voltage over a frame duration. The remaining sections deal with the operations performed after quantized samples with correct timing have been generated.

3.2 Single User Receivers

The single user receiver is the basic receiver design for a DS/CDMA system. Each user that the base station expects to handle has a digital receiver dedicated to the signal with a synchronous copy of the desired user's PN sequence. Other users are treated as interference, e.g., multiple access interference (MAI). The single user receiver is the simplest in complexity but its performance suffers in the presence of large MAI.

3.2.1 Correlation Receiver

A block diagram of a correlation receiver was shown in Figure 2.2. Figure 3.11 is a diagram of a correlation receiver for K users. While correlation receivers are optimum in the AWGN channel, they have several vulnerabilities. The most important facet in a wireless environment is the resistance to multipath. Here correlation receivers treat multipath reflections as noise degrading the signal because the multipath components are decorrelated with the primary component. DS/SS systems are more resistant to multipath than other modulation types because of the low autocorrelation value of PN sequences. Correlation receiver performance also degrades substantially in a CDMA environment when interfering signals have a larger signal energy than the desired signal, i.e., near-far problem. Near-far effects will always be present in a wireless CDMA environment because time-varying channels make ideal power control impossible. Multipath and near-far effects have motivated the development of receiver structures that are resistant to both theses conditions.

3.2.2 RAKE Receiver

The RAKE receiver was first introduced by Price and Green [Pri58]. For frequency selective fading, the signal bandwidth is much greater than the coherence bandwidth of the channel, therefore multipath components are resolvable and independent of each other. RAKE receivers take advantage of the energy present in multipath components by correlating with each path. The RAKE receiver is composed of several fingers which each resemble a single correlator. Each of these fingers has a different time

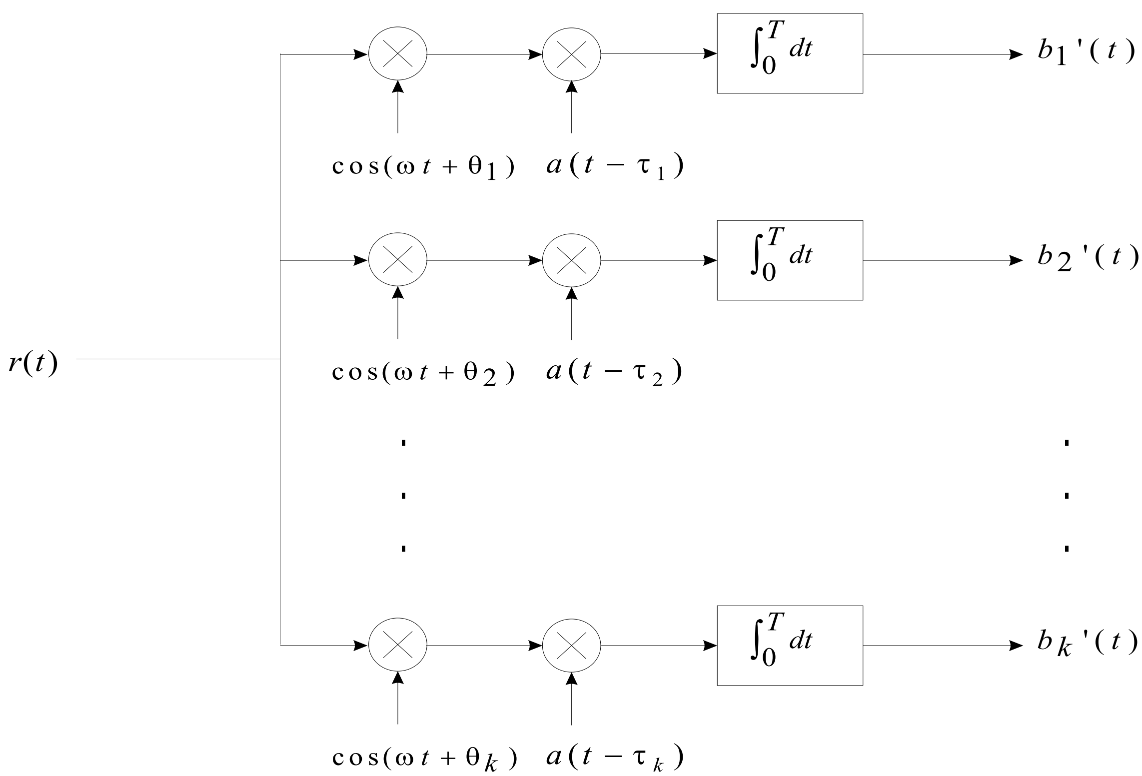

Figure 3.11: Correlation Receiver for K Users in a CDMA System

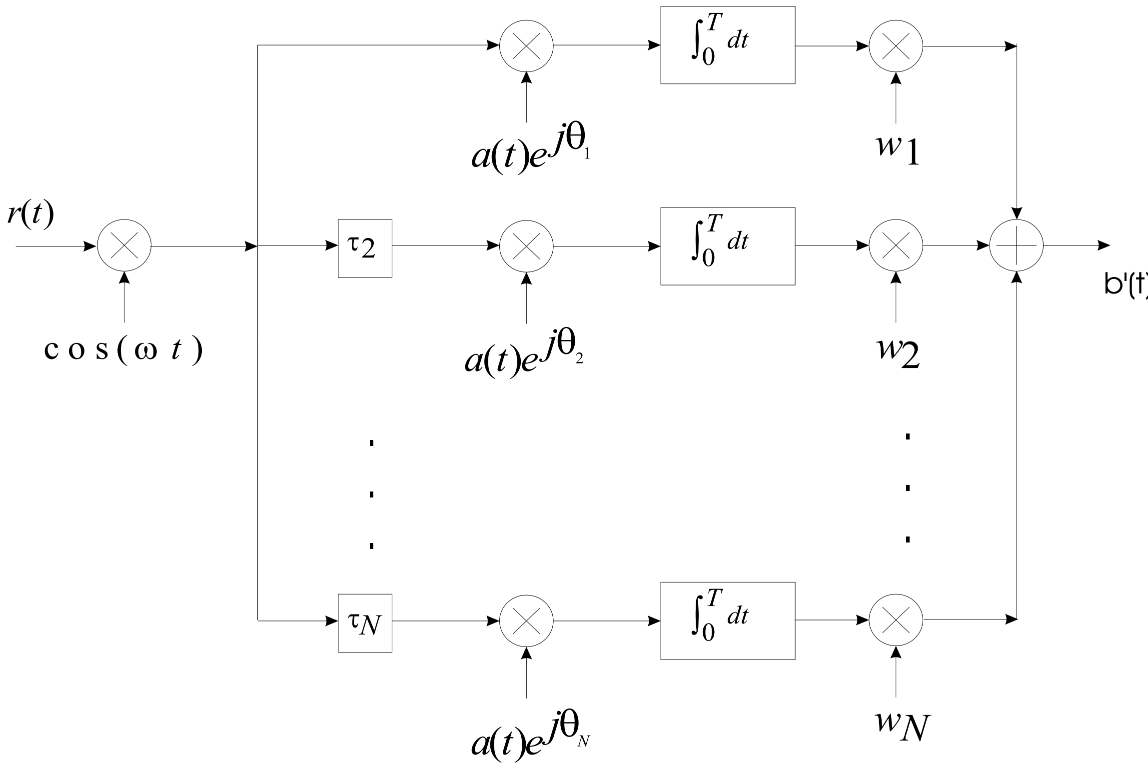

Figure 3.12: RAKE Receiver with N fingers

delay and phase rotation associated with it that is matched to a multipath component. The crosscorrelation between a spread spectrum signal and a time-delayed version should be low, therefore the RAKE receiver will be able to develop an estimate based on only the multipath component. The resolution of the RAKE (ie, the ability to resolve between separate multipaths) is dependent on the chip rate of the system. The multipath components must be separated by at least one chip period for the RAKE to resolve them. Figure 3.12 shows a generic RAKE receiver. There are several methods for choosing the weights that combine each finger [Str94]:

1) Equal Gain Combining: The weights in this scheme are chosen to all equal each other: $W_1 = W_2 = W_3 \cdots W_n = 1$. The performance of this type of combining tends to be very poor since weaker multipath components are weighted just as much as the stronger ones.

2) Selection Combining: Only one of the fingers is actually used in the decision

making. The receiver simply picks the largest of all the correlations.

$$W_i = \begin{cases} 1, & \text{if} |Z_i| = max\{|Z_1|, |Z_2|, \cdots, |Z_n|\} \\ 0, & \text{otherwise} \end{cases}$$

3) Maximal Ratio Combining: The weights are chosen so that the output SNR is maximized. This is an analytical technique that works only if we assume knowledge of the channel. That would required estimation channel parameters which can be difficult in a fast fading environment or a system that is noncoherent.

4) Empirical Rule: This method is one simple way of approximately implementing the maximal ratio combining method. The weights are chosen such that $W_i = |Z_i|$. The SNR is improved by increasing the contribution of the stronger components while reducing the that of the weaker components. Simulation shows that this technique works fairly well in practice.

After correlating each finger and multiplying by the appropriate weight, the resulting statistics are combined to form a single decision statistic. In order to constructively add these components, the phase must be known. Ideally, we would choose a sufficient number of fingers to demodulate all multipath components. RAKE receivers provide time diversity for a wideband system, taking advantage of the autocorrelation properties of PN sequences. Practically speaking, most receivers are limited to just a few fingers, typically three to five. The scheme used in this simulation is the empirical rule combining. The performance of a RAKE receiver will actually worsen in the case where there are fewer multipaths than fingers so typically a threshold is set for determining when the fingers of the RAKE are active or not.

Figure 3.13 shows an implementation of a noncoherent RAKE receiver for the IS-95 standard which is implemented in the simulations for this thesis. At the base station, up to four fingers in the RAKE receiver are used.

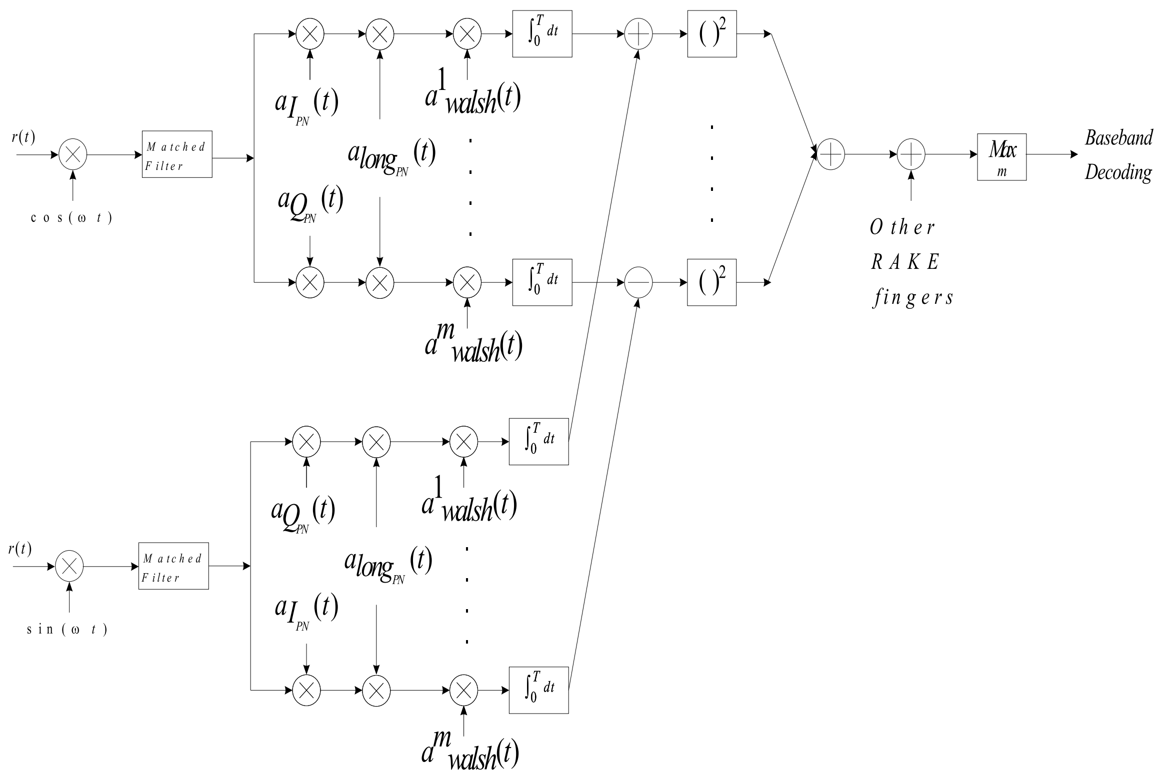

Figure 3.13: Single User Receiver for IS-95

3.3 Multiuser Receivers

Multiuser receivers are a class of receivers that use knowledge of all the PN sequences to exploit the structure of the MAI. Instead of being separately estimated, as in a single user detection, the users are jointly detected for their mutual benefit. Multiuser detection in CDMA was introduced in [Sch79]. A multiuser system with interference cancellation was introduced in [Koh83]. For the AWGN channel, Verdu presented an optimum multiuser receiver [Ver86]. This optimum technique however requires *a priori* knowledge of the signal amplitudes and phases and involves a high degree of computational complexity. Extensive work has followed developing suboptimum multiuser detection and interference cancellation schemes in hopes of reducing complexity while maintaining good performance. This work tends to be a mix of analytical and simulation results because of the inherent difficulty analyzing multiuser receivers.

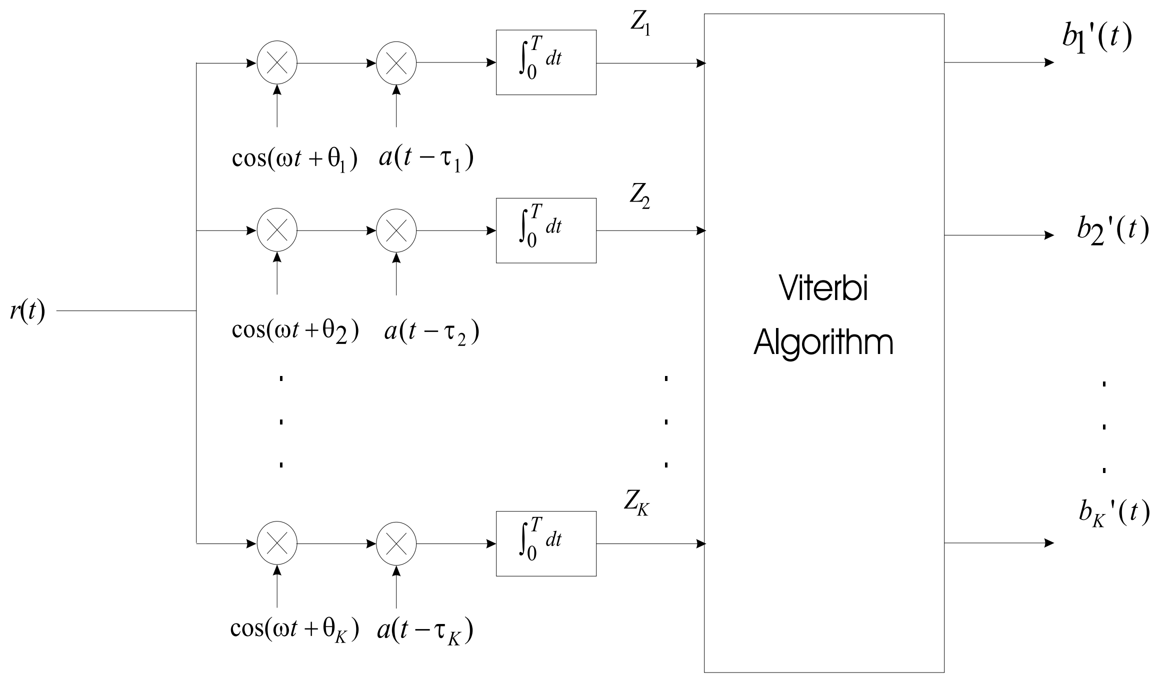

Figure 3.14: Optimum Multiuser Receiver

The focus of this section, however, will be mainly on the successive and parallel interference cancellation schemes which have reasonable complexity for handling at base stations.

The optimum receiver presented in [Ver86] is shown in Figure 3.14. The optimum receiver consists of a bank of K single user receivers whose outputs are then fed to a maximum likelihood Viterbi decision algorithm. The optimum receiver requires *a priori* knowledge of the signal amplitudes and phases in order to derive a maximum decision statistic in the decoder. This decoder will introduce a considerable delay to achieve optimality and will have complexity on the order of 2^K for every bit decision required. However, it was shown that the receiver is near-far resistant regardless of received power levels with significant improvement over the single user receiver. Because 2^K computations are needed for every user's bit decisions, it should be obvious that for a high capacity system the receiver will not be capable of sustaining such a load.

Several different types of sub-optimum receivers have been studied in the literature.

A decorrelating receiver was presented in [Lup89]. The decorrelating receiver consists of K single user receivers. The receiver generates decision statistics for the K users and also creates a matrix of crosscorrelations of the users' PN sequences. A vector of the correlator decision statistics is multiplied by the inverse of the crosscorrelation matrix. Bit decisions are then made on the resulting vector. The decorrelation receiver performs well at high SNR because the MAI is eliminated by the inversion of the crosscorrelations. Unfortunately, as with any matrix inversion, the operation is very computationally intensive and numerically sensitive. Decorrelation also performs poorly at a lower range of SNR's because the noise is multiplied by the inverse crosscorrelation matrix.

Modifications of the optimum receiver represent another class of sub-optimum receivers. Most of these replace the Viterbi ML algorithm with a reduced complexity algorithm. Some variations include sequential decoding, minimum mean squared error (MMSE) detection, weighted least square (WLS), and decision feedback equalizers (DFE) [Due93]. Other sub-optimum receivers use interference cancellation to remove the interfering signals during detection. In an interference cancellation scheme, the signal is first passed through a bank of correlators and then each user's signal is reconstructed and cancelled from the received signal. This process may be repeated for multiple stages. The effectiveness of the cancellation is a function of the quality of the estimation and reconstruction. Performance of interference cancellation is tied to the signal parameters and whether they are known. Figure 3.15 is a block diagram of such a structure. Several implementations of interference cancellation exist, but the two covered in this work are successive and parallel interference cancellation.

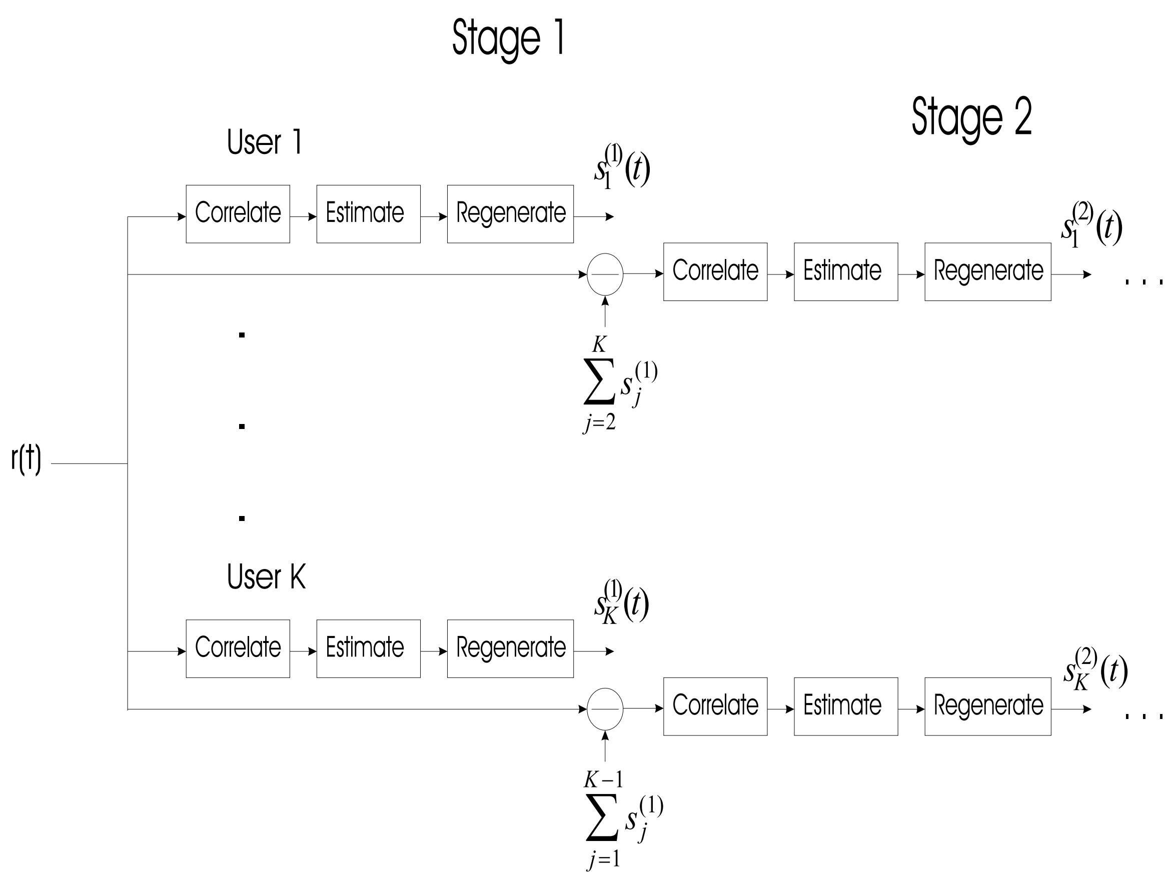

Figure 3.15: Multiuser Multistage Interference Cancellation Receiver

3.4 Successive Interference Cancellation

The successive interference cancellation scheme uses the algorithm shown in Figure 3.16. At each iteration of the scheme, all the user's signals are estimated. The signal with the largest power is then regenerated and subtracted from the buffered received signal. The remaining signals are now re-estimated and a new largest user is selected. The process will continue until all the users' signals have been recovered or the maximum allowable number of cancellations is reached. The decision statistic for the kth user after users 1 through $k-1$ have been removed is

$$z^{(k)} = \int_0^T \hat{r}^{(k)}(t) a_k(t-\tau_k) dt \tag{3.9}$$

where $\hat{r}^{(k)}(t)$ is the received signal after users 0 through $k-1$ have been cancelled, given by

$$\hat{r}^{(k)}(t) = r(t) - \frac{2}{T} \sum_{j=1}^{k-1} z^{(k)} a_k(t-\tau_k) cos(\omega t + \theta_k) \tag{3.10}$$

Successive interference cancellation has been shown to be very robust to imperfect power control in a DS/CDMA system [Pat94]. This comes from the strongest users (and thus best estimated) all having been cancelled from the received waveform. Successive interference cancellation is considered one of the simplest forms of interference cancellation because of the single stage of cancellation. However, the processor performing the cancellation must perform all the cancellations while maintaining the necessary data rate.

Figure 3.17 is the block diagram of successive interference cancellation for the DS-BPSK system introduced in Chapter 2. This will be expanded later to include the more complicated issues involved in a cellular CDMA system.

Estimating the power of the user is fairly straightforward in a coherent DS-BPSK system. Here, we have the knowledge of the amplitudes and phases of the user's signal and can reconstruct a good estimate of the user's signal for cancellation. Noncoherent reception forces the receiver to use the output of the correlators as the only statistics for regenerating the signal.

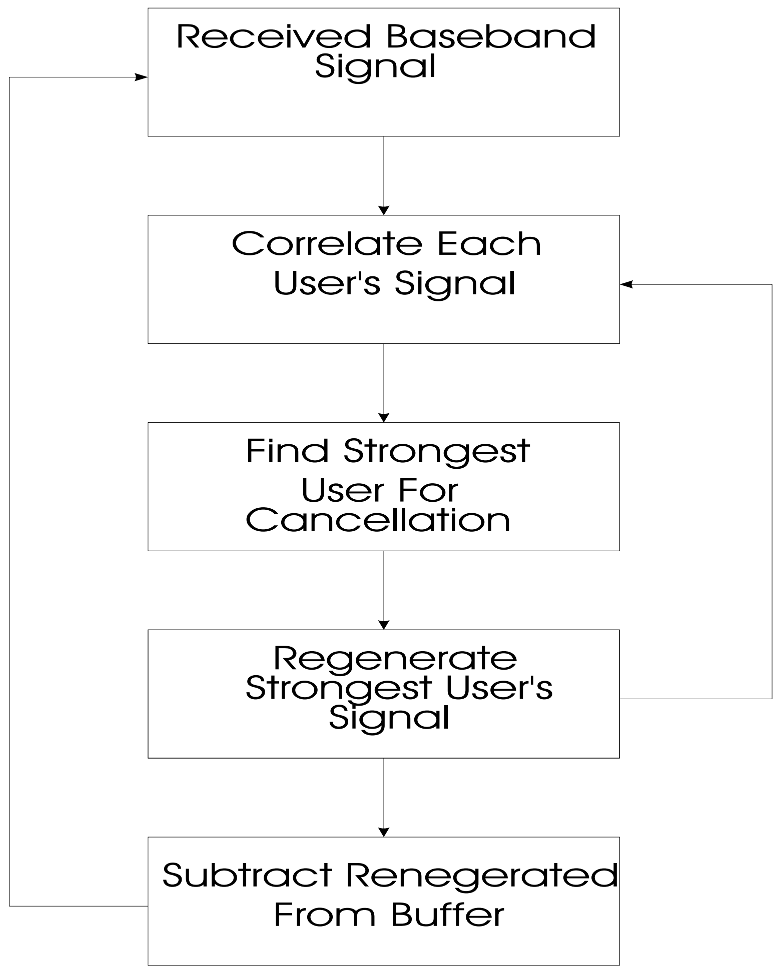

Figure 3.16: Algorithm for Successive Interference Cancellation

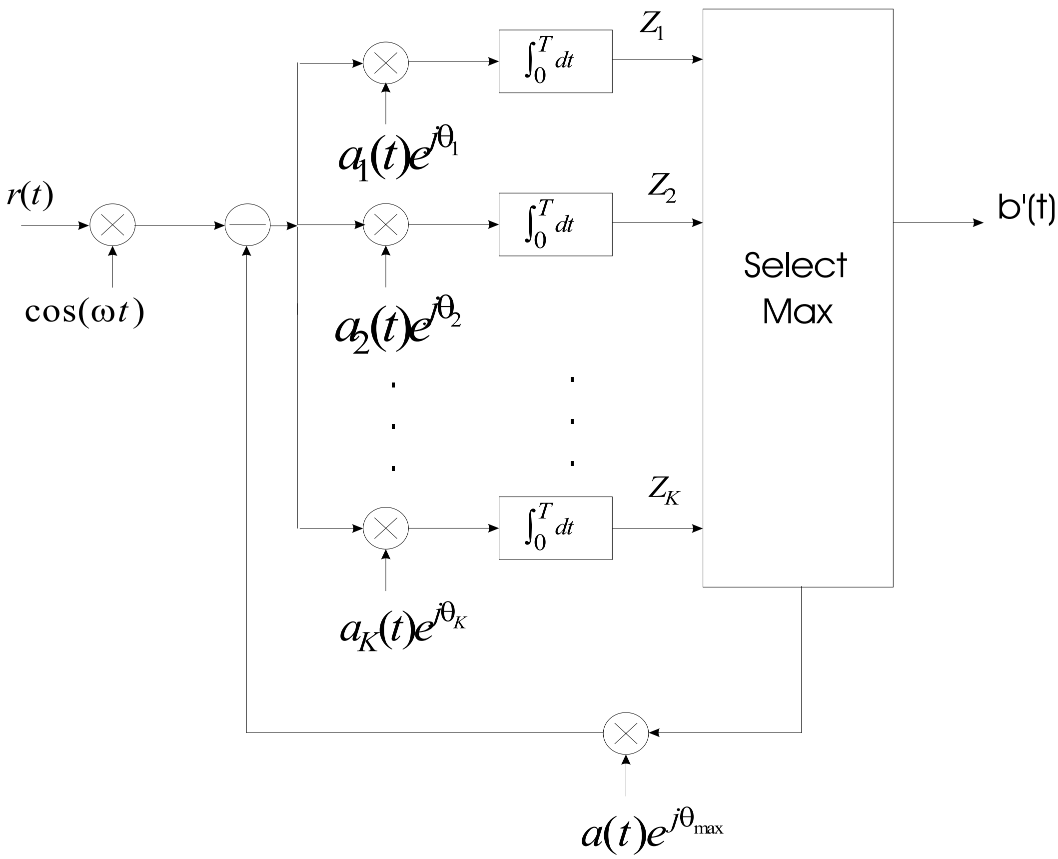

Figure 3.17: Successive IC for BPSK modulation

3.5 Parallel Interference Cancellation

A popular method for interference cancellation was presented by Varanasi and Aazhang [Var90]. The model for parallel interference cancellation in a DS/SS-BPSK system is shown in Figure 3.18. The first stage of this receiver consists of a bank of correlators that are used to generate decision statistics for every bit i for the kth user, $Z_{k,i}$. These decision statistics then generate the estimate of the user's signal, $\hat{s}^{(k)}$. In the next stage, a new estimate for the kth user is formed by taking the received signal and subtracting from it all $\hat{s}^{(j)}$ such that $j = 1, \cdots, N; j \neq k$. This process may be repeated for an arbitrary number of stages. Consequently, the received signal at stage s for the kth user's signal path is

$$r_k^{(s)}(t) = r(t) - \sum_{\substack{j=1 \\ j \neq k}}^{K} \hat{s}_k^{(s)}(t - \tau_k)$$

The decision statistic for the ith bit of user k after s stages of interference cancellation is then

$$Z_{k,i} = \int_{iT+\tau_k}^{(i+1)T+\tau_k} r_k^{(s)}(t) a_k(t - \tau_k) cos(\omega_c t + \phi_k) dt.$$

Kaul [Kau95] has done extensive work with parallel interference cancellation including developing analytic bounds and demonstrating an optimal number of stages. It was shown that three to four stages of interference cancellation approach the lower bound for the case of an infinite stages. Even one stage of cancellation seemed to do well, showing promise of minimizing complexity while still improving performance. Yang [Yan95] combined convolutional coding with parallel interference cancellation. Buehrer [Bue96] compared several techniques to that of parallel interference cancellation and also quantified the number of operations required for each method. The number of operations for parallel interference cancellation is greater than for successive cancellation but operation in the base station means that more processing power may be used. Individual processors may be used for receiving and regenerating users' signals when compared to the single processor that must be used for successive interference cancellation.

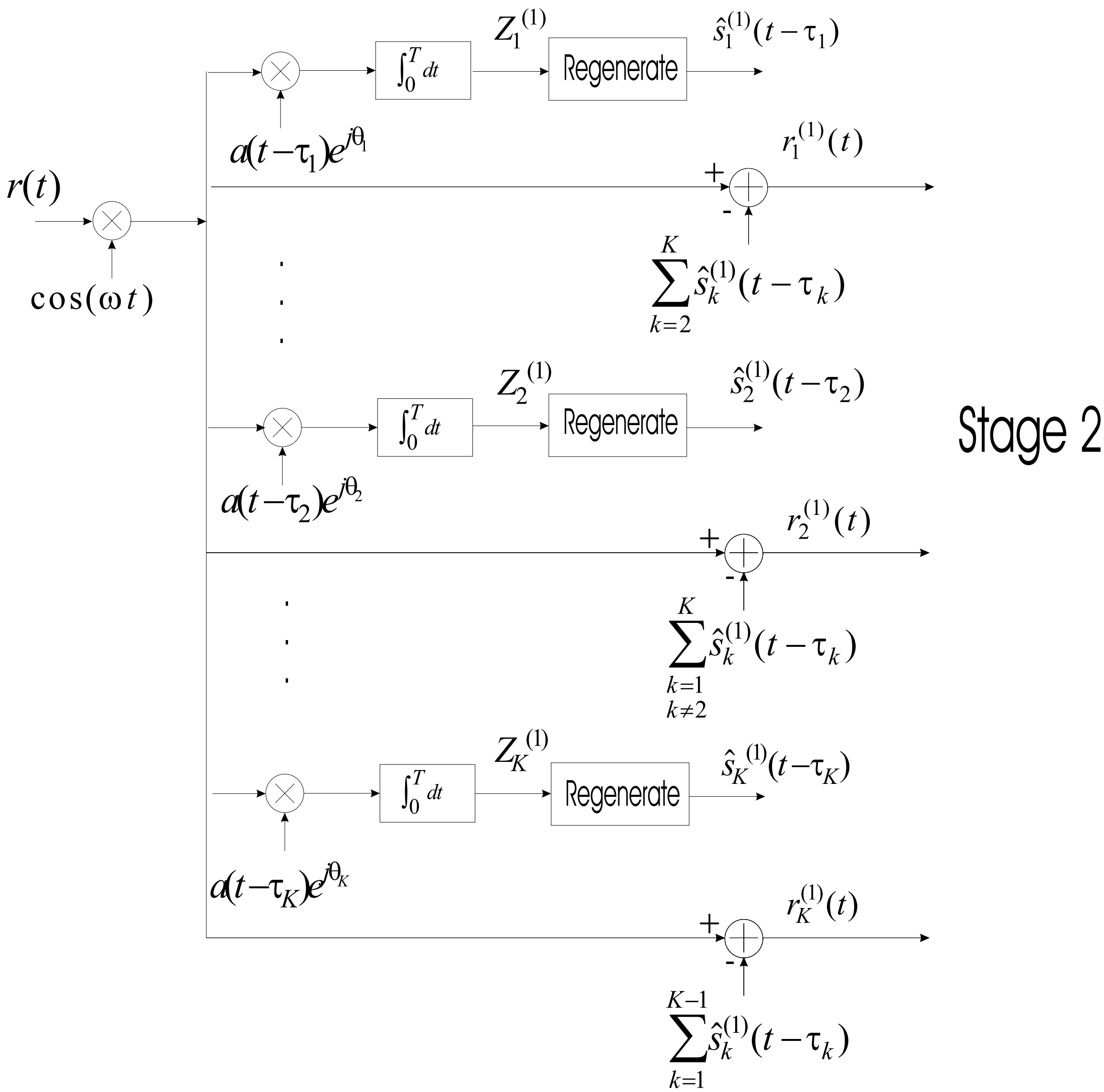

Figure 3.18: Block diagram of of first stage in parallel IC scheme for BPSK modulation

3.6 Chapter Summary

Several forms of receiver structures have been presented in this chapter. Literature exists that gives analytical and simulation methods for the analysis of receiver structures in CDMA. Most of this literature has used the BPSK-DS/SS modulation method as the core of the work, because of its reduction of complexity in analysis and the minimal computation required in simulation. Work has been presented recently that has compared the performance of different interference cancellation implementations [Due95] [Bue96]. Little work has been done, however, in the area of quantization effects in a system. Some analytical work for the performance of and ADC combined with a CDMA system resembling IS-95 was presented by Gaudenzi [Gau94]. Two CDMA systems, one with orthogonal codes and the other without, were used as system models. One distinct feature of the analysis was the assumption that the matched filtering operation would be performed by analog circuitry. This paper also used simulations to present some values of threshold levels for the AGC system.

Chapter 4

Simulation of the System

In this chapter, we present the computer model for the IS-95 reverse channel system. The mathematical representation for the simulation is given, along with the techniques used to simulate each component. We also present the models for several implementations of multistage interference cancellation for a cellular CDMA system. Successive and parallel interference cancellation schemes are developed for the IS-95 standard. The software written for these simulations allows for variation in the type of decisions made by the Viterbi decoder. Simulations were run for hard and soft decisions. In addition to these cases, quantization effects were also simulated. A variable number of bits in a quantizer was used to determine the performance effects in a standard CDMA receiver and the interference cancellation schemes studied. The simulation uses the AWGN channel model as a baseline for comparison. The multipath phenomenon is also used with a unique channel impulse response for each user present.

4.1 Baseband Representation

Signals in the wireless are propagated by modulating an RF carrier. Simulation of a system operating in the RF band would require millions of samples to represent a single symbol. While an RF level simulation would simulate the system precisely, it is very advantageous to simulate only the information signal and not the carrier frequency. Simulations are commonly performed at the baseband level, simulating only the information signal not the carrier signal. Any bandpass signal can be expressed in the form [Cou93]

$$s(t) = a(t)cos[2\pi f_c t + \theta(t)] \tag{4.11}$$

where $a(t)$ is the amplitude of the signal, $\theta(t)$ is the phase of the signal, and f_c is the carrier frequency. Using trigonometric identities we may expand this expression to the form

$$\begin{aligned} s(t) &= a(t)cos(\theta(t))cos(2\pi f_c t) - a(t)sin(\theta(t))sin(2\pi f_c t) \\ &= a_I(t)cos(2\pi f_c t) - a_Q(t)sin(2\pi f_c t) \end{aligned} \tag{4.12}$$

where $a_I(t)$ and $a_Q(t)$ are called the in-phase and quadrature components, respectively, and are defined as

$$a_I(t) = a(t)cos(\theta(t)) \tag{4.13}$$

$$a_Q(t) = a(t)sin(\theta(t)) \tag{4.14}$$

We define the complex envelope as

$$\tilde{a}(t) = a_I(t) + j a_Q(t) \tag{4.15}$$

This complex envelope representation is independent of the carrier frequency f_c. This may be converted back to a bandpass representation (Equation 4.12) by the following operation

$$s(t) = Real\{\tilde{a}(t)e^{j2\pi f_c t}\} \tag{4.16}$$

Partitioning the signal into in-phase (I) and quadrature(Q) channels eliminates any need to simulate the high frequency carrier while maintaining the correct mathematical model for the signal. The complex envelope representation will be used throughout this work to explain the simulations models used.

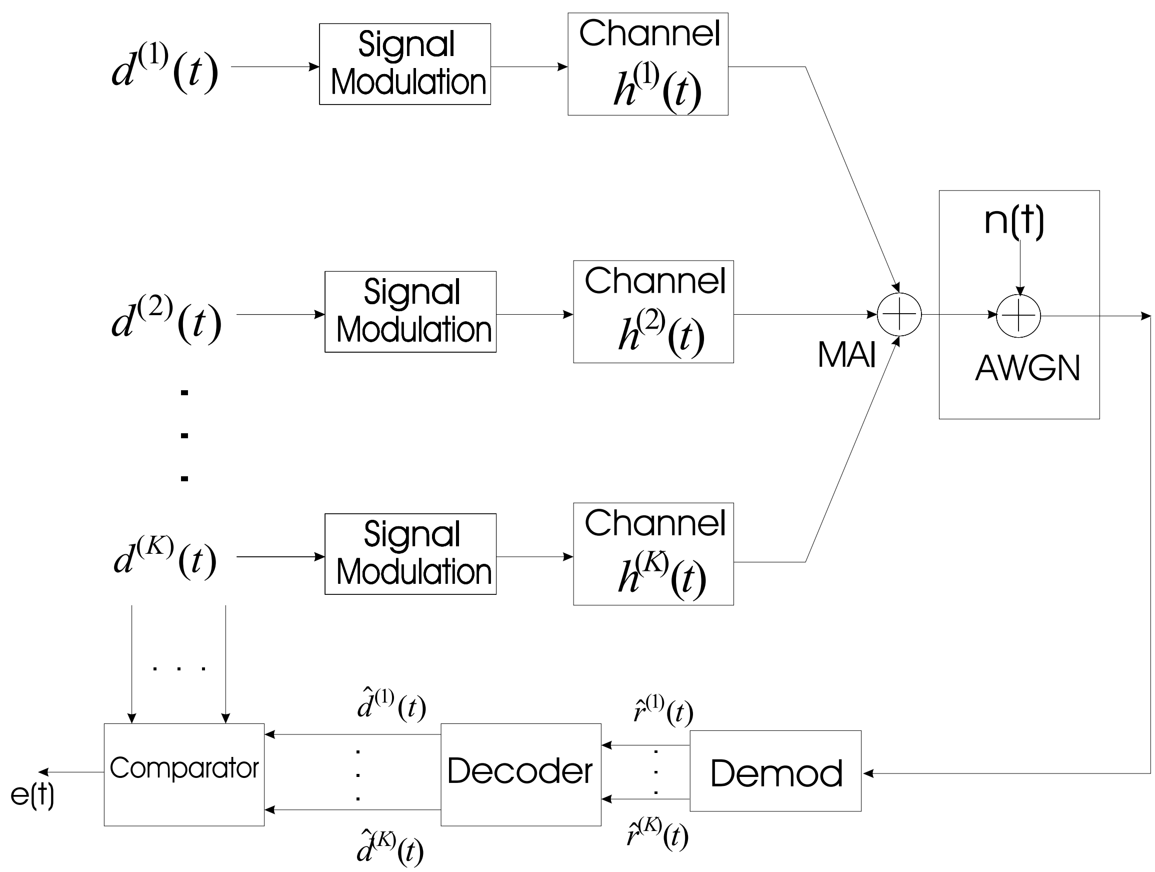

Figure 4.19: Block Diagram of Simulation Model

4.2 Generation of Bit Stream

Each incoming bit stream, $d^{(k)}(t)$, as shown in Figure 4.19, consists of a series of pseudorandom binary values. These binary numbers have an equal probability of being a 1 or 0. Several methods exist for generating uniformly distributed deviates. The difficulty lies in choosing a technique that has a very large period so as to approximate randomness as much as possible. A modified L'Ecuyer congruential generator with a period greater than 2^{18} [Pre92] is used for the generation of random deviates. A separate stream is generated for each user, which is then stored for comparison with the output bit stream, $d'^{(k)}(t)$. The software developed for this simulation allows for bit error rate (BER) comparison and frame error rate (FER) comparison. Frame error rate is becoming a popular method for measuring the outage probability in voice and packet-based systems. The rate of damaged voice packets is often a better indicator of the received speech quality than a given bit error rate. Recent simulation work of IS-95 has focused solely on FER comparisons [Pad94]. There are some disadvantages to FER estimation. To achieve good FER estimates a large number of frames must be simulated which will increase the simulation time by at least two orders of magnitude. When errors are randomly distributed the FER is yields no more information than the BER since bits bits may be treated as a series of Bernouilli trials.

4.3 Signal Modulation

As explained in Section 2.2, the signal is encoded and interleaved prior to orthogonal modulation. The data bit stream, $d^{(k)}(t)$, is sent to the convolutional encoder for encoding and the resulting code symbols, $c^{(k)}(t)$ are interleaved. For the orthogonal modulation and long code spreading, the symbols are still represented by 1's and 0's. The orthogonal modulation replaces every six code symbols with 64 modulation symbols, $c^{(k)}_{Walsh}(t)$. Modulo-2 addition is used to spread the signal with the long code PN sequence, $a^{(k)}_{longPN}(t)$,

$$c^{(k)}_{longPN}(t) = c^{(k)}_{Walsh}(t) \oplus a^{(k)}_{longPN}(t) \tag{4.17}$$

resulting in a new sequence of symbols, $c^{(k)}_{longPN}(t)$, which are now at 1.2288 Mcps. To account for the higher rate, the array storing the symbols is expanded at each operation.

Prior to pilot PN spreading, the symbol array is copied to I and Q channels which are then added to the pilot PN sequences, $a^{(k)}_{Ipilot}(t)$ and $a^{(k)}_{Qpilot}(t)$, by modulo-2 addition

$$
\begin{aligned}
c_I^{(k)}(t) &= c_{longPN}^{(k)}(t) \oplus a_{Ipilot}^{(k)}(t) && (4.18)\\
c_Q^{(k)}(t) &= c_{longPN}^{(k)}(t) \oplus a_{Qpilot}^{(k)}(t) && (4.19)
\end{aligned}
$$

At this point, the symbols are sampled at the desired sampling rate. For all the presented results (Chapter 5), the sampling rate was fixed at four samples per PN chip. The samples are separated by 203.45 ns. This conveniently matches the rate of the filter coefficients of the baseband filters which eliminates the need for interpolating the filter coefficients. Each symbol is converted to an impulse with value 1 or -1 followed by three zeroes. We do, however, demonstrate a case where the sampling rate has been increased to eight samples per chip. This will demonstrate whether artifacts from aliasing are present with a sampling rate of four samples per chip. Representing each symbol with an impulse instead of a rectangular pulse saves the convolution operation with an inverse sinc(x) pulse prior to pulse shaping. The Q channel is delayed by 2 samples (1/2 PN chip) and then I and Q channels are convolved with the baseband filters, $h_{lpf}(t)$

$$
\begin{aligned}
s_I^{(k)}(t) &= c_I^{(k)}(t) * h_{lpf}(t) && (4.20)\\
s_Q^{(k)}(t) &= c_Q^{(k)}(t - \frac{T_c}{2}) * h_{lpf}(t) && (4.21)
\end{aligned}
$$

4.4 Reverse Channel Model

The reverse channel model in most early work consisted of only AWGN. In order to better emulate conditions, multipath models were added along with interference from other users. This simulation uses the multiple access interference (MAI) which typically limits the capacity of a CDMA system in addition to the standard AWGN model. Multipath channels models are also used in the simulation. Each user is generated for simulating MAI and each user sees a unique channel model. It would not be necessary to simulate each user individually if it were not for the interference cancellation schemes used. Multiuser detection implies the presence of multiple distinct signals. If only single user receivers were simulated, modelling the MAI as AWGN leads to a more efficient simulation.

4.4.1 Multipath Model

In this research, multipath propagation is used to add some realism to the performance of a channel in a true wireless environment. For a wideband signal, the channel bandwidth is considerably smaller than the signal bandwidth leading to frequency selective fading. The received signal will consist of multiple copies of the original signal attenuated and delayed in time. This leads to ISI in the time domain. While frequency selective fading describes the brief snapshot of the channel a user's signal encounters, it is necessary to define the rate of change of the channel impulse response in time. A slow fading channel occurs when the rate of change of the channel characteristics is much slower than the symbol duration of the signal. Fast fading occurs when the channel changes faster than a symbol. To minimize computation, only slow fading was considered in this simulation; the channel impulse response was maintained constant over a frame duration.

The baseband impulse response of a channel may be mathematically represented as [Gur92]

$$h(t, f) = \sum_{n} a_n exp(-j\omega\tau_n) exp(-j2\pi f_D t) \tag{4.22}$$

where a_n and τ_n are the complex gain and time delay of the nth multipath component and f_D is the Doppler shift. By assuming wide sense stationarity over a small-scale time interval then the channel impulse response may be simplified to

$$h(t) = \sum_{n=0}^{N-1} a_n exp(-j\theta_n) \delta(t - \tau_n) \tag{4.23}$$

The weights a_n are assumed to be Gaussian and θ_n is uniformly distributed in the interval $[0, 2\pi)$. To compare multipath channels, mean excess delay and rms delay spread are often used. The mean excess delay is defined as

$$\bar{\tau} = \frac{\sum_n a_n^2 \tau_n}{\sum_n a_k^2} \tag{4.24}$$

and the rms delay spread is given by

$$\tau_{rms} = \sqrt{\frac{\sum_n a_n^2 \tau_n^2}{\sum_n a_k^2} - (\bar{\tau})^2} \tag{4.25}$$

Typical values for rms delay spread in a 910 MHz suburban and urban environment were given in [Cox72] and [Cox75]. Most of the rms delay spread was concentrated in the 200-300 ns range for suburban case with the urban rms delay spread concentrated about 1.3 μs. In some cases, the urban rms delay spread would exceed 3 μs. Rappaport showed in [Rap90] that in some cases rms delay spread may surpass 20 μs albeit these occurrences are rare. Given Equation 4.24 and some of the measured characteristics, we may formulate channel models for the system.

A tap delay line model was used to simulate the channel encountered by each user with either two or three rays in each channel profile. When only two rays are present and the power is equal in both rays, the rms delay spread is equal to one half the the time delay between the two rays.

4.4.2 Multiple Access Interference

After each user's signal is passed through the channel, all the signals are then combined. To model the reverse channel, the users are assumed to be asynchronous with a uniformly distributed delay in the range of $[0, T_c]$ relative to the first generated user, where T_c is the chip period. In the simulation, each chip is sampled four times therefore the delay may vary from 0, $1/4T_c$, $1/2T_c$, or $3/4T_c$. The I and Q signals at the receiver may then be expressed as

I channel

$$r_I(nT_s) = \sum_{k=1}^{K} (s_I^{(k)}(nT_s - \tau_k) * h_I^{(k)}(nT_s) - s_Q^{(k)}(nT_s - \tau_k) * h_Q^{(k)}(nT_s)) \tag{4.26}$$

Q channel

$$r_Q(nT_s) = \sum_{k=1}^{K}(s_I^{(k)}(nT_s-\tau_k)*h_Q^{(k)}(nT_s)+s_Q^{(k)}(nT_s-\tau_k)*h_I^{(k)}(nT_s)) \quad (4.27)$$

where K is the total number of users present, $s_I^{(k)}(nT_s)$ and $s_Q^{(k)}(nT_s)$ are the kth user's signals, $h_I^{(k)}(nT_s)$ and $h_Q^{(k)}(nT_s)$ are the kth user's channel impulse response, and τ_k is the random time delay for each user.

4.4.3 AWGN

Additive white Gaussian noise is used in this simulation. The noise, $n(t)$, is added to the transmitted signal so that the received signal is given by

$$r(t) = s(t) + n(t) \quad (4.28)$$

which for baseband complex envelope is

$$\tilde{r}(t) = \tilde{s}(t) + \tilde{n}(t) \quad (4.29)$$

where $\tilde{s}(t)$ is the signal at the input of the receiver prior to the addition of noise and $\tilde{n}(t)$ is the baseband complex envelope representation of the Gaussian noise process. the noise may be separated into in-phase, $n_I(t)$, and quadrature, $n_Q(t)$, components,

$$\tilde{n}(t) = n_I(t) + jn_Q(t) \quad (4.30)$$

To simulate a particular signal to noise ratio, the power of the signal relative to the noise power must be fixed. In this simulation the signal power is normalized to unit value and the noise power is set to a desired signal to noise ratio. A measure of signal to noise in a digital communications system is E_b/N_o, where E_b is the energy used to transmit each information bit and N_o is a funciton of the noise power spectral density. To generate an E_b/N_o value, the noise added to the signal must be scaled properly. Assuming a two-sided noise power spectral density of $N_0/2$, the noise power σ^2 is related to the occupied bandwidth,

$$\sigma^2 = \frac{N_o B_N}{2} \tag{4.31}$$

where B_N is the noise bandwidth of the receiver filter. The noise bandwidth of a filter is calculated by [Jer94]

$$B_N = \frac{\sum_{m=0}^{M} H(mT_s)^2}{(\sum_{m=0}^{M} H(mT_s))^2} \tag{4.32}$$

For the filter (see Chapter 2) used in this simulation, B_N is equal to 3.904. The noise variance is then equals

$$\sigma^2 = \frac{E_b B_N}{2(E_b/N_o)}$$

where E_b is

$$E_b = P_{out} T_{bit}$$

The output power is fixed to a nominal value of 1.0. The duration of a bit, T_{bit}, is equal to the number of samples representing each bit. Because of coding and spreading, T_{bit} is

$$T_{bit} = G_p N_s$$

where G_p is the processing gain (128 for this simulation), and N_s is the number of samples per output chip (4 for the simulation). The variance of the added noise is then

$$\sigma^2 = \frac{N_s G_p B_N}{2(E_b/N_o)} \tag{4.33}$$

which is a function of the system parameters and the desired E_b/N_o ratio. Random normal deviates (Gaussian deviates with a mean of zero and variance of 1) are first generated, x_{norm}, and then multiplied by the standard deviation. The in-phase and quadrature noise components have identical variances

$$n_I(nT_s) = \sigma x^{(i)}_{norm} \tag{4.34}$$

$$n_Q(nT_s) = \sigma x^{(i)}_{norm} \tag{4.35}$$

The noise components are then added to the signal as shown in Equation 4.29.

4.5 Receiver Implementation

Several architectures were investigated in this work. This section describes in greater detail the modelling used for each portion of the receiver. In all cases, a four finger RAKE receiver was used. Perfect timing was assumed in synchronizing with the direct and any multipath components. Synchronization with the PN sequences was also assumed.

4.5.1 Quantization

Prior to quantization, the signal must be scaled to prevent clipping in the quantizer. The optimum threshold level for clipping must be found. For a CDMA system with many active users, the probability distribution function that describes the signal environment will be Gaussian. Figure 4.20 shows the output SNR of a uniform quantizer with an input Gaussian signal of different variances.

As a conservative effort, the signal is scaled relative to the largest sampled magnitude in the frame. This will prevent clipping in the quantizer, but since the desired signal is 21 dB below the noise floor it shouldn't cause a large amount of distortion. The quantizer uniformly quantizes the received signal to the nearest of 2^N levels, where N is the number of bits specified. The number of bits used in the quantizer is varied from 1 to 8 bits. All simulations which do not specify a particular level of quantization do not use a quantizer and are instead limited by the floating point accuracy of the computer simulation. We call this the infinite quantization case.

The received signal is separated into in-phase and quadrature components prior to quantization. After quantization the I and Q channels are

$$r_I(nT_s) = \alpha_{AGC}(nT_s)r_I(t) + n_{quant}(nT_s) \quad (4.36)$$
$$r_Q(nT_s) = \alpha_{AGC}(nT_s)r_Q(t) + n_{quant}(nT_s) \quad (4.37)$$

Each sampled value is multiplied by a coefficient, $\alpha_{AGC}(nT_s)$, which represents the scaling by the AGC. The noise added by the quantizer is represented by $n_quant(nT_s)$,

$$n_{quant}(nT_s) \cong \left(\frac{2V}{2^N}\right)^2 /12 \quad (4.38)$$

where V is the full scale range of the device and N is the number of bits.

4.5.2 RAKE Receiver

The RAKE receiver used in the receiver is non-coherent but perfectly synchronized with all the multipath components present (up to a maximum of four). The RAKE has knowledge of all resolveable multipaths and only activates fingers which can track a multipath component. Therefore, there is no loss from tracking spurious components. Figure 4.21 shows the RAKE receiver structure used to generate bit estimates. For every finger of the RAKE, both I and Q channels are matched filtered and the output is sampled at the chip period. Because of the 1/2 chip offset in the Q channel, the I channel is buffered for 1/2 chip period so that the data is kept synchronized. After filtering, the signal is correlated with the corresponding pilot PN sequence and long PN sequence. In order to noncoherently combine the signals, the cross-correlation of the two signal components is found. The in-phase signal is correlated with the quadrature arm with an equivalent operation performed for the quadrature signal. Thus there are now four outputs from the correlators. The correlations for the jth modulation symbol of the kth user are equal to

$$Z_{II,j}^{(k)} = \int_{jT_{Walsh}+\tau_k}^{(j+1)T_{Walsh}+\tau_k} r_I(t)a_{IpilotPN}(t-\tau_k)a_{longPN}^{(k)}(t-\tau_k) * h_{lpf}(t)\,dt \quad (4.39)$$
$$Z_{IQ,j}^{(k)} = \int_{jT_{Walsh}+\tau_k}^{(j+1)T_{Walsh}+\tau_k} r_I(t)a_{QpilotPN}(t-\tau_k)a_{longPN}^{(k)}(t-\tau_k) * h_{lpf}(t)\,dt \quad (4.40)$$

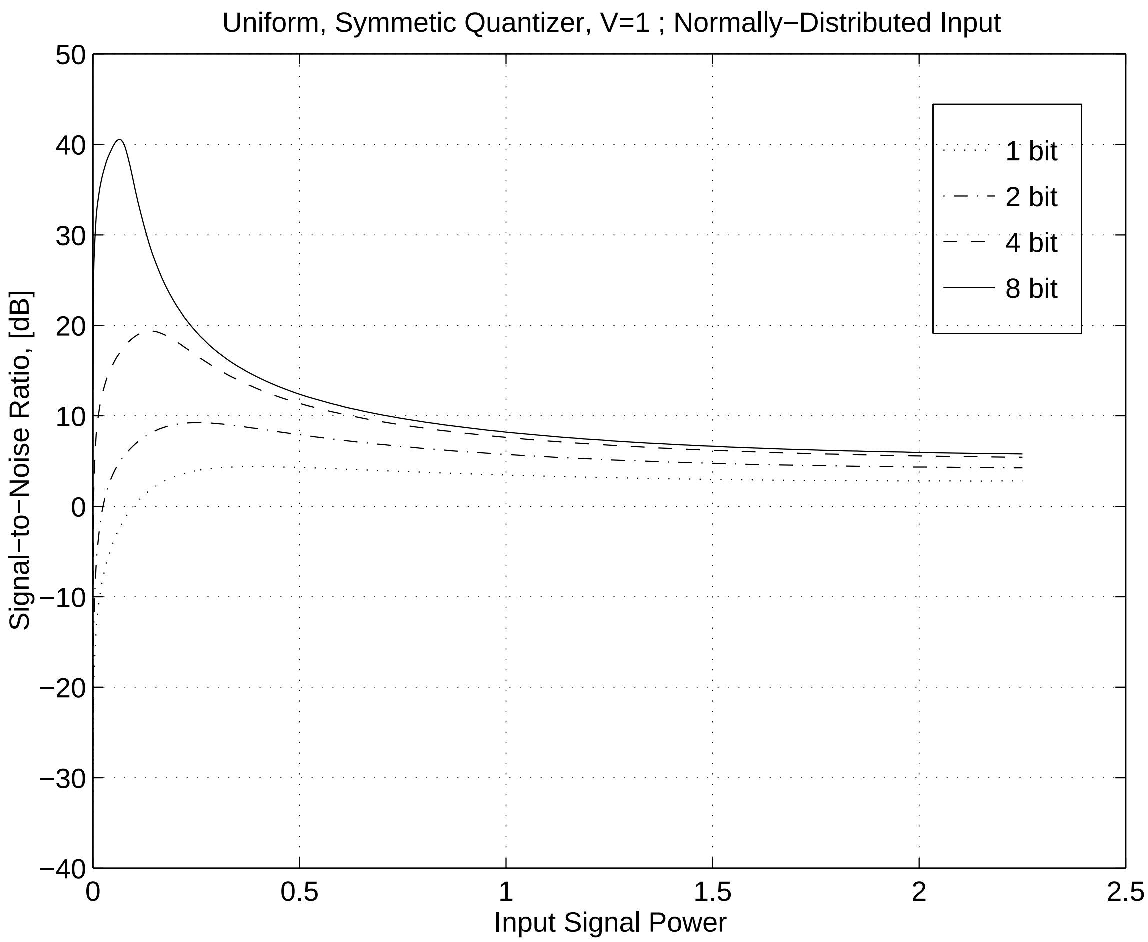

Figure 4.20: Quantization results for an input Gaussian signal with a full scale range of 1 V and b bits used in the quantizer

$$Z_{QI,j}^{(k)} = \int_{jT_{Walsh}+\tau_k}^{(j+1)T_{Walsh}+\tau_k} r_Q(t) a_{IpilotPN}(t-\tau_k) a_{longPN}^{(k)}(t-\tau_k) * h_{lpf}(t)\, dt \tag{4.41}$$

$$Z_{QQ,j}^{(k)} = \int_{jT_{Walsh}+\tau_k}^{(j+1)T_{Walsh}+\tau_k} r_Q(t) a_{QpilotPN}(t-\tau_k) a_{longPN}^{k}(t-\tau_k) * h_{lpf}(t)\, dt \tag{4.42}$$

where $a_{longPN}^{(k)}(t)$ is the long PN sequence for user k, $a_{IpilotPN}(t)$ and $a_{QpilotPN}(t)$ are the pilot PN sequences for the I and Q channel, respectively, and $h_{lpf}(t)$ is the lowpass matched filter.

Each of these outputs is then correlated with all 64 rows of the Walsh function, so that for every mth row of the Walsh function there is an output correlation. These correlations are for every ith code symbol

$$Z_{II,i,m}^{(k)} = \int_{iT_{symb}}^{(i+1)T_{symb}} Z_{II,j}^{(k)}\, a_{Walsh}^{(m)}(t)\, dt \tag{4.43}$$

$$Z_{IQ,i,m}^{(k)} = \int_{iT_{symb}}^{(i+1)T_{symb}} Z_{II,j}^{(k)}\, a_{Walsh}^{(m)}(t)\, dt \tag{4.44}$$

$$Z_{QI,i,m}^{(k)} = \int_{iT_{symb}}^{(i+1)T_{symb}} Z_{II,j}^{(k)}\, a_{Walsh}^{(m)}(t)\, dt \tag{4.45}$$

$$Z_{QQ,i,m}^{(k)} = \int_{iT_{symb}}^{(i+1)T_{symb}} Z_{II,j}^{(k)}\, a_{Walsh}^{(m)}(t)\, dt \tag{4.46}$$

where $a_{Walsh}^{(m)}(t)$ is the mth row of the Walsh function. In a system employing coherent demodulation, it would be sufficient to add the I and Q channel decision statistics, but in noncoherent systems, square-law detection is used. The correlated values are combined for noncoherent demodulation with the following equation

$$Z_{i,m}^{(k)} = (Z_{II,i,m}^{(k)} + Z_{QQ,i,m}^{(k)})^2 + (Z_{QI,i,m}^{(k)} + Z_{IQ,i,m}^{(k)})^2 \tag{4.47}$$

These equations describe the output of one set of correlators. For multipath channels, the decision statistics of all active RAKE receiver fingers would combine to form the decision statistic for the receiver. If we generalize Equation 4.47 to account for an active RAKE finger, then we have

$$Z_{i,m}^{(k,l)} = (Z_{II,i,m}^{(k,l)} + Z_{QQ,i,m}^{(k,l)})^2 + (Z_{QI,i,m}^{(k,l)} + Z_{IQ,i,m}^{(k,l)})^2 \tag{4.48}$$

where $Z_{i,m}^{(k,l)}$ is the output decision statistic of the kth user's lth RAKE finger. The outputs of the RAKE fingers are combined to form the complete decision statistic for the RAKE receiver

$$Z_{i,m}^{(k)} = \sum_{l=1}^{L} W^{(k,l)} Z_{i,m}^{(k,l)} \tag{4.49}$$

where $W^{(k,l)}$ is the weight for that finger. The maximum of the 64 decision statistics is then found for the estimate of the ith code symbol

$$Z_i^{(k)} = \underset{m}{max} [Z_{i,m}^{(k)}]; m = 1, \ldots, M \tag{4.50}$$

It is then converted to 6 estimates as described in Section 2.2.4. When only the RAKE receiver is used, i.e., no interference cancellation, these decision statistics are deinterleaved and then sent to the Viterbi decoder.

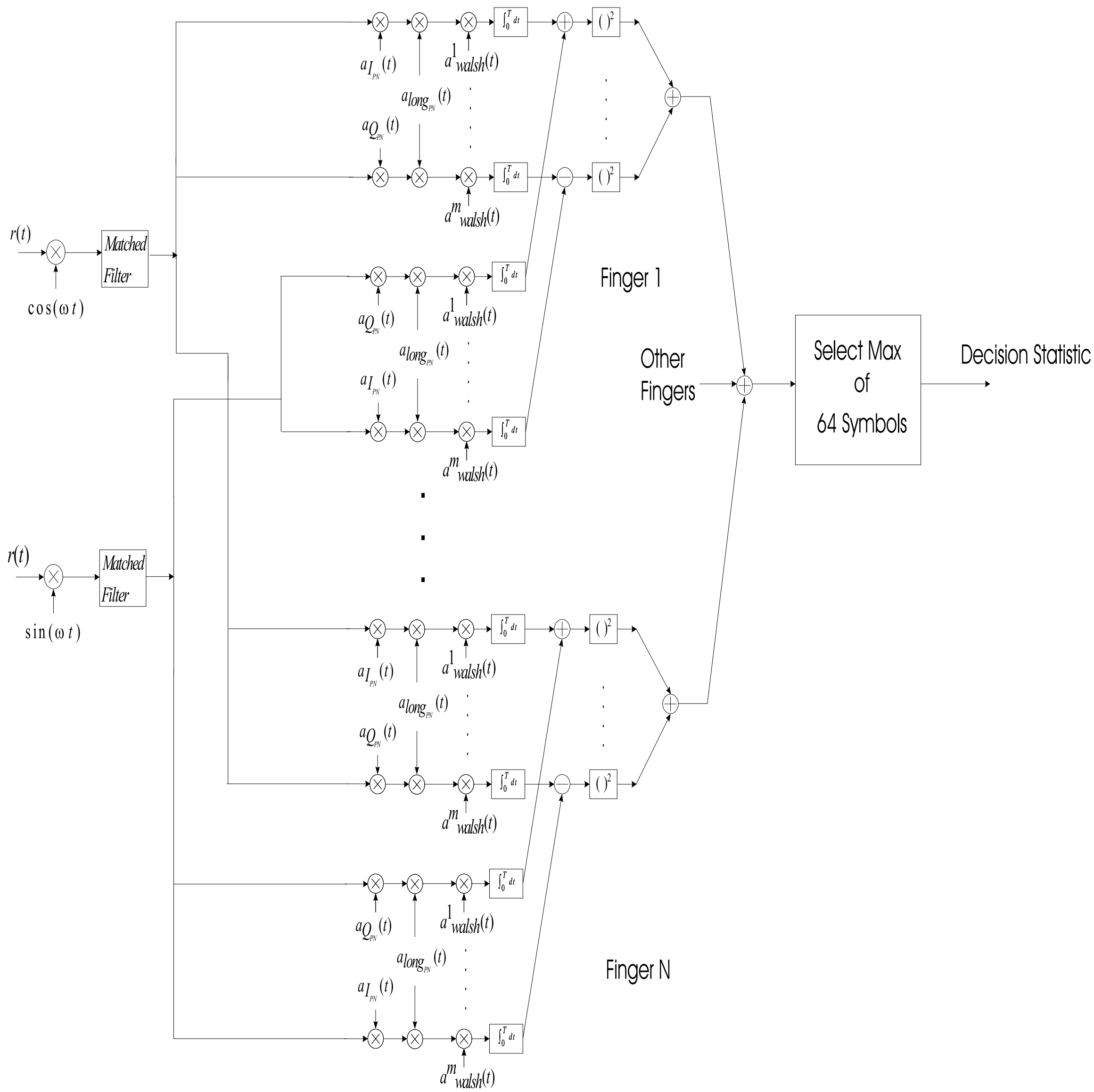

Figure 4.21: Model for the RAKE Receiver

4.5.3 Successive Interference Cancellation

Figure 4.22 shows a a block diagram of the successive interference cancellation scheme used for the noncoherent receiver. The robustness of interference cancellation schemes strongly depends on the accuracy of the interferers' power estimates. In this case the outputs of the correlators are used as power estimates but the correlations are averaged over the entire frame duration (20 ms) so that a better decision as to the most powerful user is made. Interference cancellation is performed prior to deinterleaving and Viterbi decoding.

For every 20 ms frame received, the users' signals are demodulated and correlation values are created as described above. These correlations are averaged over the entire frame period such that

$$\bar{Z}^{(k)} = \frac{\sum_{i=1}^{I} Z_i^{(k)}}{I} \tag{4.51}$$

where I is equal to the number of code symbols present in a frame (576). Given the frame average correlation of all the users, the users are ranked in order of the strongest correlation. The strongest user's I and Q channels are regenerated based upon the estimated code symbols found in Equation 4.50.

In the presence of resolveable multipath components, separate correlations are saved for each finger of the RAKE receiver. The interference cancellation scheme is integrated with this RAKE receiver. In addition to cancelling the strongest multipath component, the technique common to most simple interference cancellation schemes, all multipaths resolveable by the RAKE are cancelled. The I and Q channels are regenerated (including the cross-correlation components) and weighted by the appropriate decision statistic ($Z_{II}^{(l)}, Z_{QQ}^{(l)}, Z_{IQ}^{(l)}, Z_{QI}^{(l)}$) and then subtracted from the received signal buffer by the equations

$$\hat{r}_I^{(k)}(t) = r_I(t) - \sum_{j=1}^{k-1} \sum_{l=1}^{L} \left(\frac{\bar{Z}_{II}^{(j,l)}}{T} a_I^{(j)}(t-\tau_j) + \frac{\bar{Z}_{IQ}^{(j,l)}}{T} a_Q^{(j)}(t-\tau_j) \right) \tag{4.52}$$

$$\hat{r}_Q^{(k)}(t) = r_Q(t) - \sum_{j=1}^{k-1} \sum_{l=1}^{L} \left(\frac{\bar{Z}_{QQ}^{(j,l)}}{T} a_I^{(j)}(t-\tau_j) + \frac{\bar{Z}_{QI}^{(j,l)}}{T} a_Q^{(j)}(t-\tau_j) \right) \tag{4.53}$$

where $\hat{r}_I^{(k)}(t)$ and $\hat{r}_Q^{(k)}(t)$ are the kth user's I and Q signals after $k-1$ users have been estimated and removed. All the PN sequences and the lowpass filtering have been lumped together into the functions $a_I^{(j)}(t-\tau_j)$ and $a_Q^{(j)}(t-\tau_j)$ in order to simplify notation. Note that all L multipaths tracked by the RAKE receiver are removed from the signal buffer. This process is iterated until user K (the weakest user) is reached, at which point all of the stronger users will have been subtracted from the received signal.

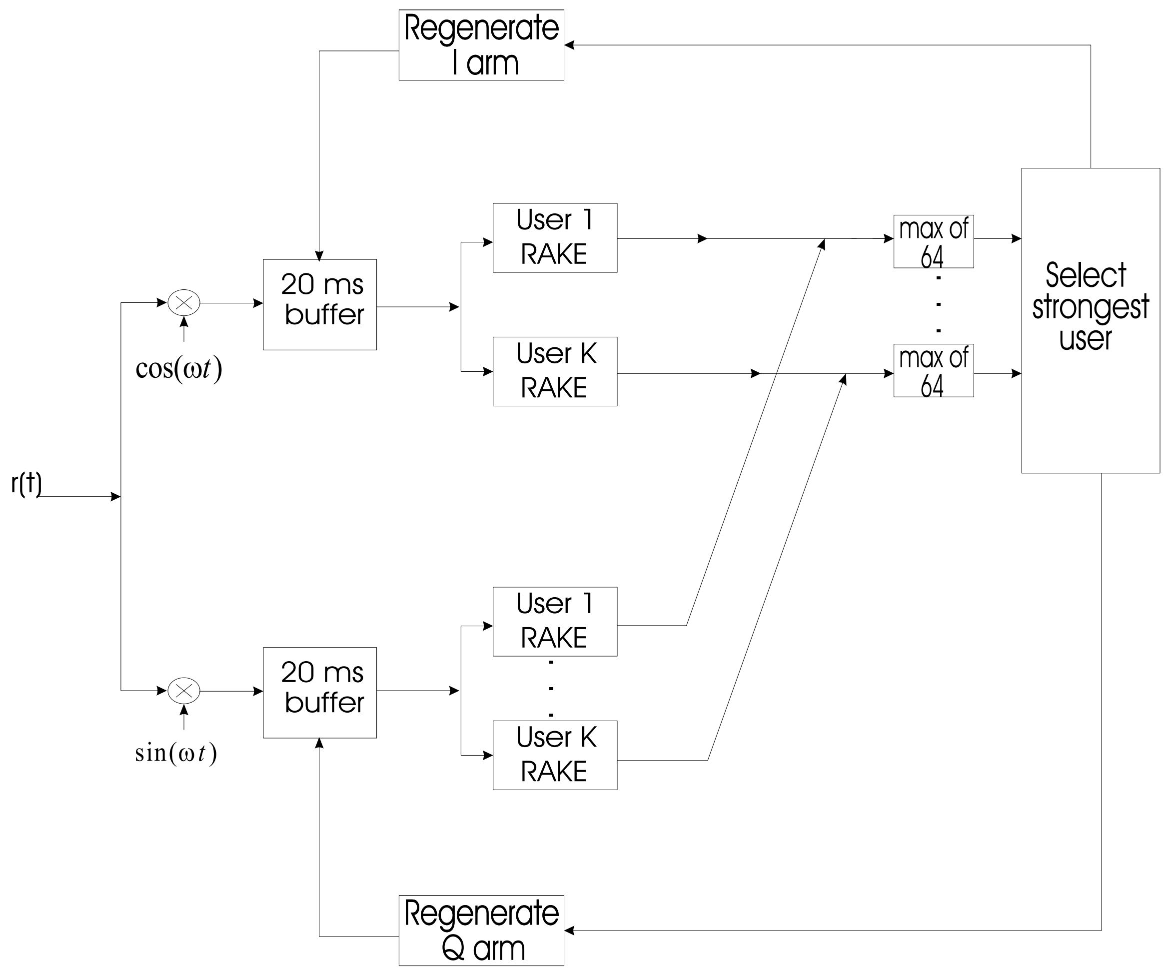

Figure 4.22: Model for Successive Interference Cancellation Scheme

4.5.4 Parallel Interference Cancellation

Figure 4.23 is a block diagram of the parallel interference cancellation scheme used in the simulation. For this particluar receiver implemenation, only one stage of cancellation is performed before the estimates are sent through the deinterleaver and Viterbi decoder. This is done to minimize the computations and delay prior to decoding the data. A separate copy of the received signal buffer is maintained for each user. For this algorithm, the first estimates are made and then each user's signal is regenerated. Once all the users' signals have been regenerated, each user has all other regenerated signals subtracted from that particular signal buffer. As in the case of successive interference cancellation, when multipaths are present each multipath component is removed by weighting with the correlation output values of the RAKE receiver for every finger. The average correlation outputs over a frame duration are used to weight the regenerated signal. The regenerated signal for each user is given by

$$\hat{s}_I^{(k)}(t) = \sum_{l=1}^{L} \left(\frac{\bar{Z}_{II}^{(k,l)}}{T} a_I^{(k)}(t) + \frac{\bar{Z}_{IQ}^{(k,l)}}{T} a_Q^{(k)}(t) \right) \tag{4.54}$$

$$\hat{s}_Q^{(k)}(t) = \sum_{l=1}^{L} \left(\frac{\bar{Z}_{QQ}^{(k,l)}}{T} a_Q^{(k)}(t) + \frac{\bar{Z}_{QI}^{(k,l)}}{T} a_I^{(k)}(t) \right) \tag{4.55}$$

where $\bar{Z}_{II}^{(k,l)}$, $\bar{Z}_{IQ}^{(k,l)}$, $\bar{Z}_{QQ}^{(k,l)}$, $\bar{Z}_{QI}^{(k,l)}$ are the correlation outputs of the RAKE receiver fingers averaged over the duration of one frame. Once again the all the PN sequences, Walsh function, and low pass filtering for the I and Q channel of each user have been compressed into $a_I^{(k)}(t)$ and $a_I^{(k)}(t)$ in order to simplify notation. The new received signal for the kth user is found by

$$\hat{r}_I^{(k)}(t) = r_I(t) - \sum_{\substack{i=1 \\ i \neq k}}^{K} \hat{s}_I^{(i)}(t) \tag{4.56}$$

$$\hat{r}_Q^{(k)}(t) = r_Q(t) - \sum_{\substack{i=1 \\ i \neq k}}^{K} \hat{s}_Q^{(i)}(t) \tag{4.57}$$

This new received signal estimate is passed once again through a RAKE receiver for each user to yield the bit estimates sent to the decoding unit. The resulting correlation outputs are then

$$Z'^{(k)}_{II,i} = \int_{iT}^{(i+1)T} \hat{r}^{(k)}_I(t)\, a^{(k)}_I(t)dt \tag{4.58}$$

$$Z'^{(k)}_{IQ,i} = \int_{iT}^{(i+1)T} \hat{r}^{(k)}_I(t)\, a^{(k)}_Q(t)dt \tag{4.59}$$

$$Z'^{(k)}_{QI,i} = \int_{iT}^{(i+1)T} \hat{r}^{(k)}_Q(t)\, a^{(k)}_I(t)dt \tag{4.60}$$

$$Z'^{(k)}_{QQ,i} = \int_{iT}^{(i+1)T} \hat{r}^{(k)}_Q(t)\, a^{(k)}_Q(t)dt \tag{4.61}$$

These values are then noncoherently combined yielding a final code symbol decision statistic

$$Z'^{(k)}_i = \left(Z'^{(k)}_{II,i} + Z'^{(k)}_{QQ,i}\right)^2 + \left(Z'^{(k)}_{IQ,i} + Z'^{(k)}_{QI,i}\right)^2 \tag{4.62}$$

$Z'^{(k)}_i$ is then sent to the deinterleaving and decoding stage.

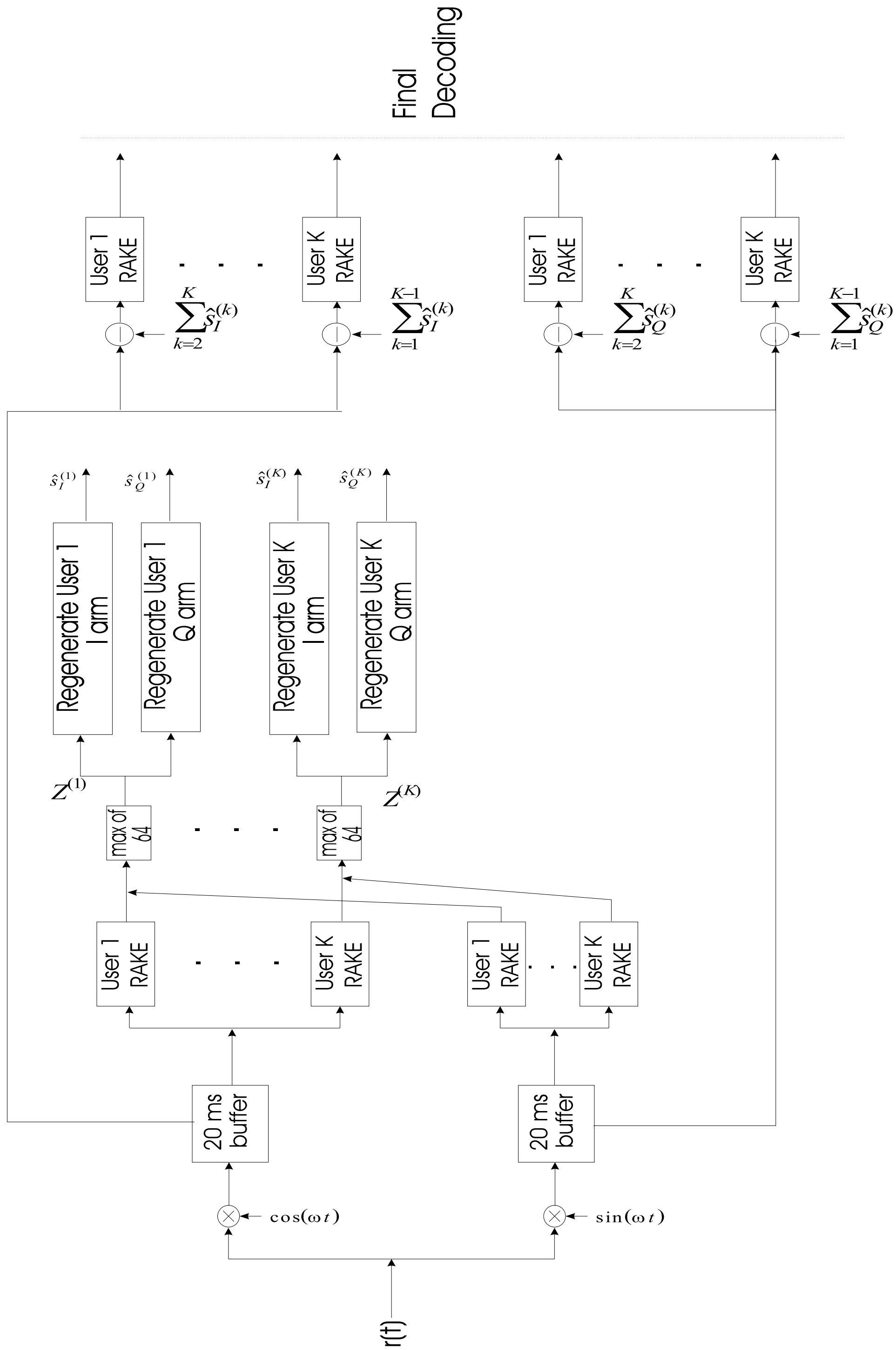

Figure 4.23: Model for IS-95 Parallel Interference Cancellation

4.5.5 Deinterleaving and Viterbi Decoding

The deinterleaver performs the reverse operation of the interleaver as described in Chapter 2. In order to allow flexibility in the decoding operations, the deinterleaver operates on memory elements using floating point rather than assuming conversion to integer symbols.

The Viterbi algorithm provides a maximum likelihood decoding (MLD) of a convolutional code [For73]. The decoder has knowledge of the structure of the convolutional code so that a trellis may be generated showing the number of paths to a particular state of the encoder. Each branch of the trellis has a metric associated with it: Hamming distance for hard decision decoding or the squared Euclidean distance for soft decision decoding. The metric of a path may be found by stepping through the trellis and accumulating the metric at each branch. In order to reduce computational effort the Viterbi decoder used in the simulation software allows for two different implementations. In the case of hard decisions, the estimates from the output of the deinterleaving operation are converted to ones and zeroes before being sent to the decoder. Otherwise, the estimates themselves are sent through the decoder for soft decisions. Soft decision decoding takes significantly longer because all operations are done using floating point rather than integer operations. For most of the simulations, hard decisions were used to minimize the computation time. The decoder uses a finite number of memory elements (44 elements) for developing the trellis. This is approximately 5 times the constraint length so performance should be near optimum. The memory depth (44 in this case) is the coding delay in the receiver. All output bit estimates are delayed by 44 bit periods relative to the original data source.

4.6 Error Estimation

The bits at the receiver output are compared with a delayed version of the input bit stream. When a received bit is different from a transmitted bit an error is recorded. The simulation can count the errors for a single user or multiple users providing flexibility in simulation of the near far effect. After the errors are counted the bit error rate is calculated by dividing the number of errors by the total number of bits counted. A minimum of 100 bit errors are generated for each iteration over either the E_b/N_o or the number of users. This maintains a fairly tight confidence interval for the error estimate. Given a binomial distribution for the errors, 100 independent error events will result in an estimate that is within a 1.3 factors of the actual probability of error.

4.7 Chapter Summary

This chapter reviewed the simulation model used in the software. We represented the signal in a mathematical form using baseband complex envelope notation which simplifies simulation. Models for MAI, AWGN, and multipath characteristics were given. In addition, we described the various receiver implementations used in the software in detail.

Chapter 5

Simulation Results

In this chapter, we present the results of the simulations. The system described in Chapter 2 is simulated using the concepts and models presented in Chapters 3 and 4. The simulations provide results for performance of the IS-95 reverse channel with successive and parallel interference cancellation implemented. Results are provided for the performance of the system in a multipath environment as well. Quantization results are also given for the IS-95 reverse channel; in addition the performance of a BPSK DS/SS system with quantization effects is given for a comparative view.

Certain assumptions were used throughout to simplify the simulation. These include perfect acquisition and synchronization of the PN sequences for each user; [Bue96] shows the performance degradation because of timing errors. We have also assumed that the data rate of all the users is fixed at 9600 bps. Since the data rate is not varying, the capacity is not increased by voice activity detection. While this may be considered a worst case scenario, the current trend towards handling voice and data applications may make maximum rate connections more common. For many of the simulations, perfect power control was also assumed. This assumption fixes all user powers to the specified E_b/N_o.

5.1 Performance of IS-95

Results for IS-95 without interference cancellation are provided here as a form of comparison to the results provided in the remainder of the chapter. The results present a range of users and E_b/N_o levels. Figure 5.24 gives a curve of the BER versus number of users for the IS-95 reverse channel in AWGN. E_b/N_o is fixed at 10 dB for a range of 10 to 30 users with perfect power control. This plot clearly shows the gradual degradation in performance of a CDMA system, thus leading to the claims of a "soft capacity" system. The two curves representing different E_b/N_o levels also show the IS-95 reverse channel approaching an interference related performance floor. As the number of users loading the systems surpasses 22, the 5 dB power increase has a diminishing effect on the BER. When the number of users equals 20, an E_b/N_o of 15 dB improves the BER by more than two orders of magnitude compared to that of 10 dB. When the system load is increased to 30 users, this same advantage is reduced to less than one order of magnitude. Note that these are full are users so that the actual system capacity is two to three times larger if voice activity detection is taken into consideration

A comparison is given for the performance of the receiver with hard and soft decisions made at the receiver. As explained in Chapter 4, it is possible to improve the performance of a Viterbi decoder by using the probabilistic outputs of the demodulator as inputs to the decoder rather than performing a decision on the code bit. While requiring more memory and floating point operations, soft decision decoding can significantly improve the performance of convolutional codes. Figure 5.25 shows the performance of the IS-95 reverse channel in AWGN with 25 users present in the system in a range of E_b/N_o values. Perfect power control is assumed for all the users. The advantage of using soft decisions in the decoder is fairly constant; approximately 2 dB of coding gain is provided for this number of users. Since the complexity and cost of the receiver equipment is limited to the base station unit, it is desirable to maximize the performance using soft decision decoding.

A brief look at the effect of sampling is given in Figure 5.26. Here, a curve for the sampling rate at four samples per chip and another with eight samples per chip are shown. This plot shows that increasing the sampling rate does not depict a large capacity improvement. In some cases, aliasing effects may further degrade a signal so it is necessary to sample at more than twice the information rate. Selecting the sampling rate is very critical in a CDMA simulation because of exponential increases in simulation time with increasing sampling rates. For a CDMA system, however, we would expect the signal to be resistant to aliasing effects just like any other form of interference. In addition, the pulse shaping used in IS-95 has reduced sidelobes further minimizing aliasing effects.

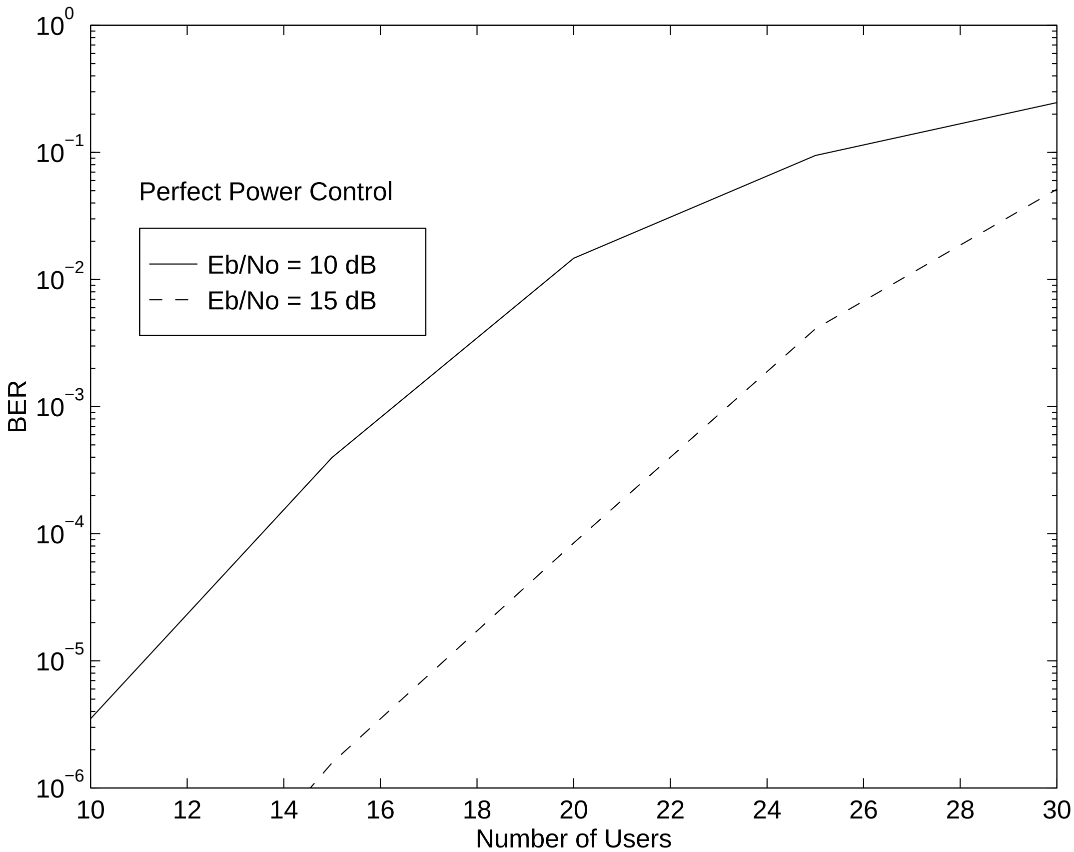

Figure 5.24: BER vs. number of users for IS-95 reverse channel with a conventional receiver in AWGN, using an Eb/No=10dB and 15dB. Perfect power control is assumed (hard decision decoding).

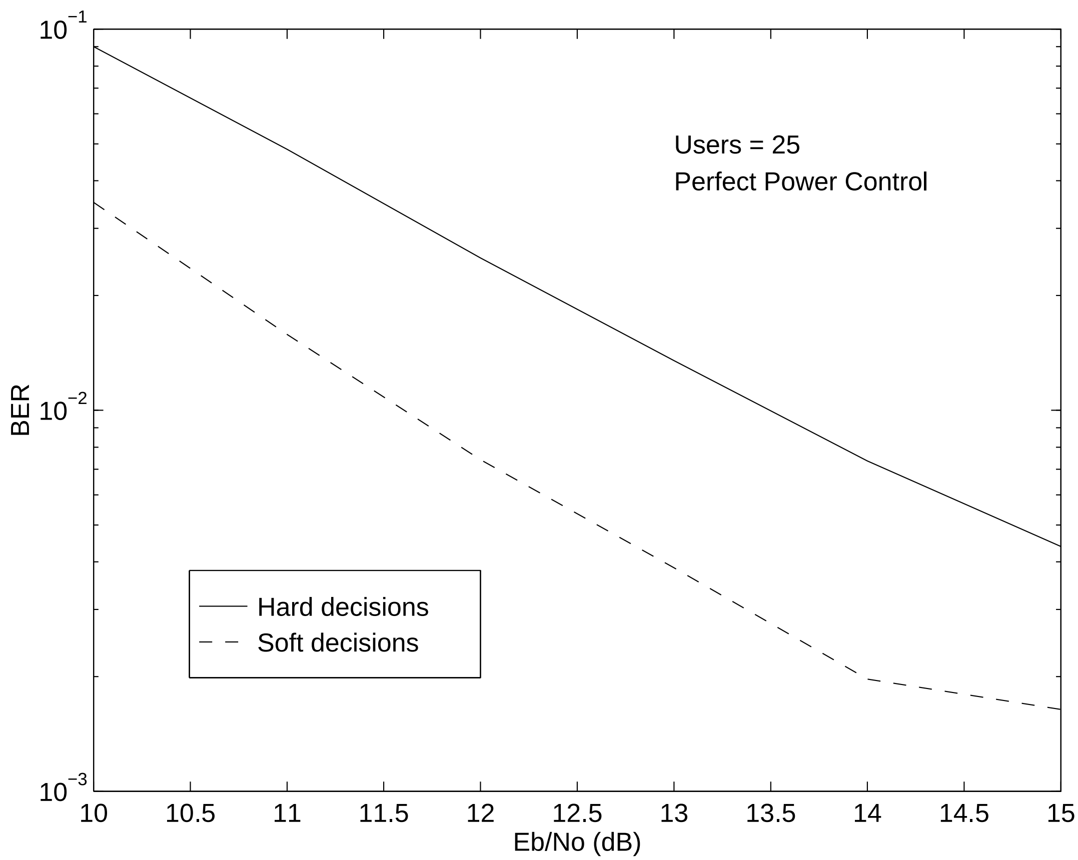

Figure 5.25: BER vs. E_b/N_o for IS-95 reverse channel in AWGN using hard and soft decisions in the Viterbi decoder. There are 25 users present with perfect power control.

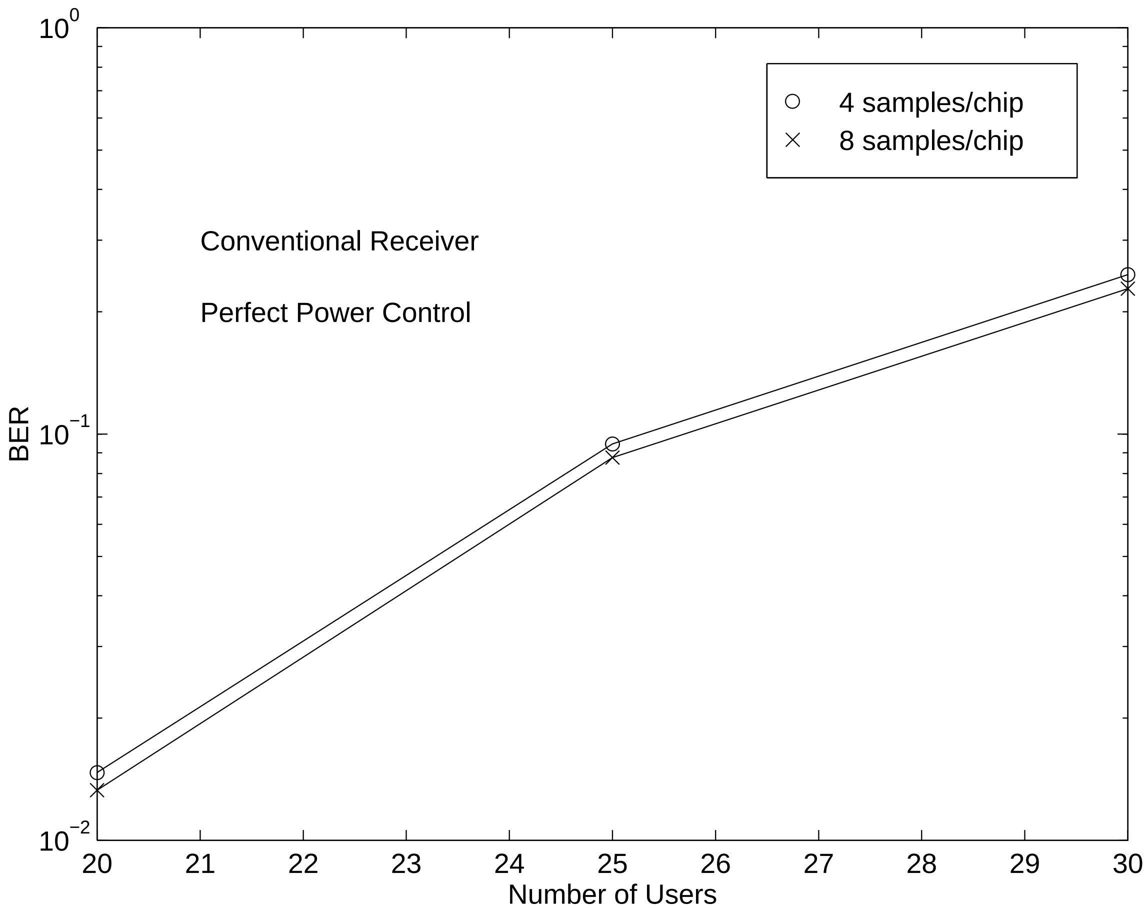

Figure 5.26: BER vs. number of users for IS-95 reverse channel in AWGN using 4 and 8 sample per chip. Perfect power control is assumed with an E_b/N_o of 10 dB (hard decoding).

5.2 Performance with Interference Cancellation

Two implementations of interference cancellation are compared in this section: successive and parallel interference cancellation. For successive interference cancellation, $K-1$ cancellations were performed where K is the total number of users. In the case of parallel interference cancellation, only one stage of cancellation was used, however, all users are regenerated and cancelled in that one stage. In this section, only AWGN is assumed for the channel model. The multipath channel is covered in a later section. Ideal power control is assumed for this section also. Ideal power control assumes that the base station (and mobile) are capable of maintaining a desired E_b/N_o for the length of a connection.

Figure 5.27 shows a performance curve for all three receiver implementations over a range of users with a fixed E_b/N_o equal to 10 dB. Hard decisions are used in the decoding. Figure 5.27 clearly shows that capacity increases are possible with the implementation of the interference cancellation schemes presented in this work. It is also clear that performance gains from using interference cancellation are a function of the current load on the system. For a fixed E_b/N_o, all the receiver implementations begin to converge rapidly with increasing system load. If the system were attempting to maintain a BER of 10^{-3}, successive interference cancellation could increase capacity by approximately 15% and parallel interference cancellation could increase capacity by 25%. While 10^{-3} is considered a minimum for voice communications, it may be too high for data applications and high quality voice. Both interference cancellation schemes show potential for increasing capacity by even greater amounts at lower BER values.

Figure 5.28 demonstrates the performance improvement when the system load is fixed and the E_b/N_o of all the users is increased. The number of users is fixed at 25 with perfect power control in an AWGN channel. Hard decision decoding is used with the Viterbi algorithm. The successive interference cancellation scheme shows approximately 2 dB effective E_b/N_o gain relative to the conventional receiver structure. The parallel interference cancellation scheme shows an even greater improvement in BER. The disparity between the conventional receiver and multiuser receivers increases as

E_b/N_o increases suggesting that the interference floor is being reduced by the multiuser receivers.

Figure 5.29 is a plot depicting the performance improvement using soft decision and hard decision decoding with successive interference cancellation. The number of users is fixed at 25 with perfect power control and an E_b/N_o ranging from 10 to 15 dB. Just as in Figure 5.25 there is 2 dB coding gain evident from the use of soft decision decoding. This indicates that the threshold E_b/N_o level for improving performance with convolutional codes has been reached for this particular constraint length. We would expect a 2 dB coding gain for using soft decision decoding over hard decision decoding in any of the implementations.

The performance of multiuser receiver structures is best compared to that of the single user receiver with only one user present in the system. The single user case would ideally exist if all the MAI were effectively removed by the multiuser receiver. It is not possible, however, to simulate the single user case accurately. The bit error rate for only one user in an AWGN environment with convolutional coding would be well below 10^{-6} for the E_b/N_o values used throughout the other simulations.

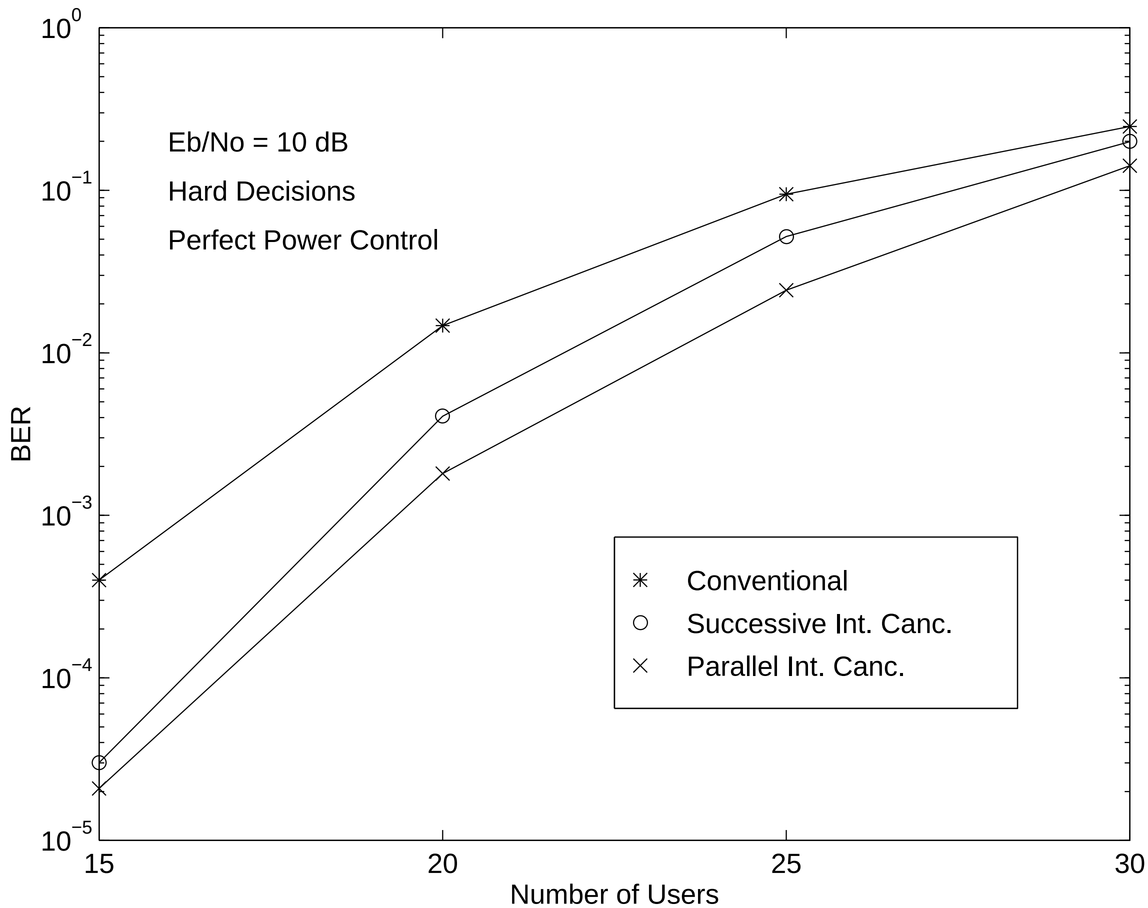

Figure 5.27: Capacity curves for IS-95 with different receiver implementations in AWGN. The users all have perfect power control and operate at an E_b/N_o=10dB (hard decision decoding).

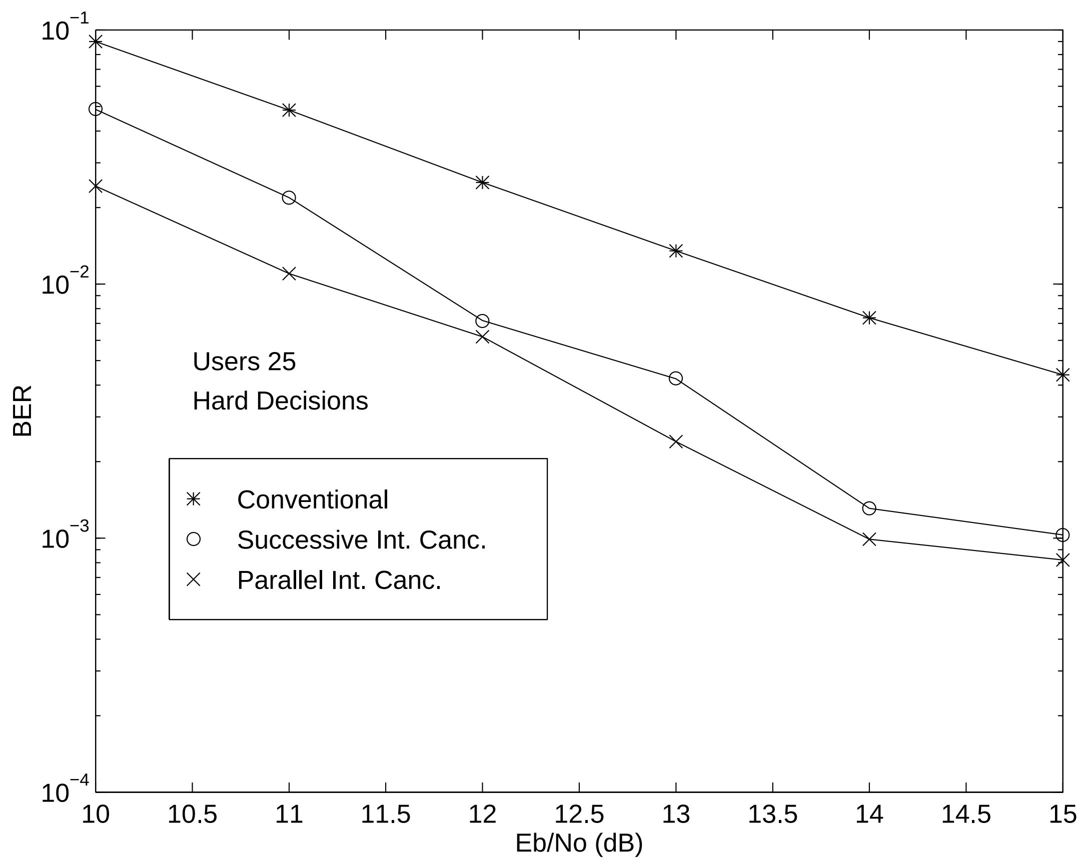

Figure 5.28: BER curves for IS-95 with different receiver implementations in AWGN. There are 25 users with perfect power control (hard decision decoding).

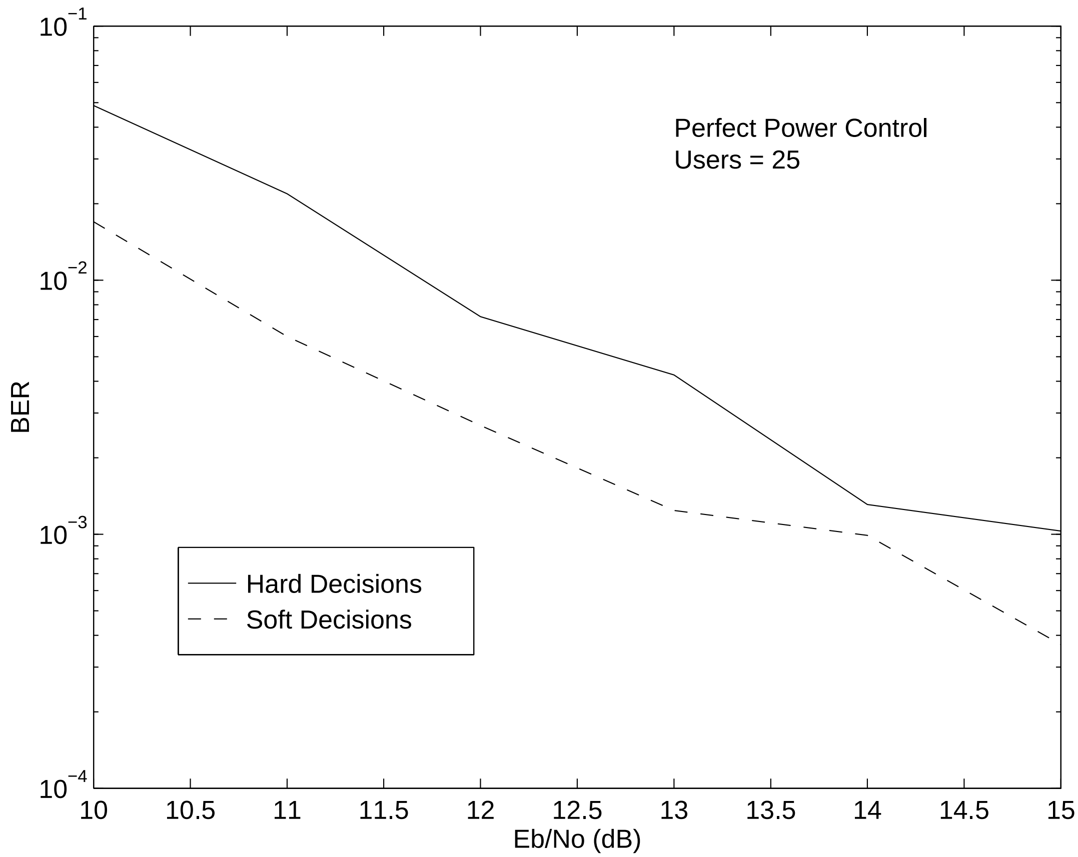

Figure 5.29: BER curves for IS-95 with successive interference cancellation using hard and soft decision decoding. There are 25 users with perfect power control in an AWGN channel.

5.3 Performance in Near-Far Conditions

In this section, the receiver structures' performances in near-far conditions induced by imperfect power control are examined. To simulate the near-far effect, half the users are set 3 dB below the desired power level and the other half are set 3 dB above the desired level. Consequently, there is a 6 dB power differential between the two groups of users. The bit error rates for weaker group of users are examined. The stronger group of users performs significantly better and in all cases achieved bit error rates below 10^{-6}. It is not surprising that the stronger users have lower BERs; it is more important for the system designer to maintain acceptable BERs for the weaker users in order to prevent dropped calls or low quality connections. Resistance to performance degradation under near-far conditions would eliminate dependence on stringent power control. Strict power control is difficult to realize in cellular CDMA because of shadowing that may occur in urban environments. It is also a function of the update rate of the power control (in the closed loop case) and the resolution steps of the power level updates. All these parameters complicate the selection of efficient power control algorithms.

Figure 5.30 depicts the performance of the three structures in an AWGN channel when the five of the ten users are 6 dB weaker than the other five users. The desired user is present in the weaker group. Hard decision decoding is used. The conventional receiver clearly performs poorly in near-far conditions. Both successive and parallel interference cancellation schemes show significant improvement and a reduction in the MAI noise floor. It is notable that the successive interference cancellation shcheme did not perform better than the parallel interference cancellation scheme.

Figure 5.31 is a performance measure of BER versus desired $\overline{E_b/N_o}$ with 20 users present. Half of the users including the desired user are 6 dB below the other half of the users. Hard decision decoding is used in an AWGN channel. This curve depicts the performance of the IS-95 reverse channel under heavily loaded conditions with a large amount of variation in the power levels of the users. Clearly, the conventional receiver is not capable of supporting the weaker users. Both of the multiuser receivers show potential for supporting wide power variations in a heavily loaded system. By increasing E_b/N_o the BER could also be increased.

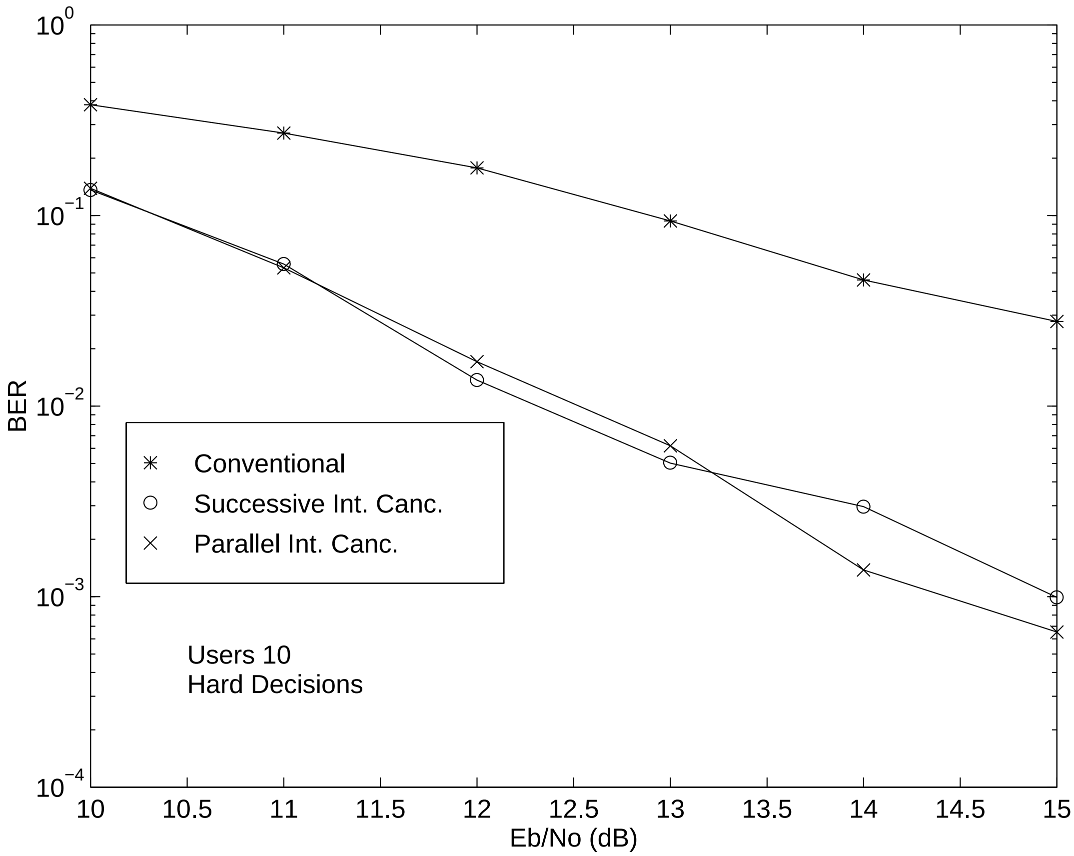

Figure 5.30: BER curves for IS-95 receiver structures in AWGN for five of the ten users (including the desired) 6 dB below the other 5 users (hard decision decoding).

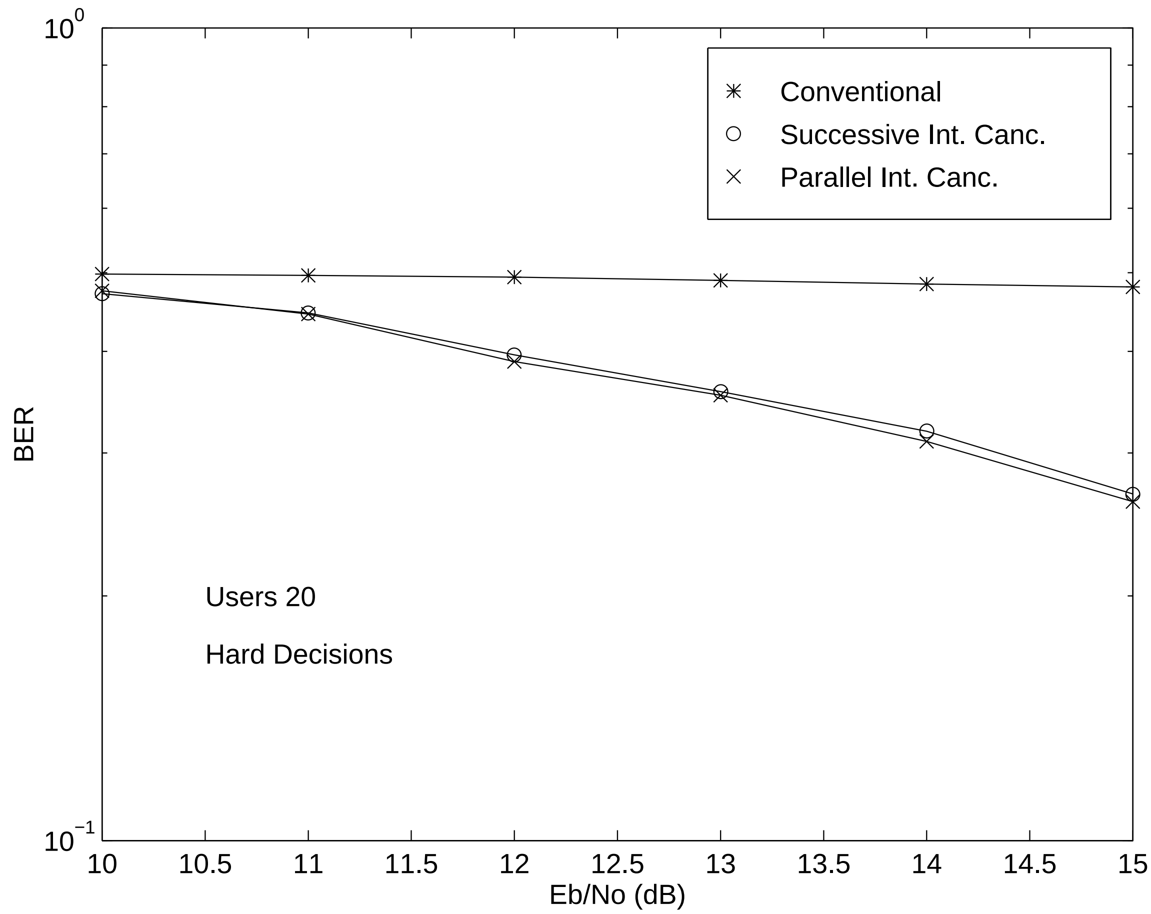

Figure 5.31: BER curves for IS-95 receiver structures in AWGN for 10 of the 20 users (including the desired) 6 dB below the other 10 users (hard decision decoding).

5.4 Performance in Multipath

This section provides a preliminary performance evaluation of the conventional single user and multiuser receiver in the presence of multipath. To minimize computational complexity, the multipath conditions were limited to a two-ray model with a fixed time delay between the two rays. The total power in any of the channel impulse responses is normalized. Perfect synchronization with the multipaths is assumed. The two rays used in the model were assumed to be static, i.e., no fading distribution was assumed for either of the components. This is a simplistic model that allows us to verify the performance of the combinined RAKE and interference cancellation schemes. The static impulse response might also be representative of a wireless local loop application where none of the handset units are moving.

For one of the two-ray equal power channel models, the time delay is equal to 5 μs. Under these conditions the rms delay spread is then equal to 2.5 μs. The two-ray equal power channel model is typically a worst case scenario. The 2.5 μs delay spread is a reasonable figure common in many suburban and urban areas [Cox75] [Rap90]. Figure 5.32 is a plot of the receiver structures' BER versus E_b/N_o in such an environment. There are 15 users present with perfect power control, and hard decision decoding is used. Because the outputs of the individual RAKE fingers are used in the interference cancellation scheme, the BER performance of the multiuser receiver is not reduced in multipath.

The second channel impulse response used a two-ray model. Again, both rays were separated by 5 μs. The second ray, however, was 3 dB lower in power than the first primary ray. Using Equations 4.24 and 4.25 we may readily calculate the rms delay spread, $\tau_{rms} = 2.3\mu s$. Fifteen users are present with perfect power control and hard decision decoding used at the receiver. Again, the multiuser receivers clearly operate as expected in multipath conditions.

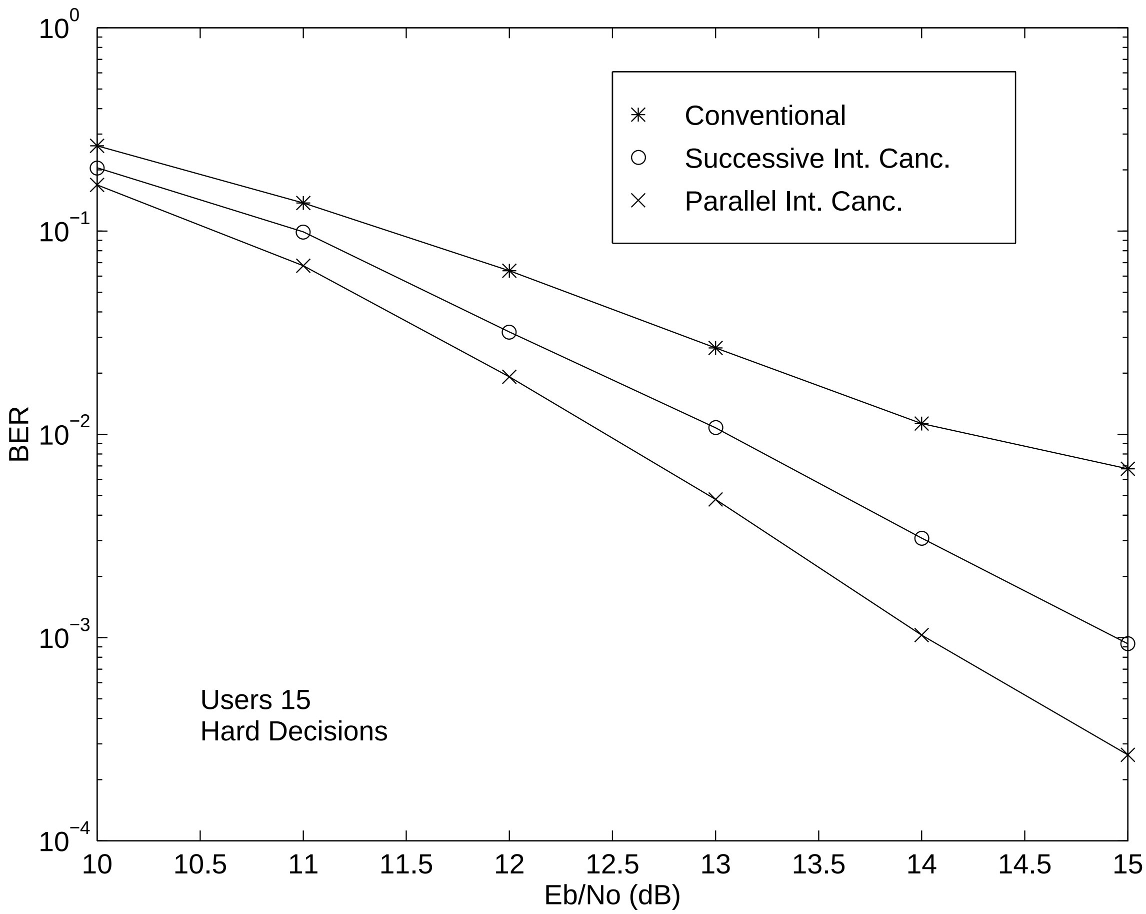

Figure 5.32: BER vs. E_b/N_o for receiver implementations in a 2-ray multipath channel with $\tau_{rms} = 2.5\mu$s. There are 15 users with perfect power control (hard decision decoding).

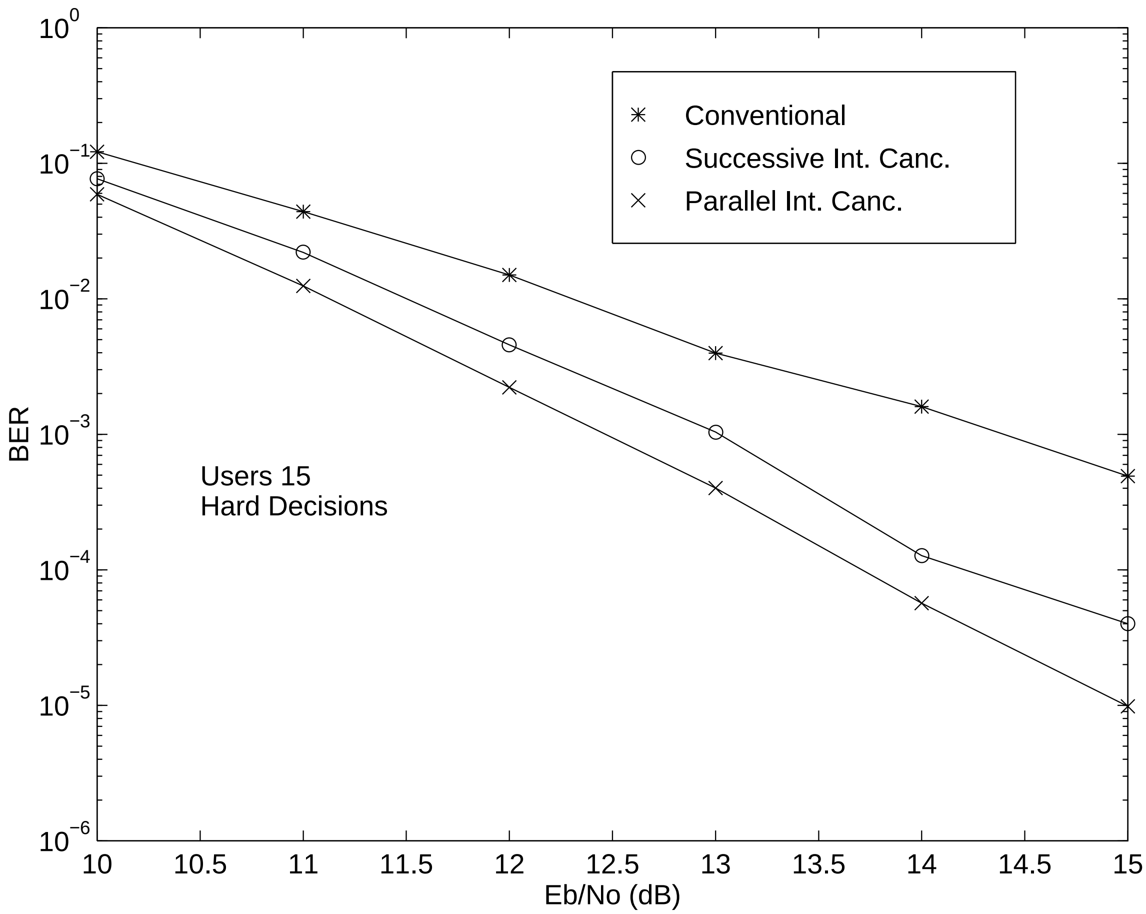

Figure 5.33: BER vs. E_b/N_o curves for receiver implementations in a 2-ray multipath channel with $\tau_{rms} = 2.3\mu$s. There are 15 users with perfect power control (hard decision decoding).

5.5 Quantization Results

Next we explore the effect of the quantization introduced by the ADC on receiver performance. All quantization results were obtained by using an AGC that scaled to the largest magnitude over a frame duration. The ADC is a uniform quantizer operating at the system sampling (equal to four times the chip rate) with a given number of bits. The term "infinite bits" implies the floating point limitation of the compiler and the computer, which in most cases is essentially infinite.

5.5.1 BPSK DS/SS with Quantization

The BPSK DS/SS system uses a processing gain (G_p) of 128. The users are phase asynchronous but time synchronous. The spreading codes for the users are randomly generated. The purpose of this simulation is to generate a comparison to the IS-95 quantization results. Convolutional coding is not used for this system. Coherent reception is implemented at the receiver.

Figure 5.34 is a plot of BER versus the number of users in the system assuming perfect power control. Only AWGN is used with an E_b/N_o equal to 10 dB. The plot shows that near optimal performance may be obtained with 4 or 8 bits in the quantizer. There is almost no loss in capacity when implementing 4 bits in the quantizer. Using 1 or 2 bits in the quantizer yields similar results; the capacity of the system is reduced by 45%.

Figure 5.35 is a plot of BER versus E_b/N_o in a system of 25 users assuming perfect power control. The simulation is done under AWGN conditions with E_b/N_o varying from 10 to 15 dB. The plot shows that 4 and 8 bit quantizers give near optimal performance for DS/SS-BPSK. The performance loss for using fewer than 4 bits is about 4 dB.

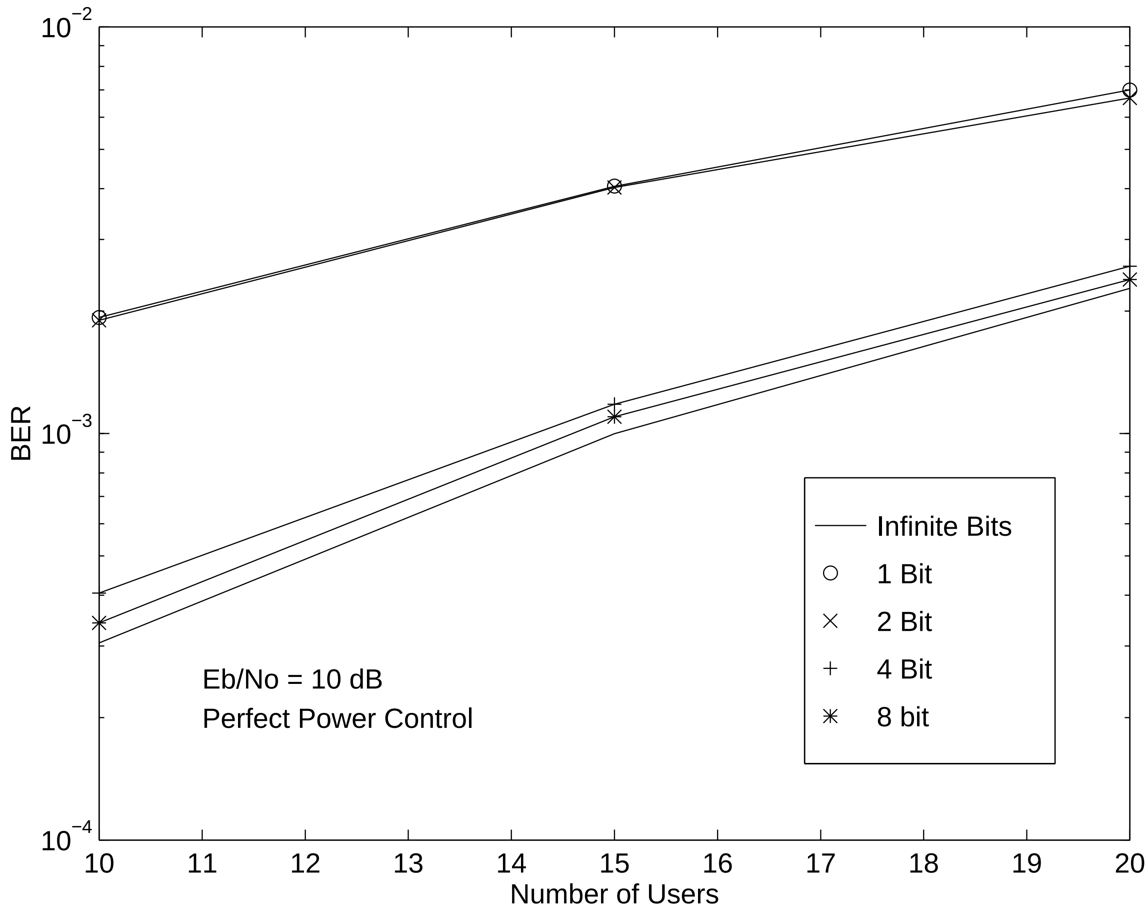

Figure 5.34: BER vs. number of users for number of quantizing bits in a BPSK DS/SS system with $G_p = 128$. Perfect power control with an Eb/No=10dB is assumed.

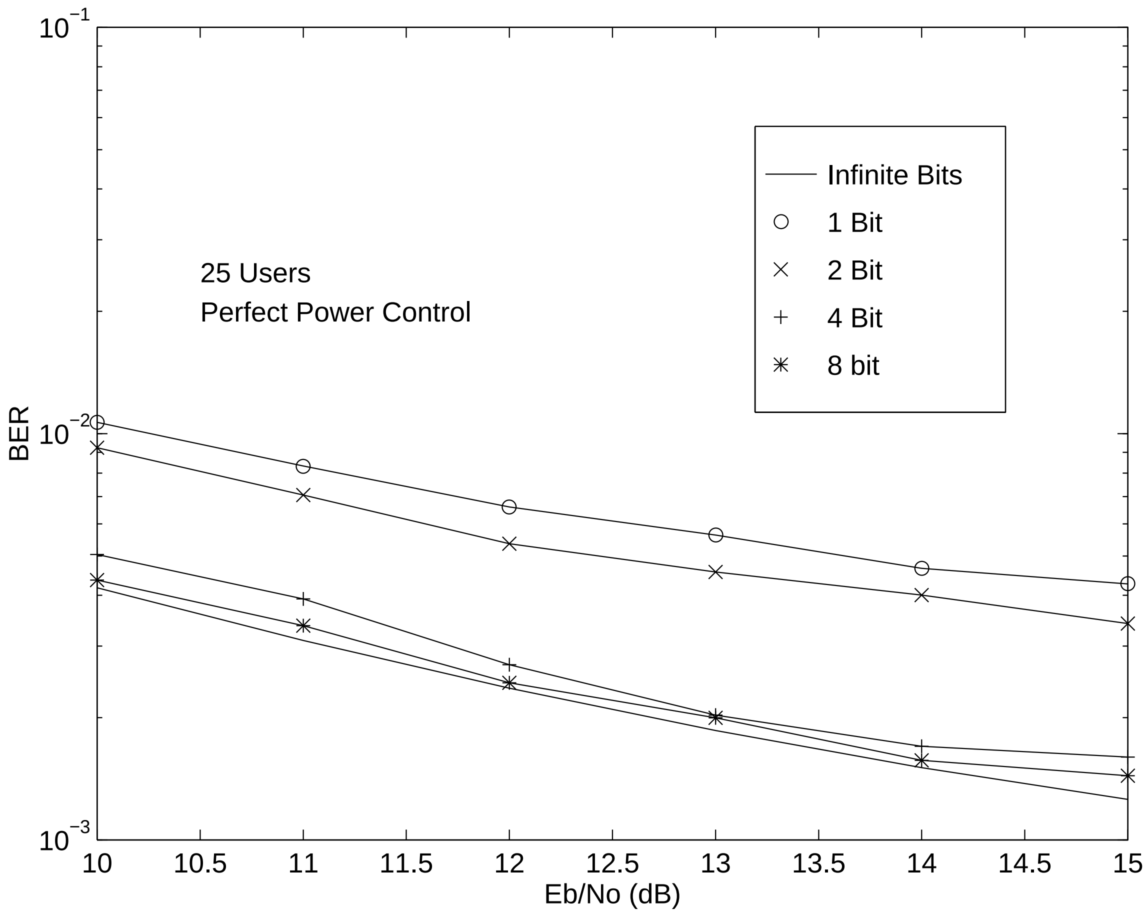

Figure 5.35: BER curves vs. E_b/N_o for number of quantizing bits in a BPSK DS/SS system with $G_p = 128$. There are 25 users with perfect power control in AWGN.

5.5.2 IS-95 with Quantization

For the IS-95 quantization results, the aforementioned AGC and ADC were used. Since IS-95 has a processing gain of 128, we would expect similar quantization effects as in the DS/SS-BPSK system. Figure 5.36 depicts the BER of the IS-95 reverse channel versus E_b/N_o for different levels of quantization. The conventional receiver in AWGN was used with 25 users present. Perfect power control was assumed and the Viterbi decoder used hard decisions. The 8 bit quantizer performed identically with the infinite quantization. The 4 bit quantizer resulted in a loss of 0.75 dB. The 1 and 2 bit quantizers performed almost identically and appear to be insufficient for quantization.

Figure 5.37 demonstrates the effect of ADC quantization on the information used for soft decision Viterbi decoding. From these results it is apparent that the ADC does not affect the Viterbi decoder using soft decisions anymore than the hard decision decoder.

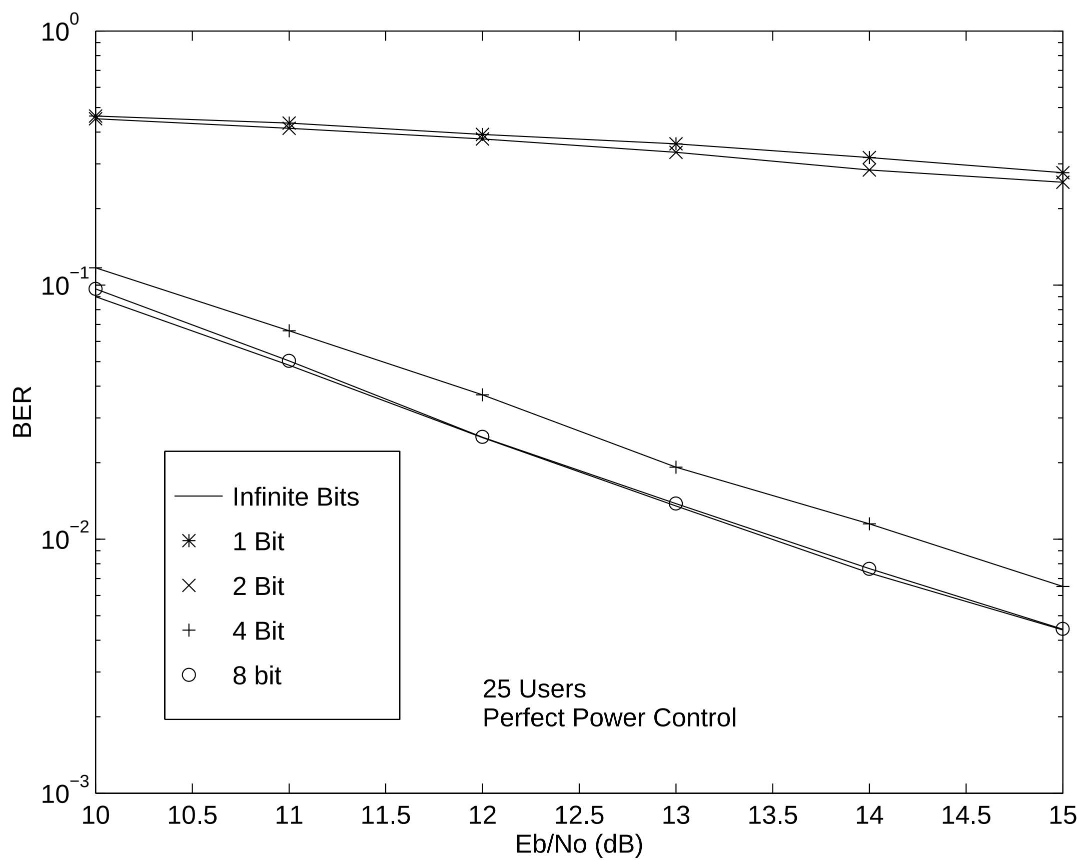

Figure 5.36: BER curves vs. E_b/N_o for number of quantizing bits with an IS-95 conventional receiver. There are 25 users with perfect power control in an AWGN environment (hard decision decoding).

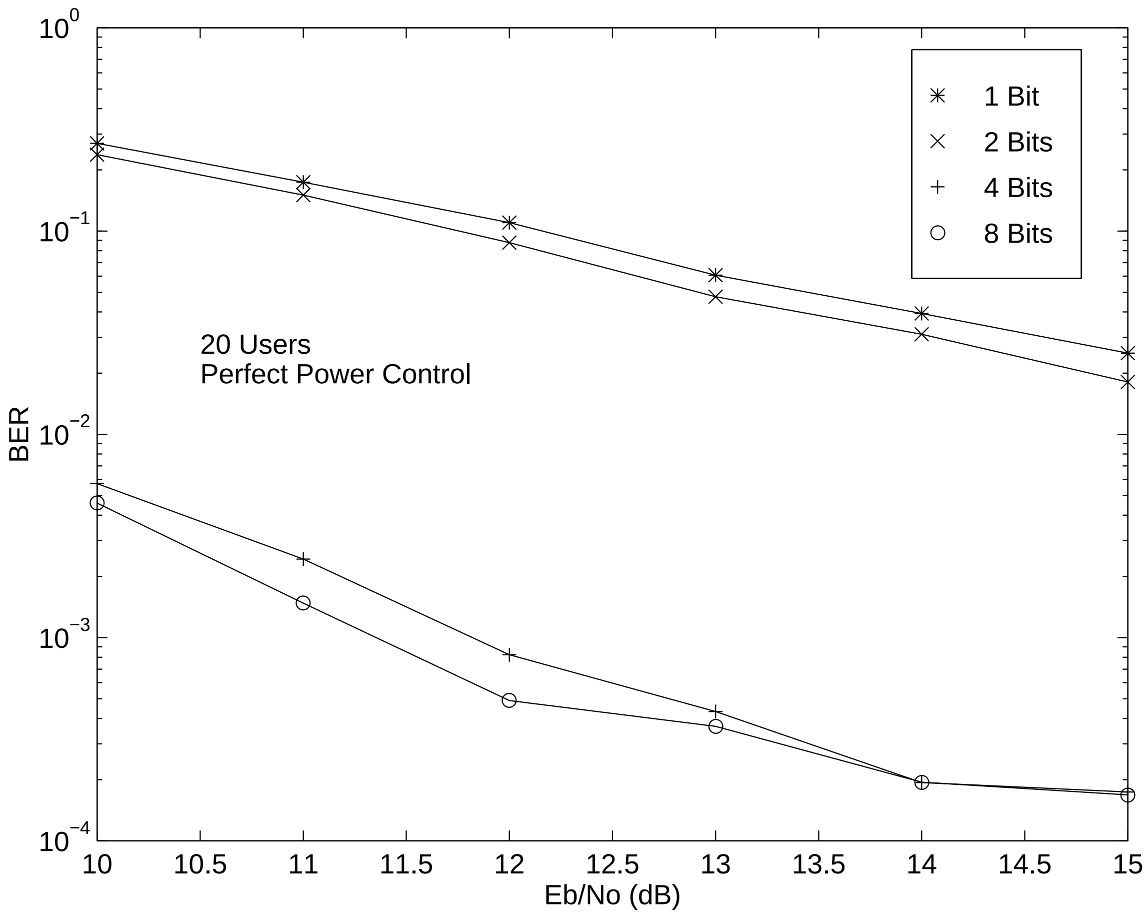

Figure 5.37: BER vs. E_b/N_o for number of quantizing bits with an IS-95 conventional receiver. There are 20 users with perfect power control in an AWGN environment (soft decision decoding).

5.6 Simulation Time

As discussed in Chapter 1, there is a tradeoff between the complexity of any simulation and the running time necessary to complete such a simulation. Much of the work in the literature has focused on simple DS/SS-BPSK systems in order to minimize the computational complexity. This thesis has recreated, with reasonable accuracy, the IS-95 reverse channel. To appreciate this complexity, a table is presented which contains samples indicating the approximate length of time it takes to complete a particular simulation. The simulations shown in the table were all run on a Sun SPARC 20 workstation as background processes in order to minimize disruption to the network. Clearly, the interference cancellation schemes can significantly increase the

Table 5.3: Simulation time for different simulation points presented.

Receiver Type	Number of Users	Simulation Time	Referencing Figure
Conventional	20	3.5 hrs	Fig. 5.24
Successive IC	20	27 hrs	Fig. 5.24
Parallel IC	20	58 hrs	Fig. 5.24

simulation time. This is due to the regeneration, cancellation, and re-estimation that must be performed in the interference cancellation methods. As mentioned previously, the number of computations required for successive interference cancellation is fewer than the that of parallel interference cancellation which is apparent in Table 5.3. In a hardware architecture, however, it would be possible to use parallel processors to implement parallel interference cancellation. In addition to the added complexity of using interference cancellation, the reduced BER requires a greater number of simulated bits to achieve similar confidence intervals on the estimates. Simulations that include multipath would take even longer because of the convolution operation for the channel.

5.7 Chapter Summary

This chapter provided a concise summary of the performance of IS-95 and two forms of multiuser detection in several environments. The effects of hard and soft decision decoding on IS-95 was demonstrated. Capacity curves for the multiuser receivers were presented for the AWGN and multipath channel case. The receivers' resistance to near-far was demonstrated by plotting the BER of users being drowned out by stronger interferers. The effects of quantization on both DS/SS-BPSK and the IS-95 reverse channel were also simulated. Discussion of these results is contained in the following chapter.

Chapter 6

Conclusions

In this chapter, we summarize the research performed for this thesis. We also review the observations made from the results presented in Chapter 5. Topics for future areas of research are suggested in this chapter.

6.1 Summary of Research

A bit error rate simulation tool for the IS-95 CDMA standard has been presented. This software permits the simulation of three classes of receiver architectures: conventional single user, multiuser successive interference cancellation, and multiuser parallel interference cancellation. Although the simulation results presented in this work limited the parallel interference cancellation to one stage the software allows for multiple stages of cancellation. The transmitted signals are represented in baseband complex envelope notation and convolved with a user defined channel impulse response. The user may include multiple channel profiles to emulate each user experiencing a different channel response. A few simple two-ray channel models have been used in this simulation. Multiple access interference and additive white Gaussian noise have been included in the simulation. Simulation of the near-far effect is also an option available.

The BER degrades gracefully as the system load increases for the IS-95 reverse channel. The capacity is also a function of the E_b/N_o power level selected for all the users. The simulations in this work focused on a range of E_b/N_o from 10 to 15 dB. In most cases this was sufficent to obtain a BER of 10^{-3}. The number of multiple access interferers limits the system performance. There is a diminishing return from increasing the E_b/N_o when using a conventional single user receiver at the base station. A comparison of the benefits of using soft decision decoding was made. We show that in a conventional and multiuser receiver approximately 2 dB of coding gain may be realized through the use of soft decisions in the decoder.

The two types of multiuser receiver analyzed in this work both improved the system performance and increased system capacity. The parallel interference cancellation method performed slightly better than the successive method. The advantage of using a multiuser receiver was more evident when the system was moderately loaded (approximately 15-20 users).

Under near-far conditions both multiuser receivers did significantly better than the conventional receiver. Both multiuser receivers were very robust to even 3 dB deviations from the desired power level, whereas the conventional receiver's capacity was reduced by more than 45% with similar imperfect power control. Multiuser receivers are a viable alternative solution to the complicated issues of ensuring perfect power control. Parallel interference cancellation performed on par with successive interference cancellation in the same near-far conditions.

The multipath conditions simulated in this work were fairly simple two-ray channel impulse responses. The purpose of these simulations was to show robustness to multipath for the multiuser receivers. This robustness was achieved by taking advantage of the multiple fingers of the RAKE tracking the multipath components. Each multipath was, in essence, regenerated and cancelled from the received signal taking advantage of the signal energy contained in each component. Performance decreased as the rms delay spread increased for all the receiver types, but more importantly the advantage of using multiuser detection was maintained throughout.

Quantization was the other focus of this research. We showed that in the DS/SS-BPSK system the quantization may be near optimal with as few as four bits of quantization. The threshold, however, is rather steep. One and two bit quantizers have identical performance characteristics but the performance loss is very large. Since quantization noise is often modelled as the addition of white Gaussian noise, we hoped for an extension of these simple results to that of the IS-95 standard. The separation in performance was almost identical. Both four and eight bit quantizers performed near optimum for the IS-95 reverse channel, while one and two bit quantizers performed far worse. We also showed that the same performance change is seen when soft decisions are used in the Viterbi decoder.

6.2 Future Work

The simulation software created for this work provides a flexible vehicle for future simulations of both IS-95 and various receiver structures in CDMA. Several extensions to this work remain available topics for future study.

If a particular receiver structure presented in this work was selected for further study, simulations might include more detailed channel impulse profiles, possible from real-world site measurements. These channel impulse response may be readily incorporated with the simulator. Future simulations might examine the effect of vehicle speed on the system performance by simulating the Doppler shift. More complicated analytic channel models may also be simulated such as the N-ray Rayleigh and N-ray Ricean model. Studying the effects of timing errors on the receiver is another topic worth pursuing. The work presented here has limited the scope of the interference to originate from within the cell of interest. Research has shown that much of the interference comes from other cells. It may be possible for base stations to share information between each other to cancel the interference form other cells. Several models of multicellular interference in a CDMA environment have already been developed [Aga95] and can be added to the interference modelling.

A modification to the current IS-95 standard has been accepted that would allow an increase of the data rate from 9600 bps to 14400 bps. This also requires a minor change in the convolutional coder. In addition to modifying the maximum data rate, accounting for voice activity detection may be added to the simulator. This would give a more realistic performance analysis rather than the worst case scenario presented in this work. A frame error rate analysis may also be simulated for the system. With increasing interest in data transmission, it may be useful to simulate the performance of different network layer protocols operating over an IS-95 radio link, such as ATM or TCP/IP.

This simulation used the Walsh matrix to correlate with the received signal. It is possible to take advantage of the symmetry and structure of the Walsh matrix and perform a differential correlation of the received structure. The complexity of any interference cancellation is directly proportional to the computational effort required to perform an inverse Walsh function. The number of cancellations performed in a successive interference cancellation scheme is a limited by the time required to perform the inverse matrix operation. For parallel interference cancellation, the delay introduced is proportional to the number of stages of cancellation and time to perform an inverse Walsh operation. More efficient implementation of the Walsh transform implies a large number of cancellations are possible.

This simulation demonstrated the effect of ADC quantization bits on the system performance. Other issues in the implementation of a digital receiver may also be analyzed and simulated. Selecting a threshold for optimal performance in a CDMA system may be one topic for simulation. Quantization errors in the interference cancellation stage due to fixed point arithmetic in a digital signal processor may also be simulated.

Appendix A

Software Documentation

The software used for the simulation was written in ANSI C. Each of the routines used in the simulation is documented in this section. For ease of simulating multiple structures simultaneously, several copies of the software have been placed in different directories representing each receiver structure. A *Makefile* is present in the directory; this file controls the compilation of the C programs. To compile the software the following commands are executed:

make clean
make

The executable file *IS95sim* will be created which may be invoked to run the simulation.

A.1 Simulation Files

There are several files that contain the source code for the *IS95sim* simulation software.

A.1.1 IS95sim.c

This file sets the initial conditions of the simulation such as the number of users, the E_b/N_o ratio to iterate over, and the power control conditions. It also controls the writing of the output results to a file. This subroutine calls *transmitter.c* and *receiver.c* to perform the transmit and receive functions.

initialize()
This routine takes an array of floats of given length and initializes all the elements to zero. The routine is used throughout the software.

A.1.2 transmitter.c

This file calls all the functions necessary for generating the transmitted signal for each user. This includes the generation of data, spreading the signal, and scaling the power level. It also performs the channel convolution for each user.

gen_data()
Each bit of random data is generated by this routine.

gen_power_levels()
Imperfect power control is simulated with this routine. Given a power level difference in dB, half the users present have their powers increased by this amount. The other half have their levels reduced by that amount.

pilotPNspread()
This spreads the I and Q channels with the appropriate pilot PN sequence using modulo-2 addition.

block_int()
This is the interleaving function for the IS-95 reverse channel.

mod_64ary()
This routine converts every 6 code symbols to a 64 chip modulation symbol. The modulation symbols are based upon a 64x64 Hadamard matrix.

LongPNspread()
This spreads the modulation symbols with the long PN code sequence using modulo-2 addition.

OQPSK_mod()
This routine performs the offset quadrature phase shift keying (OQPSK) modulation for the system. The symbols are converted to either a 1 or -1. Then each real value is sampled at the system sampling rate (4 times) by padding with 3 zeroes. The quadrature channel is delayed by 1/2 PN chip and both channels are convolved with the baseband filter.

A.1.3 genPNseq.c

This file contains the routines for generating the PN sequences. This also includes the electronic serial number (ESN) generation and the Walsh function generator.

gen_userESN()
This routine generates each user's ESN by generating a random bit sequence.

genLongPNcode()
The function generates the long PN sequence for a user for the duration of one frame (20 msec).

genWalshTable()
This function generates the 64x64 Walsh function used for othorgonal multiplication.

genLongCodeMask()
This routine generates the long code mask used in the generation of the long PN sequence.

genPilotPNcode()
This routine generates the pilot PN code for a frame duration. It is capable of generating both the I and Q pilot PN sequences.

A.1.4 filt_lib.c

This file contains the routines that perform the filtering operations used in the simulation. It also contains files that control the reading in of files containing filter coefficients.

conv_causal()
This routine performs the real convolution of two arrays.

matched_filter()
This routine does the matched filtering for the receiver. Both I and Q channels are matched filtered and the delay from the filtering is removed.

shift_left()
This function shifts an array by a given number of elements to the left.

shift_right()
This function shifts an array by a given number of elements to the right.

load_filter()
This function loads the filter coefficients from the file *filter.dat*.

phase_shift()
This function performs a complex phase shift on real and imaginary arrays.

A.1.5 channel_lib.c

This file contains the routines that load in the channel models. It also contains functions that generate the AWGN channel.

load_channel_params()
This routine loads channel parameters from the file *channel_params.dat*. This file contains the number of channel profiles and the length of each profile.

load_channel()
This routine loads the channel profiles from the file *channel.dat*. This file contains the I and Q channel characteristics of each channel profile. The I and Q components are sequentially placed in the file, i.e., the I and Q parameters of the first sample

are read, then the I and Q of values of the second sample, etc. The routine loads a channel profile from *channel.dat* every time it is called. When the end of *channel.dat* is reached, the routine restarts from the beginning of the file.

awgn()
This function generates and adds the AWGN to the I and Q channels.

channel_conv()
This function performs the comples convolution of the I and Q signal components with the I and Q channel components.

rake_tracking()
This function is used to synchronize the RAKE receiver fingers to the largest multipath components present. The delays of the largest components are stores for later use.

A.1.6 receiver.c

This file contains the routines for the implemented receiver. The routines perform the sampling, quantization, demodulation, interference cancellation (if any), decoding, and error counting for each user.

sample_sig()
This function samples the output of the I and Q matched filters.

block_deint()
This function performs the de-interleaving operation for the IS-95 reverse channel.

detecterror()
This function compares the output bit stream of the decoder with the input bit stream.

ViterbiDecoder()
This routine performs a threshold operation on the output correlations if the decoder is to perform hard decoding. It then calls the decoding routines.

par_interfer_cancel()
This routine controls the flow of the parallel interference cancellation scheme. The number of stages of cancellations is definable by the user.

regen_sig())
This function regenerates a user's I and Q channel signals, including all multipath components (if any), based upon output correlator statistics. It calls routines found in **transmitter.c**.

succ_interfer_cancel()
This routine controls the flow of the successive interference cancellation scheme. The number of cancellations performed is definable by the user.

A.1.7 RAKE_rec.c

This file contains the routines that perform the correlating functions with all the PN sequences for the multiple fingers in the RAKE. The number of fingers in the RAKE is user definable.

Walsh_corr()
This function calculates the output correlation of a given set of inputs with a row of the Walsh matrix. This is later used to find the row giving the maximum correlation.

RAKE_rec()
This routine performs the separate I and Q channel correlations, including matched filtering, sampling, PN correlation, and Walsh function correlations. This is done for all the fingers in the RAKE receiver.

dec2bin()
This function is used to convert the decimal row number of the Walsh matrix to 6 binary symbols.

A.1.8 rand_lib.c

This file contains the routines used to emulate stochastic properties. Most of these routines were developed in [Pre92].

ran2()
This function generates a uniform deviate based upon a modified L'Ecuyer generator.

rand_norm()
This functions generates a normally distributed deviate given uniform deviate seeds.

rand_bit()
This function converts a uniformly distributed deviate on [0,1) to either a 1 or 0.

rand_uni()
This function produces a uniformly distributed deviate on [0,1) by seeding with a part of the time function.

A.1.9 codec.c

This file contains the code for the convolutional encoder and Viterbi decoder. This code was take from Li's work [LiY93]. Complete documentation may be found there.

Bibliography

[Aga95] Parag Agashe and Brian D. Woerner, "Analysis of Interference Cancellation for a Multicellular CDMA Environment," *Proceedings of the Sixth IEEE International Symposium on Personal, Indoor, and Mobile Radio Communications*, pp. 747-752, Toronto, Canada, September 1995.

[Azi96] P. M. Aziz, H. V. Sorensen, and J. D Spiegel, "An Overview of Sigma-Delta Converters,", *IEEE Signal Processing Magazine*, pp. 61-84, Jan. 1996.

[ANS95] ANSI J-STD-008- Personal Station-Base Compatibility Requirements for 1.8-2.0 GHz Code Division Multiple Access (CDMA) Personal Communication Systems, March 1995.

[Ber87] E. R. Berlekamp, R. E. Peile, and S. P. Pope, "The Application of Error Control to Communications,"*IEEE Communications Magazine*, vol. 25, no.4, pp. 44-57, Apr. 1987.

[Bue96] R. M. Buehrer, N. S. Correal, and B. D. Woerner, "A Comparison of Multiuser Receivers for Cellular CDMA," Submitted to *IEEE Transactions on Vehicular Technology*, June 1996.

[Cam92] R. A. Cameron and B. D. Woerner, "An Analysis of CDMA with Imperfect Power Control," *Proceedings of 42nd IEEE Vehicular Technology Conference*, Denver, CO, pp. 977-980, 1992.

[Cou93] Leon W. Couch II, *Digital and Analog Communication Systems*, Macmillan, 1993.

[Cox72] D. C. Cox, "Delay Doppler Characteristics of Multipath Delay Spread and Average Excess Dealy for 910 MHz Urban Mobile Radio Paths," *IEEE Transactions on Antennas and Propagation*, VOl. AP-20, No. 5, pp. 625-635, Sept. 1972.

[Cox75] D. C. Cox and R. P. Leck, "Distributions of Multipath Delay Spread and Average Excess Delay for 910 MHz Urban Mobile Radio Paths," *IEEE Trans. on Antennas and Propagation*, Vol. AP-23, NO. 5, pp. 206-213, March 1975.

[Dix84] R. C. Dixon, *Spread Spectrum Systems*, John Wiley & Sons, New York, 1984.

[Due93] A. Duel-Hallen, "Decorellating Decision-Feedback Multiuser Detector for Synchrounous Code-Division Multiple-Access Channel, *IEEE Transaction on Communications*, Vol. 41, no. 2, pp. 285-290, February 1993.

[Due95] A. Duel-Hallen, J. Holtzman, and Z. Zvonar, "Multiuser Detection for CDMA system," *IEEE Personal Communications*, vol. 2, no. 2, April 1995.

[EIA90] Electronic Industries Association, "Cellular System Dual-Mode Mobile Station - Base station Compatibility Standard," IS-54, May 1990.

[EIA92] Electronic Industries Association, "Widband Spread Spectrum Digital Cellular System Dual-Mode Mobile Station - Base Station Compatibility Standard," IS-95, April, 1992.

[Fla95] Peter Flanagan, "Personal Communications Services: The Long Road Ahead," *Telecommunications*, February 1996.

[For73] G. David Forney Jr., "The Viterbi Algorithm," *Proceedings of the IEEE*, Vol. 61, no. 3, March 1973.

[Fun91] V. Fung, "Simulation of BER performance of FSK, BPSK, $\pi/4$ DQPSK in flat and frequency-selective channels," Masters Thesis in Electrical Engineering, Virginia Polytechnic Institute and State University, Blacksburg, VA, August 1991.

[Gau94] R. De Gaudenzi, F. Gianetti, and M. Luise, "The Effect of Signal Quantization on the Performance of DS/SS-CDMA Demodulators," *IEEE Global Telecommunications Conference*, Vol. 2, pp. 994-998, 1994.

[Gil91] K. S. Gilhousen, *et. al.*, "On the Capacity of a Cellular CDMA System," *IEEE Transactions on Vehicular Technology*, Vol. 40, no. 2, pp. 303-311, May 1991.

[Gur92] S. Gurunatham and K. Feher, "Multipath Simulation Models for Mobile Radio Channels," *Proc. 42nd IEEE Veh. Tech. Conf.*, Vol. 1, Denver, CO, pp. 131-134.

[Hal96] Jason Hale, "An Implementation of an AMPS Digital Base Station with Adaptive Automatic Gain Control," Masters Thesis in Electrical Engineering, Virginia Polytechnic Institute and State University, Blacksburg, VA, June 1996.

[Jal94] L. Jalloul and J. M. Holtzman, "Performance Analysis of DS/DCMA with Noncoherent M-ary Othrogonal Modulation in Multipath Fading Channels," *IEEE Journal on Sel. Areas in Comm.*, Vol. 12, No. 5, pp. 862-871, June 1994.

[Jer94] M. C. Jeruchim, P. Balaban, and K. S. Shanmugan, *Simulation of Communication Systems*, Plenum Press, 1994.

[Jun93] P. Jung, P. W. Baier, and A. Steil, "Advantages of CDMA and Spread Spectrum over FDMA and TDMA in Cellular Mobile Radio Applications," *IEEE Transactions Vehicular Technology*, Vol. 42, no. 3, pp. 357-364, August 1993.

[Kau95] A. Kaul, "An Adaptive Multistage Interference Cancellation Receiver for CDMA," Masters Thesis in Electrical Engineering, Virginia Polytechnic Institute and State University, Blacksburg, VA, March 1995.

[Kim92] K. I. Kim, "On the Error Probability of a DS/SSMA System with a Noncoherent M-ary Orthogonal Modulation," *Proc. 42nd IEEE Veh. Tech. Conf.*, Vol. 1, Denver, CO, pp. 482-485.

[Koh83] R. Kohno, M. Hatori, and H. Imai, "Cancellation Techniques of Co-channel Interference in Asynchrounous Spread Spectrum Multiple Access Systems," *Electronics and Communications*, vol. 66-A, no. 5, pp. 20-29, 1983.

[Lee89] W. C. Y. Lee, "Spectrum Efficiency in Cellular," *IEEE Trans. on Vehicular Technology*, Vol. 38, No. 2, pp. 69-75, May 1989.

[Lee91] W. C. Y. Lee, "Overview of Cellular CDMA," *IEEE Trans. on Vehicular Technology*, Vol. 40, no. 2, pp. 291-302, May 1991.

[Lib94] J. C. Liberti and T. S. Rappaport, "Analytical Results for Capacity Improvements in CDMA," *IEEE Transactions on Vehicular Technology*, Vol. 43, No. 3, pp. 680-690, August 1994.

[Lin92] F. Ling and D. D. Falconer, "Combined Orthogonal/Convolutional Coding for a Digital Cellular CDMA System," *Proc. 42nd IEEE Veh. Tech. Conf.*, Vol. 1, Denver, CO, pp. 63-66.

[LiY93] Y. Li, "Bit Error Rate Simulation of a CDMA System for Personal Communications," Masters Thesis in Electrical Engineering, Virgina Polytechnic Institute and State University, Blacksburg, VA, August 1991.

[Llo82] S. P. Lloyd, "Least Squares Quantization in PCM," *IEEE Transaction on Information Theory*, Vol. IT-28, pp. 129-137, March 1982.

[Lup89] R. Lupas and S. Verdu, "Linear Multiuser Detectors for Synchronous Code-Division-Multiple-Access Channels," *IEEE Trans. Info. Theory*, vol. 35, no. 1, pp. 123-136, Jan. 1989.

[Max60] Joel Max, "Quantizing for Minimum Distortion," *IRE Transactions on Information Theory*, Vol. 6, pp. 7-12, 1960.

[Mil92] L. B. Milstein, T. S. Rappaport, R. Barghouti, "Performance Evaluation for Cellular CDMA," *IEEE Journal on Selected Areas in Communications*, vol. 10, no. 4, pp. 680-688, May 1992.

[Pad94] R. Padovani, "Reverse Link Performance of IS-95 Based Cellular Systems," *IEEE Personal Communications Mag.*, vol. 1, no. 3, Third Quarter, 1994.

[Pad95] J. E. Padgett, C. G. Gunther, and T. Hattori, "Overview of Wireless Personal Communications", *IEEE Commun. Mag.*, vol. 33, no. 1, pp. 28- 41, Jan. 1995.

[Pat94] P. Patel and J. Holtman, "Analysis of a Simple Successive Interference Cancellation Scheme in a DS/CDMA System," *IEEE Journal on Selected Areas in Communications*, vol. 12, no. 5, pp. 796-807, June 1994.

[Pre92] W. H. Press, *et. al.*, *Numerical Recipes in C*, Cambridge University Press, Victoria, Australia, 1992.

[Pri58] R. Price and P. E. Green, Jr., "A Communication Technique for Multipath Channels," *Proc. IRE*, vol. 46, pp. 55-570, Mar. 1958.

[Pro89] J. G. Proakis, *Digital Communications*, McGraw-Hill, New York, 1989.

[Rap90] T. S. Rappaport, "900-MHz Multipath Propagation Measurements for U. S. Digital Cellular Radiotelephone," *IEEE Transaction on Vehicular Technology*, vol. 39, no. 2, May 1990.

[Rap91] T. S. Rappaport, "The Wireless Revolution", *IEEE Commun. Mag.*, vol. 29, no.11, pp. 52-71, Nov. 1991.

[Rap96] T. S. Rappaport, *Wireless Communications: Principles and Practices*, Prentice Hall Inc., New Jersey, 1996.

[Sch79] K. S. Schneider, "Optimum Detection of Code Division Multiplexed Signals," *IEEE Trans. Aerospace Electronic Syst.*, vol. AES-15, no. 1, pp. 181-185, Jan. 1979.

[Sha80] K. S. Shanmugan, "An Update on Software Packages for Simulation of Communication Systems (Links)," *IEEE Journal on Selected Areas in Communications*, Vol. 6, No. 1, pp. 5-12, Jan. 1988.

[Sta94] H. Stark and J. W. Woods, *Probability, Random Processes, and Estimation Theory for Engineers*, Prentice-Hall Inc., New Jersey, 1994.

[Str94] S. Striglis, "A Multistage RAKE Receiver for CDMA Systems," Masters Thesis in Electrical Engineering, Virginia Polytechnic Institute and State University, Blacksburg, VA, Aug. 1994.

[Tho92] B. Thoma, “Bit Error Rate Simulation Enhancement and Outage Prediction in Mobile Communication Systems,” Masters Thesis in Electrical Engineering, Virginia Polytechnic Institute and State University, Blacksburg, VA, July 1992.

[Var90] M. Varanasi and B. Aazhang, ”Multistage Detection in Asynchronous Code Division Multiple-Access Communications,” *IEEE Transaction on Communications*, vol. 38, no. 4, pp. 509-519, April 1990.

[Ver86] S. Verdu, “Minimum Probability of Error for Asynchronous Gaussian Multiple Access Channels,” *IEEE Trans. Info. Theory*, vol. IT-32, no. 1, pp. 85-96, Jan. 1986.

[Whi94] D. P. Whipple, “The CDMA Standard,” *Applied Microwave & Wireless*, pp. 24-39, Winter, 1994.

[Wic95] S. B. Wicker, *Error Control Systems for Digital Communication and Storage*, Prentice Hall, Inc., New Jersey, 1995.

[Yan95] Ning Yang, “Multiuser Detection for CDMA Systems with Convolutional Coding,” Masters Thesis in Electrical Engineering, Virginia Polytechnic Institute and State University, Blacksburg, VA, Oct. 1995.

[Zie92] Robert Ziemer and Robert Peterson, *Introduction to Digital Communications*, Macmillan Publishing Company, New York, 1992.

Vita

George Aliftiras was born in Washington, D.C., November 4, 1973. He received the Bachelor of Science degree in Electrical Engineering from Virginia Polytechnic Institute and State University, Blacksburg, Virginia in December 1994. He joined the graduate program at Virginia Tech in September 1994, and has been a member of the Mobile and Portable Radio Research Group since July 1995. His research interests include digital communications and practical receiver implemenations. He has focused on code division division multiple access (CDMA) spread spectrum communications systems, interference cancellation, and simulation of communications systems. He was also involved in the development of flexible multimode receivers for cellular.

George is a student member of the IEEE and a member of the Eta Kappa Nu (HKN) Honor Society.